AD-A099 560 GEORGIA INST OF TECH ATLANTA ENGINEERING EXPERIMENT --ETC F/G 17/9
RADAR BACKGROUND SIGNAL REDUCTION STUDY.(U)
JUL 80 E F KNOTT, C J RAY, M S WEST F29601-79-C-0050
UNCLASSIFIED GIT/EES-A-2403-F NL

1 of 2
AD
A099560

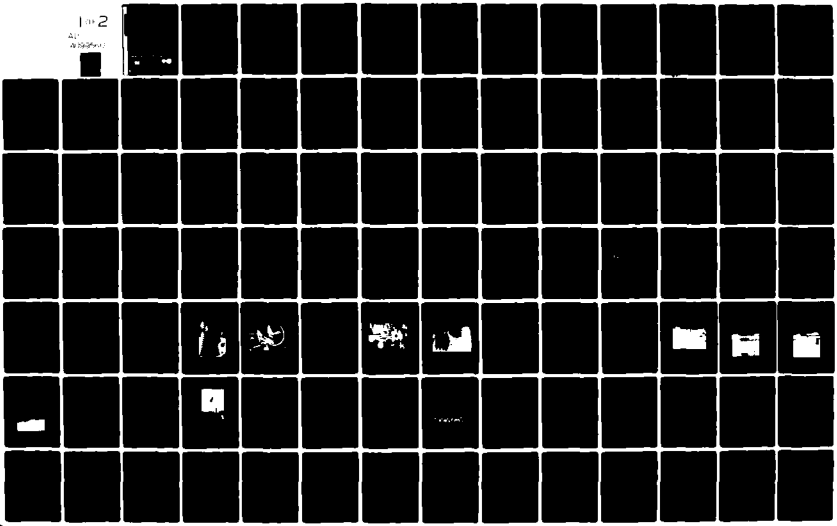

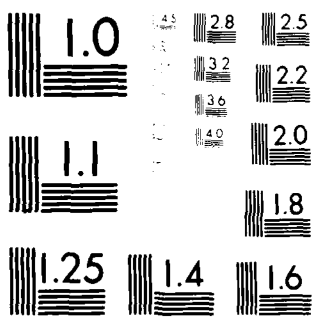

MICROCOPY RESOLUTION TEST CHART
NATIONAL BUREAU OF STANDARDS 1963 A

AD A099560

FINAL REPORT
PROJECT NO. A-2403

LEVEL II SC

RADAR BACKGROUND SIGNAL REDUCTION STUDY

By
E. F. Knott, C. J. Ray, M. S. West and R. J. Wohlers

CONTRACT NO. ~~N00039-79-C-0050~~ F29601-79-C-0050
AIR FORCE CONTRACT MANAGEMENT DIVISION
KIRTLAND AIR FORCE BASE, NEW MEXICO 87117

SEPTEMBER 1980

GEORGIA INSTITUTE OF TECHNOLOGY
Engineering Experiment Station
Atlanta, Georgia 30332

UNCLASSIFIED

SECURITY CLASSIFICATION OF THIS PAGE (When Data Entered)

REPORT DOCUMENTATION PAGE		READ INSTRUCTIONS BEFORE COMPLETING FORM
1. REPORT NUMBER	2. GOVT ACCESSION NO. AD-A099560	3. RECIPIENT'S CATALOG NUMBER
4. TITLE (and Subtitle) Radar Background Signal Reduction Study		5. TYPE OF REPORT & PERIOD COVERED Final Report
		6. PERFORMING ORG. REPORT NUMBER
7. AUTHOR(s) E. F. Knott, C. J. Ray, M. S. West ~~and~~ R. J. Wohlers		8. CONTRACT OR GRANT NUMBER(s) F29601-79-C-0050
9. PERFORMING ORGANIZATION NAME AND ADDRESS Georgia Institute of Technology Engineering Experiment Station Atlanta, Georgia 30332		10. PROGRAM ELEMENT, PROJECT, TASK AREA & WORK UNIT NUMBERS A-2403
11. CONTROLLING OFFICE NAME AND ADDRESS Air Force Contract Management Division Kirtland AFB, New Mexico 87117		12. REPORT DATE July 1980
		13. NUMBER OF PAGES 129
14. MONITORING AGENCY NAME & ADDRESS (if different from Controlling Office)		15. SECURITY CLASS. (of this report) UNCLASSIFIED
		15a. DECLASSIFICATION/DOWNGRADING SCHEDULE

16. DISTRIBUTION STATEMENT (of this Report)

DISTRIBUTION STATEMENT A
Approved for public release;
Distribution Unlimited

17. DISTRIBUTION STATEMENT (of the abstract entered in Block 20, if different from Report)

18. SUPPLEMENTARY NOTES

19. KEY WORDS (Continue on reverse side if necessary and identify by block number)

20. ABSTRACT (Continue on reverse side if necessary and identify by block number)

This report summarizes a study whose objective was to identify materials and/or techniques to reduce radar background signals for ground plane radar cross section (RCS) ranges. Background signal reduction is essential for improving the accuracy of RCS measurements and the primary application is for operations at the RATSCAT range on the White Sands Missile Range in New Mexico.

A survey of current literature revealed no new materials or techniques. A computer-aided design study showed that the control of the electrical —

DD FORM 1 JAN 73 1473 EDITION OF 1 NOV 65 IS OBSOLETE

UNCLASSIFIED

SECURITY CLASSIFICATION OF THIS PAGE (When Data Entered) properties of a target support column has few benefits, although one specific design showed substantial performance capabilities if fabrication techniques can be developed. A numerical post facto method (vector field subtraction) for background reduction was evaluated by the use of mathematically generated data. The results showed that aspect angle alignment is important and experimental verification and evaluation is clearly needed.

Column shaping was studied experimentally, but the results were inconclusive. The "volume" return from a target support column may constitute the irreducible signal, which is unaffected by shape.

Low frequency background signals are due to inadequate instrumentation and anomalies in the ground plane behavior. Diagnostic testing was suggested as a way of determining the background signal sources, and test results should indicate the corrective action to be taken.

FINAL REPORT

GIT/EES Project A-2403

RADAR BACKGROUND SIGNAL REDUCTION STUDY

by

E. F. Knott
C. J. Ray
M. S. West
R. J. Wohlers

Contract No. F29601-79-C-0050

Submitted to

AIR FORCE CONTRACT MANAGEMENT DIVISION
KIRTLAND AIR FORCE BASE, NEW MEXICO 87117

July 1980

GEORGIA INSTITUTE OF TECHNOLOGY
Engineering Experiment Station
Atlanta, Georgia 30332

TABLE OF CONTENTS

LIST OF FIGURES

LIST OF FIGURES (cont.)

LIST OF FIGURES (cont.)

LIST OF TABLES

1. INTRODUCTION

This is the final technical report under Air Force Contract F29601-79-C-0050, "Radar Background Signal Reduction Study." The objective of the study was to identify materials, or combinations of materials and techniques, which might reduce or eliminate residual radar background signals. The effort was intended primarily to improve the quality of radar reflectivity measurements conducted at the Air Force RATSCAT test site on the White Sands Missile Range near Holloman Air Force Base, New Mexico.

The technical work requirements were embedded in seven tasks, summarized below.

Task 4.1 Examine existing RATSCAT facilities, target mounting techniques, operating methods, equipment and materials, and make documented recommendations to improve background reduction techniques. For the 30 to 500 MHz frequency range, identify the sources of background and make documented recommendations to improve background reduction techniques.

Task 4.2 Investigate radar background signal reduction techniques applicable to RATSCAT over the frequency range from 0.5 to 95 GHz, to include research and evaluation of current literature. Review GFE publications to establish a baseline and minimize possible duplication of previous efforts.

Task 4.3 For the frequency range 0.5 to 95 GHz, identify suitable and available materials, or combinations of materials and techniques, which exhibit lower background characteristics than those in current use at RATSCAT. These include dielectric loading, painting, and geometric shaping and wrapping of the basic material. Evaluate and document the identified materials, or combinations of material and techniques, as to feasibility and suitability for RATSCAT application.

Task 4.4 Using the results of the investigation in Task 4.2, identify the materials that best satisfy the characteristics required by the RATSCAT operation. Determine and document via the literature search and/or laboratory measurements the radar reflectivity of the materials.

Task 4.5 Theoretically analyze the materials, or combinations of materials and techniques, which best satisfy the characteristics required at RATSCAT.

Task 4.6 Based on the theoretical analysis, fabricate models of the final column forms and measure the radar reflectivity of the models. Compare predicted and measured performance and document the results. Document those materials, or combinations of materials and techniques, which best satisfy all requirements.

Task 4.7 Examine vector subtraction techniques and make recommendations as to the feasibility for use at RATSCAT and for elimination of undesirable problems associated with vector field subtraction.

To identify the sources of low frequency (30 to 500 MHz) background signals, a site examination was conducted and discussions were held with range engineers. Due to insufficient information, the background signal sources could not be identified with certainty, but much of the problem is due to instrumentation deficiencies and ground plane anomalies. A theoretical study of trapped surface waves showed that a significant fraction of the incident energy can propagate within and just above the ground surface, for example. Judicious testing is recommended as a diagnostic procedure for defining more precisely what the background sources are and how they might best be eliminated.

To investigate high frequency (.5 to 95 GHz) background signal reduction techniques, a literature search was made and electromagnetic support column treatments were studied theoretically and experimentally. The literature search revealed that no new materials or techniques have been developed since RATSCAT began using expandable polystyrene bead foams for support columns 16 years ago. The theoretical treatment of support columns included several electrical loading ideas, most of which dispelled previous notions that loading might work. One loading scheme was identified as being potentially useful, however, but the translation of this electromagnetically desirable design into physical reality requires advanced fabrication techniques. It is recommended that the design concept be explored in more detail.

The experimental study was to be an evaluation of a circumferentially grooved column, and measurements were made of grooved and smooth test columns. But due to the small signal returns from the columns and the lack of adequate aspect angle control, the measurements were inconclusive and the advantages, if any, of a grooved shape were not established. It is recommended that the measurements be repeated at a facility where adequate sensitivity and aspect angle control are available, perhaps at RATSCAT.

The examination of vector field subtraction (VFS) was carried out using mathematically generated data. A more desirable approach would have been to use actual measurements, but none were available, nor were there any prospects of such data becoming available. Nevertheless, the study showed that VFS is a useful technique, provided the dynamic range of the background signal is limited and/or aspect angle misalignment between the data sets is minimized. It is recommended that VFS be evaluated in more detail in a comprehensive experimental program.

The structure of this report does not follow the task sequence listed above, but each task is addressed at one point or another in the text. An exception is Task 4.4, which specifies a characterization of the reflectivity of materials by measurements or from the results of the literature search. Since no new materials were identified, this could not be done. Nevertheless, the reflectivity characteristics of certain column designs and configurations are presented in Section 4 in conjunction with the analytical studies of column scattering.

2. THE BACKGROUND PROBLEM

Radar cross section (RCS) data are almost always required for a free space environment: which is to say, measurements are required of the target itself and nothing else. From the inception of the RATSCAT measurement capability, the decision was made to exploit the ground plane effect [1], which effectively quadruples the sensitivity of the radar instrumentation while still yielding the free space RCS. This sensitivity enhancement is greatest if the ground is smooth and has a high dielectric constant, but it does impose restrictions on allowable combinations of target height and antenna height above the ground.

Since it is the return from the target alone that is required, whether in a ground plane environment or not, the target support mechanism should be as invisible as possible. Lightweight plastic foams, despite their low radar visibility, do scatter a portion of the incident wave back to the instrumentation radar, thereby contaminating the measurements. Multiple interactions between the target and the rotator, as well as with the ground in the vicinity of the pit, constitute another source of error, but they cannot be measured or determined in the absence of the target. Covering the rotator and the ground in the pit area with radar absorbing material (RAM), however, can reduce this error source to acceptable levels. At low frequencies, the incident wave tends to propagate along the ground in a "trapped wave" mode, and the pit itself becomes a scatterer. Buried obstacles, such as cable runs and water lines, are other discontinuities that scatter the trapped wave.

Lightweight plastic foams, which were developed by large chemical companies strictly for commercial purposes, were discovered decades ago to be excellent materials for radar target support columns because of their "invisibility." Such support columns are not actually invisible, of course, but a well made column can have a very low radar cross section. Nevertheless, for

---

1. "RATSCAT Facilities and Capabilities," 6586th Test Group, Holloman Air Force Base, New Mexico, 1978.

modern test requirements, or even the requirements of 20 years ago, low density plastic foams often fall short of ideal performance. Unfortunately, this remains the case. The discovery of plastic foams as excellent target column support materials represented a quantum jump in RCS measurement capability, and further jumps are likely to be less spectacular. The only other comparable improvement in technology is the absorbent-covered metal pylon designed by Northrop and built by Lockheed for use at RATSCAT in the mid-seventies. Despite many of its shortcomings, this pylon offers extremely low background return for such a large structure.

The target support columns routinely used at RATSCAT are made from large blocks of expanded bead foam. The nominal density of the foam is 1 pound per cubic foot (pcf), though densities of 2 pcf may be used for high strength columns. A block of foam is not big enough to make a complete column, hence large wafers as much as 4 feet in diameter are cut from the block and stacked up to form a column of the desired height. The wafers are bonded together with a foam-in-place bonding system, and the entire column is mounted in a large, but simple, lathe fixture and turned down to the desired shape with a hot wire. The final step in column fabrication is the sanding of its surface to remove the glaze left by the hot wire and to otherwise smooth the surface.

Small targets can usually be supported with a single column mounted at the center of the rotator; larger targets may require as many as six columns. The targets are invariably guyed by several lines running from the target to the rim of the rotator. This is necessary for the safety of personnel as well as protection of the target, but the guy lines are not invisible to the radar. Measurements are often conducted in winds as high as 15 knots, and it is not uncommon for support columns to be exposed to sun and gypsum dust all day long.

Some columns are designed for a specified target; other columns are general purpose, being saved and used as needed on subsequent test programs. A column may be used for several targets of varying shape by the use of "transitions" or "saddles" made of foam blocks especially shaped to fit the target contour and to mate with the column itself. Unused columns are stored indoors out of the sun, but like everything at RATSCAT, they soon become coated with gypsum whether indoors or not. Untrained personnel occasionally abuse the delicate columns during handling, but columns often become damaged simply because of the harsh environment at the site.

For frequencies below 500 MHz, the target support column is not the dominant source of background signal, hence the background reduction techniques discussed below and in subsequent sections will have little effect at these frequencies. For frequencies in the millimeter range (35 GHz and up), the cell structure of most foams becomes an appreciable fraction of a wavelength, and it is doubtful that much can be done to reduce the background attributable to the column.

One can conceive of several ways to reduce background returns for frequencies above 500 MHz, but not all of them are useful. Below is a discussion of the advantages and limitations of several concepts.

Low density columns: Since the power reflectivity of a dielectric (foam) interface varies with the square of the density, the use of low density foams is an obvious way to reduce the scattering. A reduction in density, however, is almost always accompanied by a reduction in load-bearing properties. Thus, a larger column is required and the reduction in surface reflectivity is offset by an increase in the total surface exposed to the radar. In addition, the increased volume increases the "incoherent" return studied by Plonus [2].

Column loading: The introduction of loss in the bulk of a column is an impedance matching concept. The computer modeling study discussed in Section 4 shows that electrical losses can minimize the column return over a reasonably wide band of frequencies, but physical realization of the model may be difficult. In a uniform dispersion of carbon particles, the particles must be an appreciable fraction of a wavelength in size for the incident wave to interact with them. A more effective realization would be a network of interlaced lossy fibers, and they would have to be incorporated in the bulk of the foam

---

2. M. A. Plonus, "Theoretical Investigations of Scattering from Plastic Foams," IEEE Transactions on Antennas and Propagation, Vol. AP-13, January 1965, pp. 88-93.

during manufacture.

Joint elimination: Although it has been suggested that the bonds between adjacent sections of a built-up column are sources of reflection, no systematic study of these reflections could be identified, and the experimental tests described in Section 5 were inconclusive. Moreover, it is difficult to envision how a joint-free column might be fabricated, other than modeling the entire column with special equipment on-site.

Broadband column tuning: A cylindrical column can be "tuned" so that the reflection from its rear surface cancels the reflection from the front surface. A column can be tuned by the variation of either the radar frequency or the column diameter, but the former is much easier if the test requirements do not specify a precise frequency. Broadband tuning is a concept based on varying the effective dielectric constant across the column diameter, but, as shown in Section 4, the concept is invalid.

Contact area minimization: A University of Michigan study [3] shows that the incident field structure can be badly distorted when the incident wave propagates more than a few wavelengths parallel to the surface of a foam. This suggests that the contact surface between the target and support saddle should be minimized wherever possible. But as the contact surface is decreased, the stress over the contact area increases, and the increased force due to target guying imposes lower limits on the size of the contact area.

Column shaping: Shaping is a useful technique for RCS reduction, and RATSCAT has already employed longitudinal (fluting) shape factors to its columns. Specific shapes mentioned in the RATSCAT capabilities brochure are the teardrop and the diamond. Unfortunately, these shapes have low returns only over narrow sectors of angles centered on the edge-on direction. Complete 360-degree aspect angle measurements of targets supported by teardrop or diamond shaped columns would require that the target be repositioned several times, and a complete pattern would have to be pieced together from several

---

3. E. F. Knott and T. B. A. Senior, "Studies of Scattering by Cellular Plastic Materials," University of Michigan Radiation Laboratory Report 5849-1-F, April 1964.

patterns. An alternative is to use circumferential grooves for shape control, and such a column was in fact built and tested; this is discussed in Section 5.

Column wrapping: The column wrapping concept is based on sheathing the column with a layer of absorber or resistive material. As discussed in Section 4, the addition of the sheath serves only to raise the RCS of the columnn. Hence, this technique should be dismissed from further consideration.

RAM-coated metal pylons: The vane-shaped pylon already in use at RATSCAT is an excellent example of high technology. The pylon return is remarkably low for a structure of its size. Despite the disadvantage of requiring a solid mechanical mating with the test target (i.e., disfigurement of the target), this technique represents a reasonable compromise between reality and idealism. Another disadvantage is that target height cannot be varied unless special provisions are incorporated in the pylon design. The RAM-covered pylon idea can be extended and improved upon, as mentioned in Section 8.

RAM in the pit area: RATSCAT has recognized the need for reducing target/pit interactions, and in some test programs RAM is deployed on the ground and rotator to suppress these interactions. At lower frequencies (below 500 MHz), a different kind of RAM and a different mode of deployment may reduce scattering of the trapped wave due to the discontinuity in the ground presented by the pit itself.

Target suspension by means of thin lines: Suspending a target by nonmetallic lines can reduce background signals, but this technique is very frustrating. Lines fastened from the target to a rotator give some measure of attitude control, but the target tends to oscillate due to the strain on the lines, and the actual aspect angle is different from the angle indicated by the rotator synchros. A pair of 140-foot towers was erected straddling Pit #1 at the site for target suspension purposes, but their continued disuse is a testimony to the unpopularity of the technique.

3. LITERATURE SEARCH

Most of the prior work done on plastic foam was conducted more than 15 years ago at the University of Michigan under a subcontract with General Dynamics/Fort Worth, the prime contractor tasked with constructing and instrumenting the RATSCAT [4]. The sponsoring agency was the Rome Air Development Center at Griffiss Air Force Base, New York. The University of Michigan final report [3] was subsequently included in General Dynamic's report published by RADC [5], and was the basis for other publications and papers [2,6,7].

Three documents [5,8,9] were submitted to Georgia Tech by the Air Force as government furnished material, but were inapplicable or inappropriate. The content of [5] was a copy of the original work in [3]; the suspension devices discussed in [8] have fallen into disuse at RATSCAT; and the discussion of RAM-coated metal columns in [8] was almost completely inconclusive. The background subtraction in [9] addressed primarily the clutter return out to 90 kilofeet, and no data were presented showing the effect vector subtraction of the column return.

A computerized literature search was made to determine what, if any, published scientific or engineering data or theories were available on the RCS

---

4. H. C. Marlow, D. C. Watson, C. H. Van Hoozer and C. C. Freeny, "The RATSCAT Cross-Section Facility," Proceedings of the IEEE, Vol. 53, August 1965, pp. 946-954.
5. "Radar Cross Section Targets Supports - Plastic Materials," Technical Report RADC-TDR-64-381, Rome Air Development Center, June 1964.
6. T. B. A. Senior, M. A. Plonus, and E. F. Knott, "Designing Foamed-Plastic Target Supports," Microwaves, December 1964, pp. 38-43.
7. T. B. A. Senior and E. F. Knott, "Estimates of the 'Volume' Return from Styrofoam," Proceedings of the Radar Reflectivity Measurements Symposium held at MIT Lincoln Laboratories, Report RADC-TDR-64-25, Vol. I, April 1964, pp. 521-526.
8. "Radar Cross Section Target Supports - Metal Columns and Suspension Devices," Technical Report RADC-TDR-64-382, Rome Air Development Center, June 1964.
9. C. C. Freeny, "Radar Target Scatter Site (RATSCAT) Background Subtraction Investigation," Technical Report RADC-TDR-67-436, Rome Air Development Center, June 1964.

reduction of target support columns. Such a review was deemed necessary because the material in current use (expanded bead polystyrene foam) was selected in the mid-sixties. Manufacturers of plastic foams were also solicited for information.

The computerized literature search on plastic foams and their interaction with radar waves was performed in cooperation with professional library staff at Georgia Tech's Price Gilbert Memorial Library. The key terms used in the search were selected from a review of earlier documents for commonly used words and phrases. The key terms used were:

cellular	foam
cellular plastic	plastic
radar	thermoplastic
microwave	rigid
scatter	backscatter
reflection	

The data bases used in the search were United States Government Research and Development Reports, published by the Federal government, and INSPEC, published by the Institute of Electrical Engineers. The latter covers world literature on physics, electronics, and computers. A manual search was also conducted through the review and perusal of handbooks, texts, and the annual indexes of the Journal of Cellular Plastics. Specific review materials are listed as references [10] through [16].

---

10. "The Engineering Data Bank - Foams," Modern Plastics Encyclopedia, Vol. 54, No. 10A, 1977, pp. 485-487.
11. R. W. Barito and W. O. Eastman," Plastic and Elastomeric Foams," Chapter 7, Handbook of Plastics and Elastomers, 1975.
12. Plastic Foams, Part II, eds. K. C. Frisch and J. H. Saunders (Marcel Dekker, Inc., New York, 1973), Chapter 9, "Rigid Urethane Foams;" Chapter 10, "Polystyrene and Related Thermoplastic Foams;" Chapter 11, "Phenolic Foams;" Chapter 12, "Urea-Formaldehyde Foams Chapter 13, "Epoxy-Resin Foams;" Chapter 15, "Miscellaneous Foams;" Chapter 17, "Effects of Cell Geometry on Foam Performance;" and Chapter 21, "Military and Space Applications of Cellular Materials."
13. T. H. Ferrigno, Rigid Plastic Foams, 2nd Edition, Reinhold Publishing Corp., New York, 1967.
14. Calvin J. Benning, Plastic Foams: The Physics and Chemistry of Product Performance and Process Technology, Vol. II: Structure, Propertiesand Applications, Wiley-Interscience, New York, 1969.

The survey showed that the expandable bead foam in current use at RATSCAT is the best basic material for target support purposes. This assessment is based primarily on the density of the foam because the reflectivity of a support column has been shown to depend on the square of the density of the foam and inversely on the fourth root of its elastic modulus.

A summary of typical properties for common foams is given in Table 1, based on information abstracted from the Encyclopedia of Modern Plastics. Phenolic foam appears to be a first choice based on the density criterion, but its strength properties are questionble. The foam is characterized as friable (easily crumbled or crushed to a powder), and it is esentially an open-cell foam in its low density form. The urea-formaldehyde foams are also friable and otherwise similar to the phenolic foams.

Styrene-acrylonitrile polymer foam is also of interest in this application. A foam of this type had been investigated as a target support (Tyrilfoam, Dow Chemical Co.), but it was rated poorer for this application in comparison to expandable bead because of its high volume scattering. The large incoherent scatter was thought to be due to the large cell size which was on the order of a half wavelength at X-band, approximately 1.7 cm. Subsequent to the work with Tyrilfoam, Ingram reported on the development of a styrene-acrylonitrile copolymer foam that was not significantly different from polystyrene foam in its physical properties [17]. A 1 pcf foam (laboratory preparation) was reported to have a cell size of 0.005 to 0.013 cm and an elastic modulus of 140 to 220 psi. This elastic modulus should be compared to 207 for the Tyrilfoam and 160 to 190 for a polystyrene foam of equal density. We did not determine whether this type material is commercially available.

Polyethylene and polypropylene foams also seem potentially useful in light of the data presented in Table 1. Polyethylene foams in the density

---

17. A. R. Ingram, "Novel Foams From Styrene-Acrylonitrile Copolymers," Journal of Cellular Plastics, 1, 1965, pp. 69-75.

TABLE 1. TYPICAL PROPERTIES FOR FOAMED PLASTICS*

Material	Density, pcf	Tensile Strength, psi	Compressive Strength, psi	Dielectric Constant
Phenolic	0.33-1.5	3-17	2-15	-
Polyethylene (low density)	1.3-2.6	20-30	5	1.05 @ 10^6 Hz
Polyethylene (high density)	0.9-12.5	46-210	2.0-18.5	1.1-1.55
Polypropylene (low density)	0.6	20-40	0.7	1.02 @ 10^4 Hz
Polypropylene (cross-linked)	2.0	118-147	175-1200	-
Polystyrene (expandable bead)	1.0	21-28	13-18	1.06-1.02 @ 10^3 - 10^6 Hz
	2.0	26-68	35-45	
Polystyrene (extruded)	1.5-20	55-70	25-55 @ 5%	-
Styrene - Acrylonitrile	0.5	-	1.5 @ 5%	-
	0.8	20	6.0 @ 5%	-
	1.0	30	6.0 @ 5%	-
Urea-Formaldehyde	0.8-1.2	poor	5	-
Polyurethane (rigid, closed cell)	1.3-3.0	15-95	15-60	1.05

*Source: Modern Plastic Encyclopedia, Volume 54, No. 10A (1977).

range of 2 to 3 pcf have been compared with polystyrene foam by Skochdopole and Rubens [18]. A general comparison between polyolefin and polystyrene foams offered by Barito and Eastman [19] shows that the polyolefins are weaker but tougher. The polyolefin foams are more resiliant and can withstand repeated impact loads, but their static load bearing capabilities are not suitable for the RATSCAT operation.

Ethafoam™ is a polyethylene foam manufactured by DOW Chemical Corporation and available in a wide range of densities (2.2 to 9.0 pcf) with relatively large cells, of the order of 1 mm. Ethafoam is available in a black version, in which the coloration is due to carbon black, but the carbon concentration is not known. If it were not for its resiliance, Ethafoam might prove to be a candidate for target support applications.

Rigid polyurethane foams, which are in wide use for thermal insulation, have densities from 1.5 to 2.5 pcf. Backus and Gemeinhardt [20] state that density is the dominant factor controlling the mechanical properties of foams. Measured strengths were found to be related to density by

$$\log (\text{strength}) = \log A + B \log (\text{density}) ,$$

where A and B are constants that depend on the particular polymer from which the foam is generated. Based on averaged values for the tensile strength, a value of 574 psi can be expected for a typical polyurethane foam having a density of 1 pcf [20, p. 487]. This is somewhat higher than reported in [3]. The electrical properties of polyurethanes are not as good as those of foamed polystyrene, the permittivity being of the order of three times greater [20,p. 504].

---

18. R. E. Skochdopole and L. C. Rubens, "Physical Property Modifications of Low-Density Polyethylene Foams," Journal of Cellular Plastics, 1, 1965, pp. 91-96.
19. "Ethafoam Brand Polyethylene Foam," Dow Chemical Company Form No. 172-125-78.
20. J. K. Backus and P. G. Gemeinhardt, "Rigid Urethane Foams," in Plastic Foams, Part II, ed. K. C. Frisch and J. H. Saunders, Marcel Dekker, Inc., New York, 1973, pp. 451-524.

An extremely light polyurethane foam used in packaging applications (POL 1000, Polymer Development Laboratories, Inc.) has a density of 0.4 pcf, but it is likely to be a very weak foam. A manufacturer of rigid polyurethane foams told us that polyurethane absorbs more water than polystyrene. Since the absorption of water raises the effective dielectric constant and therefore the foam reflectivity, polyurethanes are unlikely replacements for the expandable polystyrene foams now used at RATSCAT.

Several manufacturers or representatives thereof were contacted directly as part of the literature survey and the essence of their comments are included in the above discussion. The manufacturers queried are listed in Table 2, and they were chosen from the Buyer's Guide section of the Modern Plastics Encyclopedia.

The computerized search isolated several recent documents, none of them germain to the RCS reduction of target support columns. Examples of topics included are the propagation and reflection of pressure waves in porous media, the use of foams in cable insulation, the detection of cavities in foam insulation layers by percussion testing, the measurement of ultrasonic wave velocities in foams, and the measurement of the backscattering foam a V-shaped wire. The key words chosen by the authors or catalogers of these documents were responsible for the automatic selection of the documents as potential sources of information. A few other references were only slightly more applicable: one was a theoretical determination of the fields inside and outside a pair of concentric spherical shells; another was a Russian study of the reflection of microwaves (at a fixed angle of incidence of 34 degrees) by detergent solutions as cellular or emulsive foams. The computerized search provided no indications that any work on the RCS reduction of target support columns has been done in the last few years.

A final question regarding materials was the possibility of coating or painting expandable bead columns to reduce contamination due to gypsum dust, facilitate surface maintenance and cleaning, and retard column deterioration due to exposure to sunlight. Latex paints are possible candidates for this purpose because they will not attack the polystyrene as solvent-borne coatings would. Water-borne latex paints can be pigmented to provide screening or

TABLE 2. PLASTIC FOAM SUPPLIERS CONTACTED

Company	Foam Product	Comments
BASF-Wyandotte Corp.	Polyurethane	Raw material supplier only
Borg-Warner Corp.	ABS	Cannot get ABS in 1 pcf range, sell raw materials only
Dow Chemical Co.	Polystyrene	Product literature sent. felt polystyrene only good for this application
Flexible Products	Polyurethane	Packaging foams < 1 pcf most rigid foams 1.5-2.5 pcf; water absorption may be a problem, sunlight sensitive
Hercules, Inc.	Polypropylene	Raw material supplier
ITT United Plastics Div.	ABS	Foams for automotive field only
Mobay Chemical Corp.	Polyurethane	Raw material supplier
Nortech (Div. Northern Petro-Chemical Co.)	Polystyrene Polyethylene Polypropylene	Raw materials only
Polymer Development Lab.	Polyurethane	Primarily resin supplier; density range 1.5-40 pcf, literature sent
Upjohn Co., CPR Div.	Polyurethane	2 pcf lowest density available
Wilshire Foam Products, Inc.	Polystyrene	Expandable bead 1 pcf· literature to be sent

absorption of destructive ultraviolet radiation while remaining colorless and transparent in the visual range of wavelengths. This would retard weathering changes in the polystyrene. The adhesion, washability, coverage, and any other effect of latex paint on the RCS of a support column would have to be determined empirically. Based on model studies discussed in Section 4, a thin paint film will not greatly enhance the RCS. Therefore, the great variety of latex polymers and coatings available makes the feasibility of finding or developing a coating to enhance the lifetime and usefulness of the polystyrene foams all but certain.

4. THEORETICAL STUDIES OF SUPPORT COLUMN SCATTERING

Several theoretical studies were undertaken to evaluate some of the concepts discussed in Section 2. Investigations of concepts such as column loading and broadband column tuning were carried out with the aid of computer programs previously developed at Georgia Tech. The computer-aided evaluation of the concepts is addressed in separate sub-sections below in which the column is assumed cylindrical. In the first sub-section, however, an analytical (as opposed to digital) discussion of tapered columns is presented. The sub-sections dealing with cylindrical columns all have a common goal: to assess the potential RCS reduction of a given concept. The most useful potential scheme involves the introduction of electrical losses within the interior volume of the column whose outer surface has a thin skin of relatively high dielectric constant.

A. SCATTERING FROM TAPERED COLUMNS

As pointed out by Plonus [2] and Senior, et al. [6], the radar echo of a plastic foam column can be ascribed to two mechanisms. One is a surface reflection due to the abrupt change in the medium the incident wave finds itself propagating in, and the other is an "incoherent" volume return due to millions of tiny internal scatterers (i.e., the cell structure). We consider first the surface contribution, which can be estimated by calculating the column return as if the column were metallic and then multiplying the result by a reflection coefficient appropriate to the foam/air interface. For a 1.5 pcf polystyrene foam, the power reflection coefficient is of the order of -42 dB.

The surface return from a tapered column has two components, one due to scattering from the front surface (nearest the radar) and one from the rear. Each contribution behaves approximately like a skewed sin x/x function and, because of the different slants of the front and rear surfaces with respect to the incident wave, their main lobes are angled in different directions in the vertical plane. The presence of the ground plane complicates these patterns because, in addition to the free space pattern of the column, an image pattern and a diplane pattern are introduced. Although these effects can be accounted for (see, for example, Horst, et al. [21]), we shall consider only the free space RCS.

The total free space RCS is the sum of the front and rear contributions,

$$\sigma = |\sqrt{\sigma_f} + \sqrt{\sigma_r}|^2 \tag{1}$$

where:

$$\sqrt{\sigma_f} = is\, R_f \sqrt{\frac{kd}{2\cos\varepsilon}}\, \cos(\alpha - \varepsilon)\, e^{-i(kd\cos\varepsilon - \pi/4)} \cdot$$

$$\left\{\frac{\sin[ks\sin(\alpha-\varepsilon)]}{ks\sin(\alpha-\varepsilon)}\left(1 - i\,\frac{\sin\alpha}{kd\sin(\alpha-\varepsilon)}\right) + i\,\frac{\sin\alpha}{kd\sin(\alpha-\varepsilon)}\cos[ks\sin(\alpha-\varepsilon)]\right\} \tag{2}$$

$$\sqrt{\sigma_r} = is\, R_r \sqrt{\frac{kd}{2\cos\varepsilon}}\, \cos(\alpha + \varepsilon)\, e^{i(kd\cos\varepsilon - \pi/4)} \cdot$$

$$\left\{\frac{\sin[ks\sin(\alpha+\varepsilon)}{ks\sin(\alpha+\varepsilon)}\left(1 - i\,\frac{\sin\alpha}{kd\sin(\alpha+\varepsilon)}\right) + i\,\frac{\sin\alpha}{kd\sin(\alpha+\varepsilon)}\cos[ks\sin(\alpha+\varepsilon)]\right\} \tag{3}$$

where: $k = 2\pi/\lambda$ is the free space wavenumber,

$i = \sqrt{-1}$ is the pure imaginary number,

R_f, R_r are the complex voltage reflection coefficients of the foam surface

d is the mean diameter of the column,

s is the length of its slanted surface,

α is the angle of taper of the slanted surface (i.e., the cone half angle), and

---

21. M. M. Horst, M. T. Tuley, and K. B. Langseth, "Radar Modeling Studies," Final Report on Applied Physics Laboratory Subcontract 600403, Georgia Institute of Technology, Engineering Experiment Station, July 1978.

ε is the aspect angle, measured in the positive sense from broadside toward the small end of the column (see Figure 1).

When the denonimator of the first term in brackets in (2) and (3) approaches zero, the entire bracketed term approaches unity; hence, there are no singularities in the expression. (We assume that ε remains small enough that the column is never viewed end-on.)

The reflection coefficients depend on the incident polarization and the local angle of incidence. Specifically, from [22],

$$R_f = \begin{cases} \dfrac{\cos(\alpha - \varepsilon) - [\varepsilon_r - \sin^2(\alpha - \varepsilon)]^{1/2}}{\cos(\alpha - \varepsilon) + [\varepsilon_r - \sin^2(\alpha - \varepsilon)^{1/2}} & \text{horizontal} \\[2ex] \dfrac{[\varepsilon_r - \sin^2(\alpha - \varepsilon)]^{1/2} - \varepsilon_r \cos(\alpha - \varepsilon)}{[\varepsilon_r - \sin^2(\alpha - \varepsilon)]^{1/2} + \varepsilon_r \cos(\alpha - \varepsilon)} & \text{vertical} \end{cases}$$

$$R_r = \begin{cases} \dfrac{(\varepsilon_r)^{1/2}\cos(\alpha + \varepsilon) - [1 - \varepsilon_r \sin^2(\alpha + \varepsilon)]^{1/2}}{(\varepsilon_r)^{1/2}\cos(\alpha + \varepsilon) + [1 - \varepsilon_r \sin^2(\alpha + \varepsilon)]^{1/2}} & \text{horizontal} \\[2ex] \dfrac{(\varepsilon_r)^{1/2}[1 - \varepsilon_r \sin^2(\alpha + \varepsilon)]^{1/2} - \cos(\alpha + \varepsilon)}{(\varepsilon_r)^{1/2}[1 - \varepsilon_r \sin^2(\alpha + \varepsilon)]^{1/2} + \cos(\alpha + \varepsilon)} & \text{vertical} \end{cases}$$

For incidence near broadside, all four reflection coefficients have nearly the same value. By way of illustration, Figure 2 is a plot of the calculated 3 GHz free space RCS of a column 10 feet tall with a taper (half angle) of 6 degrees and a base diameter of 3 feet. The foam density is assumed to be 1.5 pcf, hence the dielectric constant is approximately 1.034.

The two patterns represented by Equations (2) and (3) attain their peak

22. J. A. Stratton, Electromagnetic Theory, McGraw-Hill, New York and London, 1941, pp. 493-494.

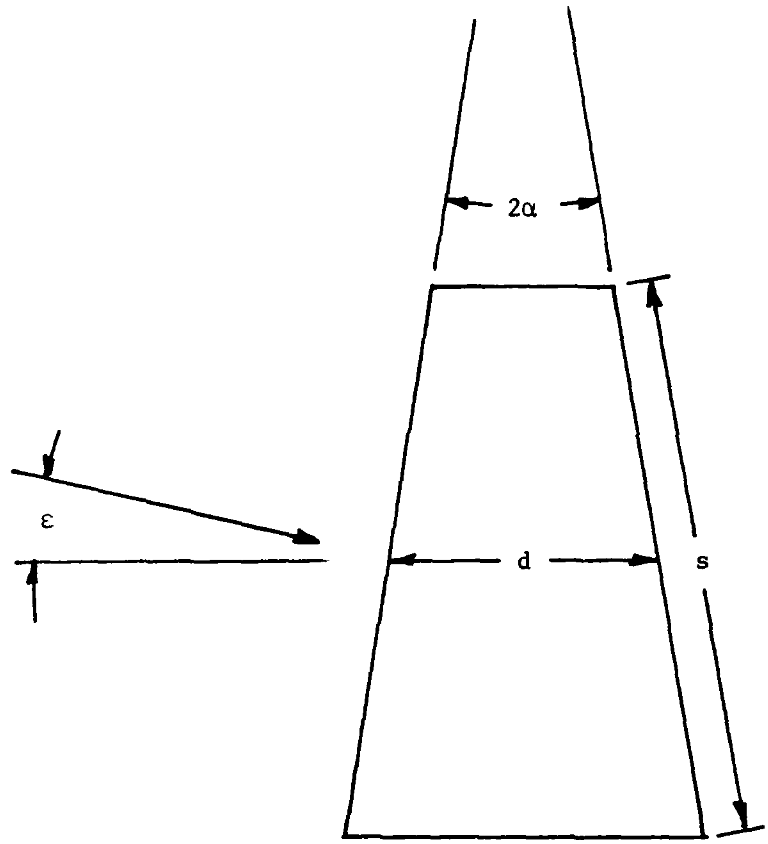

Figure 1. Geometry of a truncated cone.

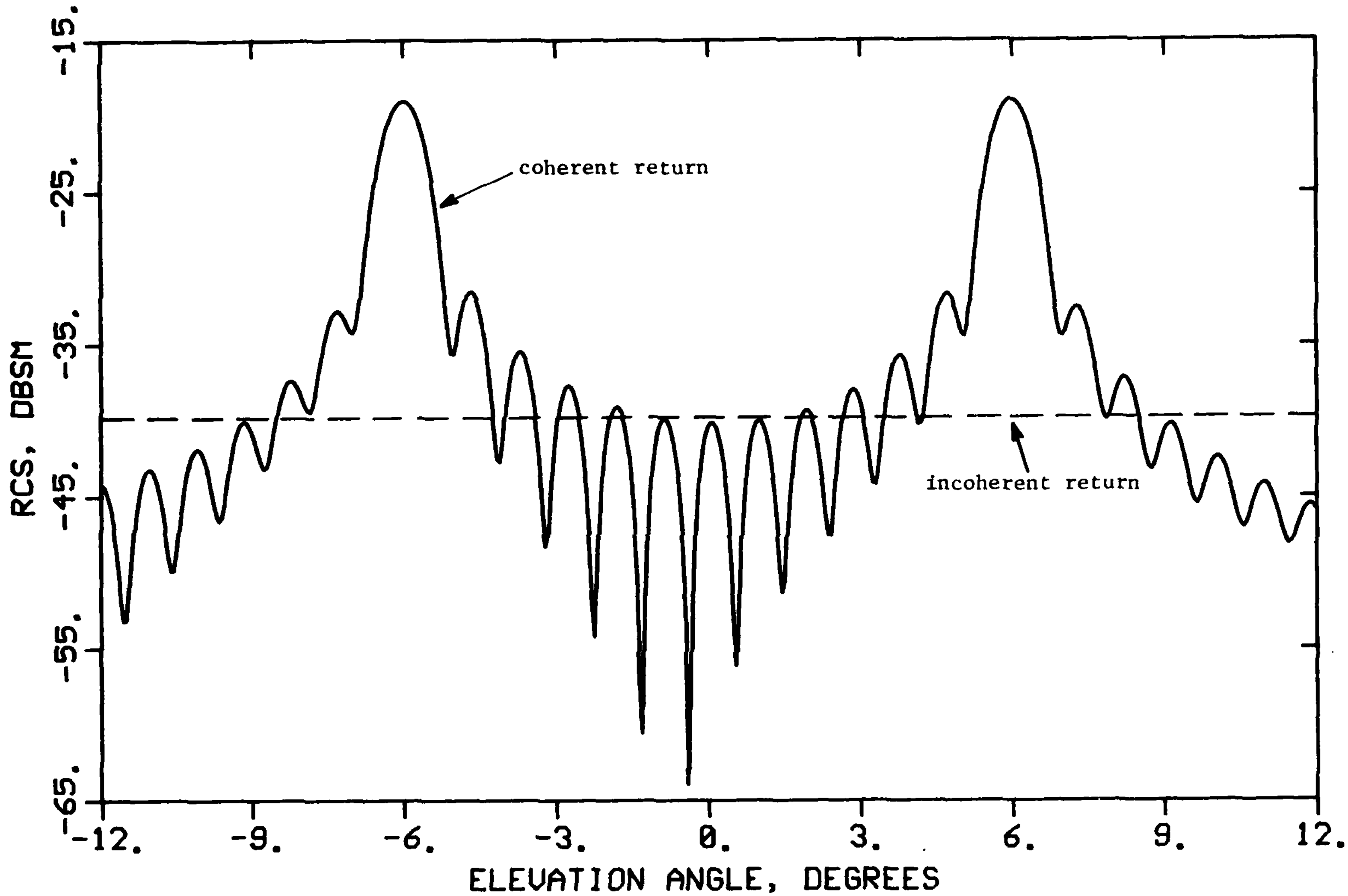

Figure 2. Theoretical free space RCS of a foam column 10 feet tall, base diameter of 3 feet, and a taper of 6 degrees at 3 GHz.

levels at quite different angular locations, with the left lobe being the reflection from the rear column surface and the right one being from the front. These peaks occur at ±6 degrees corresponding to normal incidence on one surface or the other [22]. The plot of Figure 2 is for horizontal incident polarization, and a nearly identical pattern would be observed for vertical polarization, with differences of less than 0.2 dB. Figure 3 is the predicted 9.65 GHz free space pattern of a column 56 inches tall with a 26-inch base diameter, a taper of 8 degrees, and a density of 1 pcf. These are the dimensions of a test column measured at Georgia Tech, although the measurements were very difficult to perform (see Section 5).

These are the free space returns, and entirely different patterns would be measured on a ground plane range because of the taper in the incident field strength from the top of the column to the bottom. The net return on a ground plane range would not exceed the free space value by more than 12 dB. For horizontal incidence (i.e., $\varepsilon=0$), the surface return would therefore be less than about -50 dBsm.

The other scattering mechanism mentioned above is the incoherent volume return, which Plonus attempted to relate to the cell structure of the foam [2]. The volume contribution is conceptually independent of the shape of the column and therefore irreducible; that is, column tuning can have no effect. Plonus' result for the incoherent return is

$$\sigma_i = \frac{\pi}{2} t^2 k^4 a |\varepsilon_r - 1|^2 V , \tag{4}$$

where t is the mean cell wall thickness, a is the mean cell radius, and V is the volume of the column.

Extensive experiments conducted at the University of Michigan did not confirm this prediction [3]. Because of the very small returns from test blocks and ogives, the measured data show large deviations. Nevertheless, a value of about -58 dBsm per cubic foot seems typical of the averaged data. The volume of the column taken for illustration in Figure 2 is about 61.6 cubic feet; hence, the incoherent volume return would be about -40 dBsm. This level

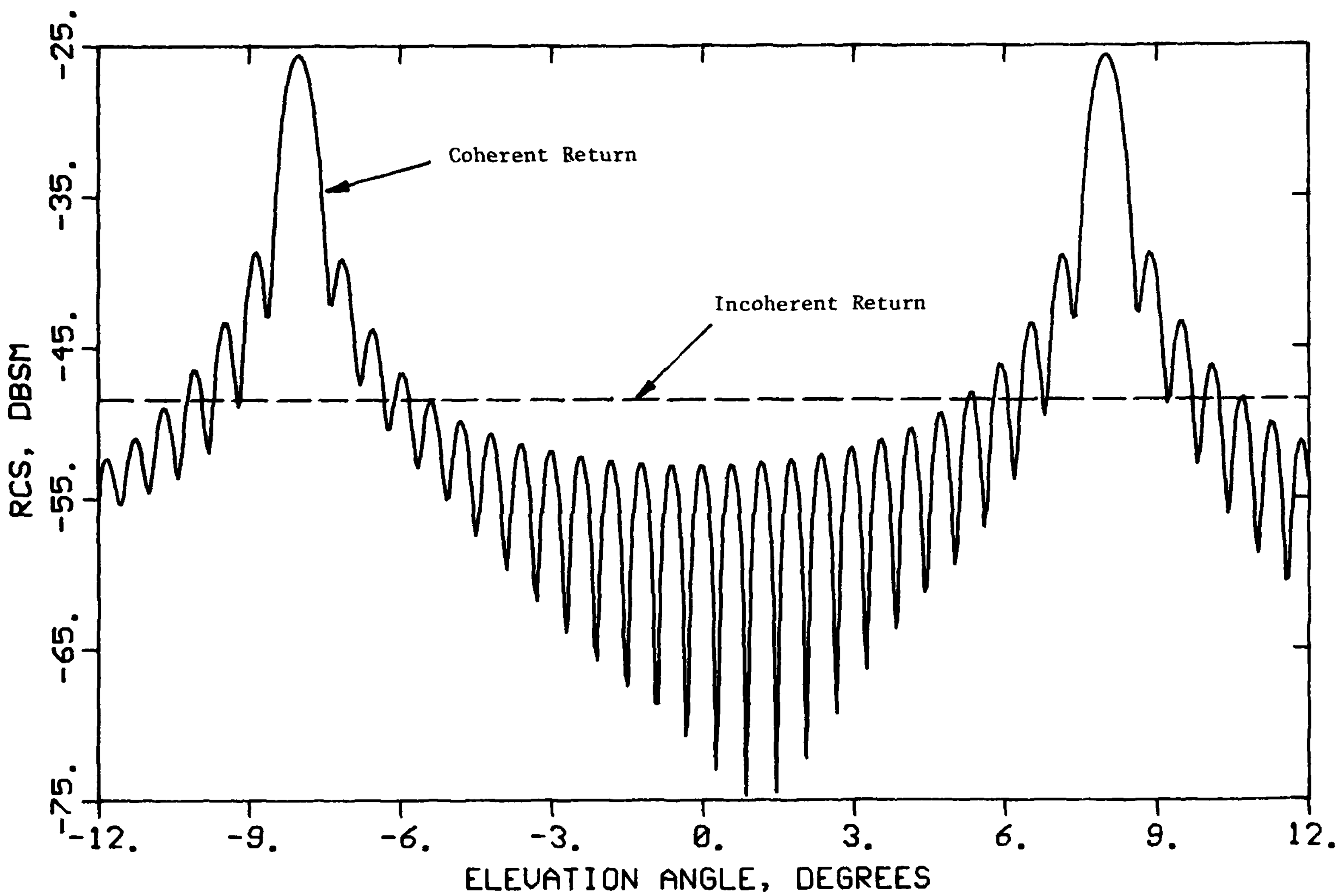

Figure 3. Theoretical free space RCS of a foam column 56 inches tall, base diameter of 26 inches, and a taper of 8 degrees at 9.65 GHz.

is indicated by the dashed lines and is somewhat above the minimal levels in the middle of the diagram for horizontal incidence. The volume return therefore appears to be the limiting level for reducing the return from a support column.

B. COLUMN WRAPPING

Some have conjectured that wrapping a foam column with a thin layer of resistive or absorbent material might reduce the column's radar echo. This turns out not to be the case, as shown by the analysis below. As with tapered columns, the front and rear sides of the column contribute to the scattered field, if the column is cylindrical, the two field components can add together constructively or destructively. To assess the effect of a thin lossy coating, we can build an approximate model of the cylinder using a thick foam slab. Such a model makes it easy to apply simple transmission line theory and gives a valid assessment, provided the cylinder is more than about a dozen wavelengths in diameter. The conceptual model depicted in Figure 4 shows a thick foam slab sandwiched between a pair of resistive sheets. Although real resistive sheets have a finite thickness, we can assume infinitely thin sheets for the purpose of analysis.

We characterize the resistivity of the sheets by a normalized resistance value ρ, the normalization being with respect to the impedance of free space. For example, $\rho = 1$ corresponds to a resistance of 366 ohms per square. From transmission line theory, the complex voltage reflection coefficient of the sheet-sheathed slab is

$$R = -\frac{1}{\rho} \frac{2\rho\sqrt{\varepsilon_r} \cos k\tau - i[1 + \rho^2(\varepsilon_r - 1)] \sin k\tau}{2(1 + \rho)\sqrt{\varepsilon_r} \cos k\tau - i[2 + \rho(\varepsilon_r + 1)] \sin k\tau} \tag{5}$$

and the power reflection coefficient is

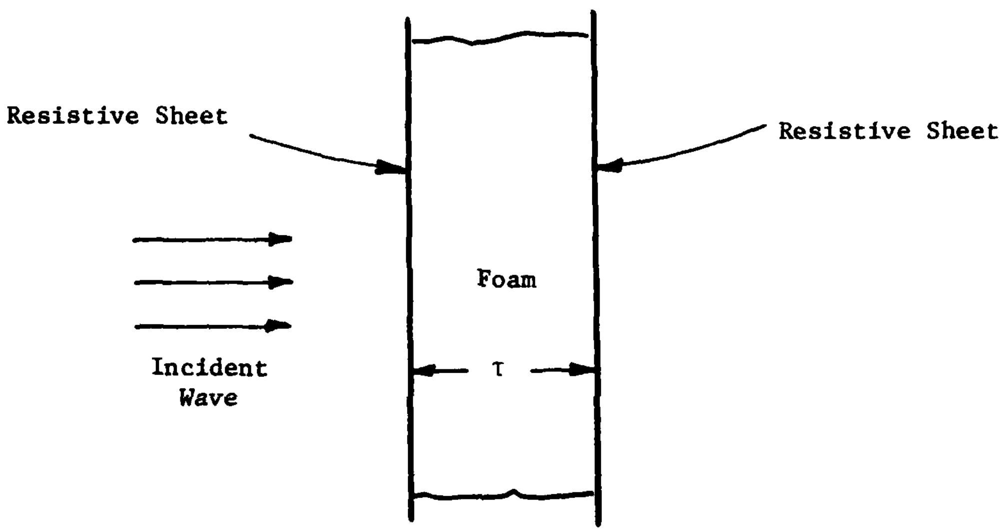

Figure 4. Geometry of a foam slab sandwich.

$$|R|^2 = \frac{1}{\rho^2} \cdot \frac{4\rho^2 \varepsilon_r \cos^2 k\tau + [1 + \rho^2(\varepsilon_r - 1)]^2 \sin^{-2} k\tau}{4(1 + \rho)^2 \varepsilon_r \cos^2 k\tau + [2 + \rho(\varepsilon_r + 1)]^2 \sin^{-2} k\tau} \tag{6}$$

where τ is the thickness of the slab.

The magnitude of the reflection coefficient oscillates between maximum and minimum values as the electrical thickness changes. To find the locations of the peaks and nulls, we may differentiate (6) with respect to $k\tau$ and find the value that forces the derivative to zero. For sheet resistivities less than a certain critical value, the maxima occur when the slab thickness is a multiple of a half wavelength, and the minima occur when it is an odd muliple of a quarter wavelength. For resistivities greater than the critical value, the locations of minima and maxima (i.e., the electrical thicknesses) interchange roles. The critical normalized resistivity for which this occurs is the largest value which satisfies the following cubic equation:

$$\rho^3(\varepsilon_r - 1) - 2\rho^2 - \rho + 1 = 0 \tag{7}$$

It will be found that

$$|R|_{max} = \begin{cases} \dfrac{1}{1 + \rho} & \rho < \rho_c \\[2ex] \dfrac{\rho^2(\varepsilon_r - 1) + 1}{\rho[2 + \rho(\varepsilon_r + 1)] + 1} & \rho > \rho_c \end{cases} \tag{8}$$

$$|R|_{min} = \begin{cases} \dfrac{\rho^2(\varepsilon_r - 1) + 1}{\rho[2 + \rho(\varepsilon_r + 1)] + 1} & \rho < \rho_c \\[2ex] \dfrac{1}{1 + \rho} & \rho > \rho_c \end{cases} \tag{9}$$

where ρ_c is the real root of (7).

These reflection coefficients are plotted in Figure 5 for a 1.5 pcf foam for illustration. Note that the minimum reflection approaches the limiting value for the maximum reflection from the slab without resistive sheets, and the maximum remains above this level; at the critical value the two interchange roles. Thus, the maximum reflection coefficient will never be less than that of the base foam slab. We conclude that column wrapping cannot improve the performance of a foam column, even if column tuning is attempted. Thus, the concept should be abandoned.

C. COLUMN LOADING

The coherent returns from the front and rear surfaces of a dielectric cylinder can be balanced against each other if the electrical diameter can be tuned for a minimum. This implies some freedom in the selection of the radar operating frequency because the support column dimensions and the dielectric constant cannot be controlled as accurately as the frequency. Unfortunately, as is the case with most cancellation schemes, the nulls are deep and narrow, which precludes the convenient use of a single column for measurements at a variety of frequencies. A computer modeling study was conducted to investigate ways to increase the bandwidth in the regions of the hulls, and mechanisms for reducing the net returns from cylindrical columns.

The objective of the study was to assess four possible approaches:

1. Introducing loss in a homogeneous cylinder,
2. Varying the refractive index of a lossless cylinder,
3. Providing a thin, lossless skin, and
4. Assessing combinations of lossless skins and the introduction of bulk losses.

The question of whether these concepts could be transformed into practical target support systems was not addressed, primarily because the performance of such columns would not likely warrant the cost of producing them. Nevertheless, it is useful to document the ideas that were pursued.

The basic tools used in the evaluation were a pair of computer programs called JMAN and CONTRAST. JMAN gives the exact solution for the scattering by a collection of infinite concentric cylinders, each of which may have an arbitrary, complex (i.e., lossy) dielectric constant. The solution of the

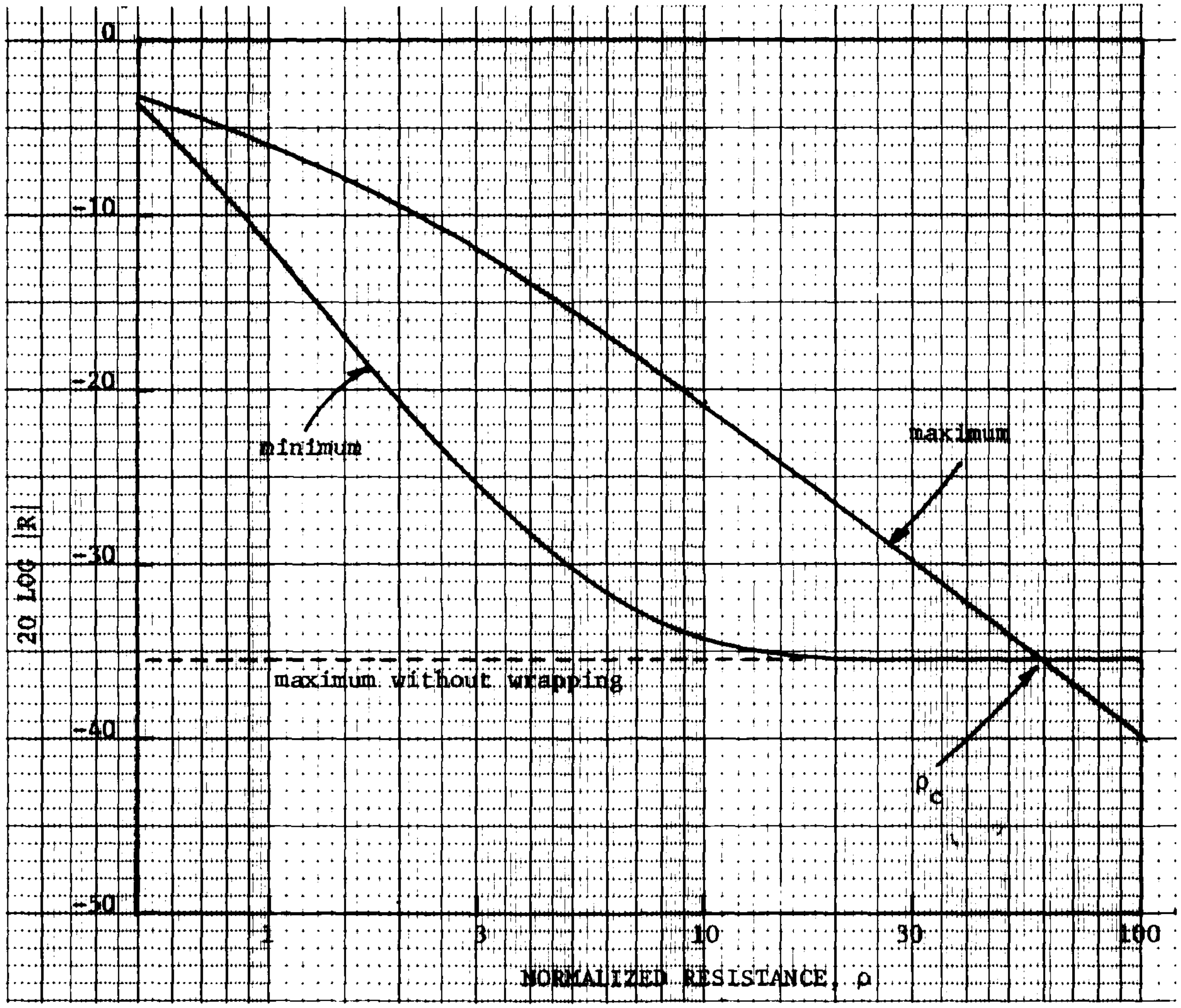

Figure 5. Net reflection coefficient of resistive sheet/foam sandwich for a 1.5 pcf foam.

two-dimension problem can easily be converted to a three-dimensional solution by a simple multiplicative factor. CONTRAST computes the normal incidence reflection coefficient of a flat multilayer dielectric backed by free space, with the individual layer properties being arbitrary and complex. The maximum electrical diameter that can be handled by JMAN is limited to about 200 radians, but any thickness can be handled by CONTRAST. The output of JMAN is the RCS of the multilayer cylinder in dBsm per unit length, and the output of CONTRAST is the magnitude of the voltage reflection coefficient expressed in dB. The absolute units are different, but the frequency dependence is similar, and one is a check of the other.

Introduction of Loss

Figure 6 shows the computed returns for a pair of homogeneous dielectric cylinders, each 40 inches in diameter. The dielectric constant of one cylinder includes a loss component; the other cylinder is lossless. The computations were performed over a narrow range of frequencies so that the interference pattern of the lossless cylinder could be inspected in detail. The lossy cylinder computations were performed only for a sufficient range of frequencies to be sure that there was no interference pattern. The attenuation of energy through the lossy column virtually eliminates the return from the rear column surface, hence the interference pattern disappears, and all that remains is the return from the front of the column. The lossy cylinder, however, reduces the return by no more than 4 dB below the maximums of the interference pattern of the lossless cylinder. This was also characteristic of other dielectric loss components ranging from -0.008 to -0.020. These results were essentially independent of the incident polarization, as is typical for large cylinders (i.e., whose diameters exceed about ten wavelengths). Figure 7 shows the maximum return as a function of the dielectric loss. For a dielectric constant of 1.03, an imaginary component of -0.013 gives the lowest maximum return. Thus, the square data points in Figure 6 suggest that the introduction of bulk losses can reduce the net return by no more than 4 dB.

Similar results were obtained for a 40-inch thick slab as modeled by the CONTRAST program, even to the point that a loss component of -0.013 minimizes the maximum return. In fact, as shown in Figures 8 and 9, a similar modest

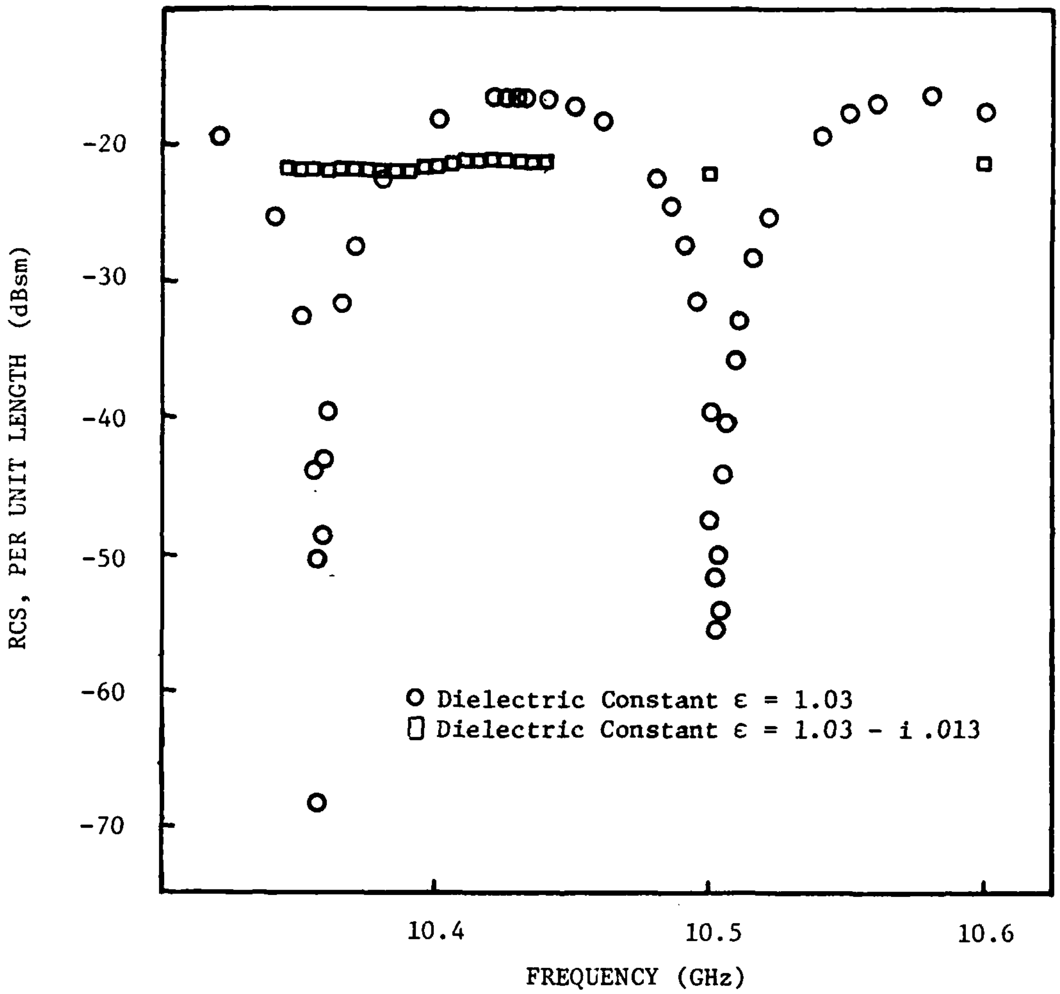

Figure 6. Comparison of lossy and lossless cylinder returns. Diameter = 40 inches.

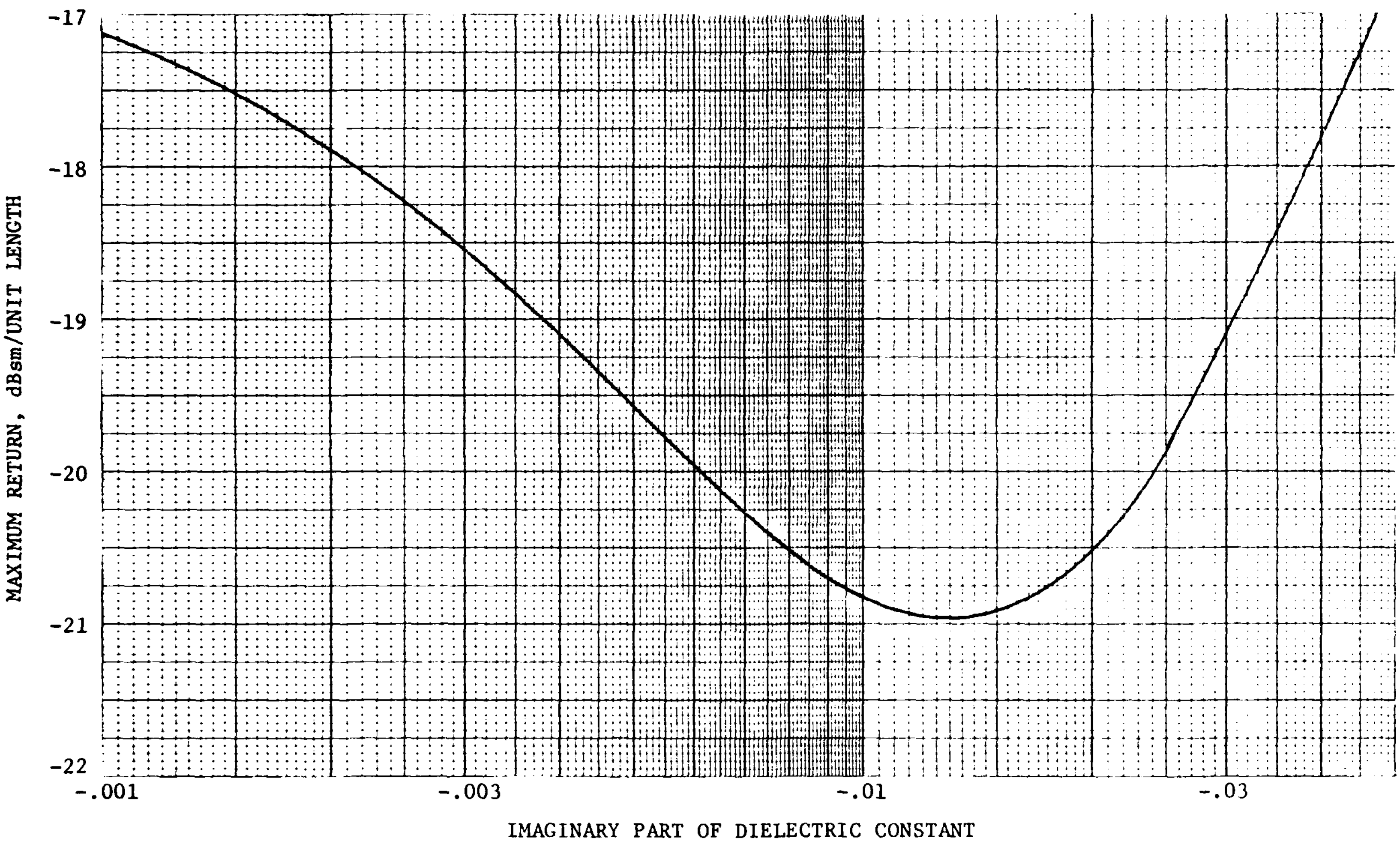

Figure 7. Maximum return from a 40 inch diameter cylinder as a function of bulk dielectric loss at 10.3-10.4 GHz. Real part of the dielectric constant is 1.03.

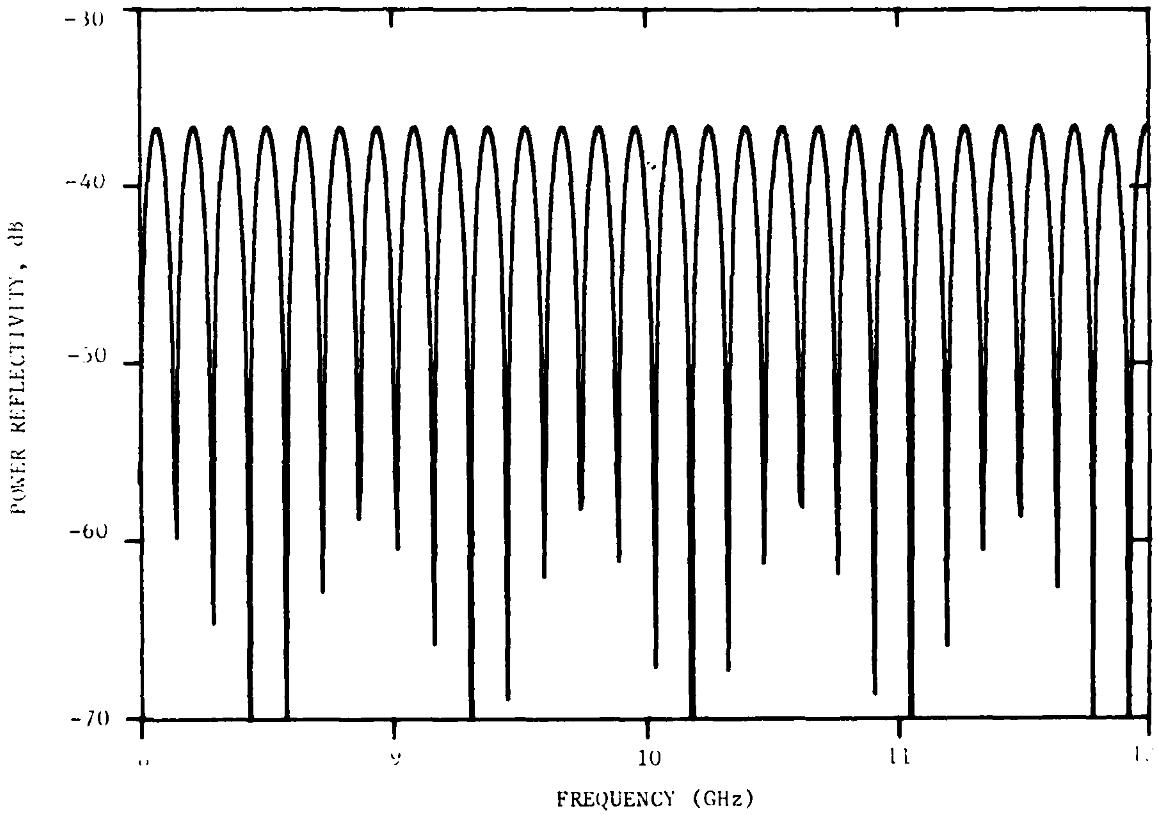

Figure 8. Reflection coefficient of a 40-inch thick lossless slab, $\varepsilon_r = 1.03$ (typical of 0 to 25 GHz).

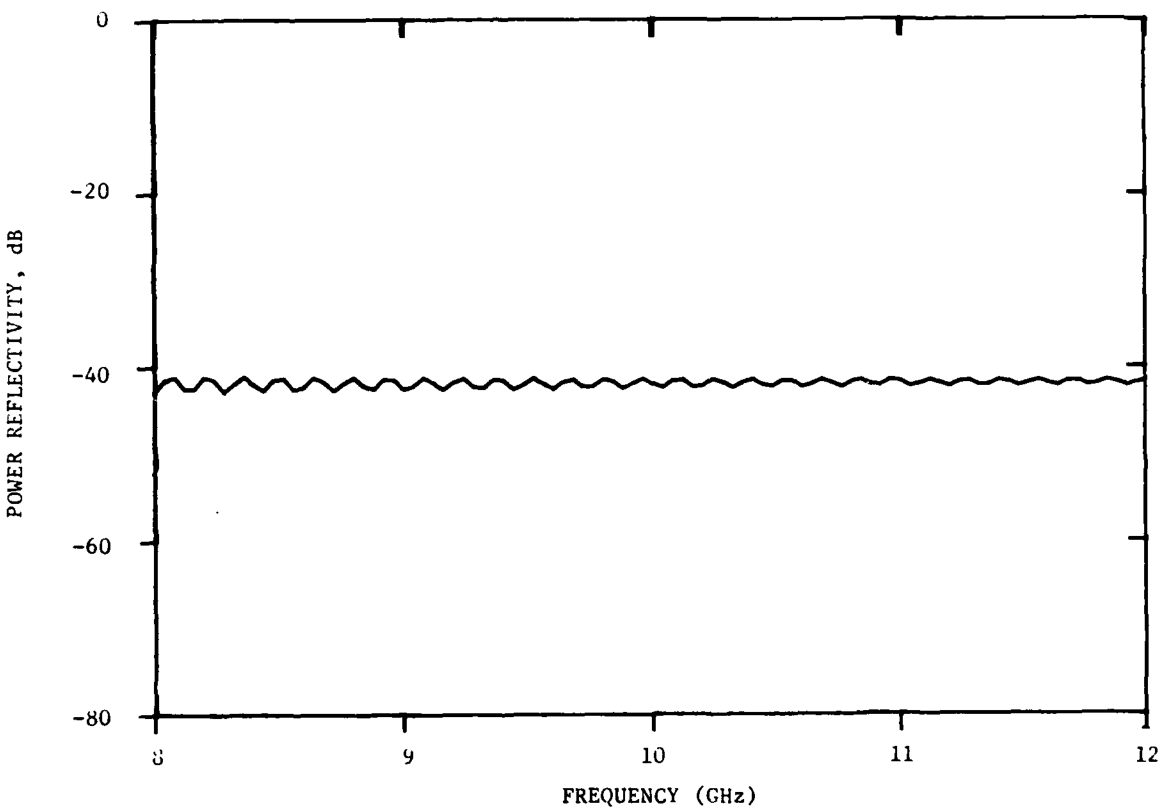

Figure 9. Reflection coefficient for a 40-inch thick lossy slab, $\varepsilon_r = 1.03 - i\,0.013$.

improvement is obtained over a broad range of frequencies. The difference between the peak values for cylinders and slabs is easily accounted for: i.e., a perfectly conducting sheet (as modeled by CONTRAST) has a reflectivity of 0 dB and a perfectly conducting cylinder (as modeled by JMAN) at 10.4 GHz has an aproximate reflectivity of 20 dBsm.

As the column diameter becomes smaller, the loss should be increased to reduce return. At 10 GHz, for example, doubling the imaginary part of the dielectric constant from -0.01 to -0.02 provides about a 0.5 dB improvement for a column of 20 inches in diameter. The maximum return for such a 20-inch diameter cylinder is -22.65 dBsm per unit length, in contrast to -20.95 dBsm per unit length for a 40-inch diameter cylinder. The maximum cylinder return is also sensitive to changes in the real part of the dielectric constant, as might be expected. For example, an increase of only 0.4% in the real part of the dielectric constant increases the return by about 1 dB.

Attempts to reduce the column RCS by varying the loss across the cylinder diameter were unsuccessful. These trials included linear variations in loss as a function of radial position, as well as a loss profile resembling a bell-shaped Gaussian function and peaking at the center of the cylinder. Results are not presented here because the homogeneous (constant) losses discussed above provided superior, albeit modest, performance. Since the introduction of constant bulk loss seems to reduce the cylinder return only 4 dB or so, this is discounted as a useful technique for the RATSCAT operation.

Variation of the Refractive Index (Lossless Case)

This RCS reduction idea is an extension of the concept of impedance matching, in which the intrinsic impedance of a cylindrical column is forced to be close to the free space value near its outer surfaces to minimize reflections, but is allowed to take on substantial values near the center to account for higher density material required for load bearing. The radial variation of the index of refraction (defined as the square root of the dielectric constant) produces a kind of two-dimensional Luneburg lens. The specific variations studied were

$$\varepsilon_r = 2 - \left(\frac{r}{r_o}\right)^2$$

$$\varepsilon_r = 1 + \left(1 - \frac{r}{r_o}\right)^2$$

$$\varepsilon_r = 1 + \frac{1}{2}\left(1 - \frac{r}{r_o}\right)^2$$

$$\varepsilon_r = 1 + \frac{1}{4}\left(1 - \frac{r}{r_o}\right)^2 \qquad (10)$$

where r is the radial position and r_o is the outer radius of the cylinder.

For each of these functions, the dielectric constant at the outer surface of the cylinder ($r = r_o$) is precisely unity, hence the impedance there is indeed matched to that of free space. To synthesize these variations in the program JMAN, however, we used a finite number of concentric cylinders of constant index of refraction, hence the actual variation was a sequence of steps, as suggested in Figure 10. If such a column were to be fabricated, it too would likely consist of a collection of concentric cylindrical shells whose densities vary from one shell to the next. Building such a cylinder would be difficult, but not impossible.

Furthermore, the electrical performance of such structures is not good at all, as illustrated by Figure 11. The RCS of a stepped cylinder is nearly two orders of magnitude higher than that of a uniform cylinder with a dielectric constant of 1.03. In comparing the performance of the stepped cylinder of Figure 11 with the uniform cylinder of figure 6, one must conclude that a stepped cylinder is useless. The reason why the cylinder has such a high return was not established, but it may be because of the cusp (discontinuity) in the dielectric constant at the center of the cylinder (see Figure 10).

Thin, Lossless Skins

The effect of thin, lossless coatings was investigated to assess their utility for protecting foam support columns against moisture and impregnation by the gypsum dust at RATSCAT. In any practical application of this idea a coating must be selected which does not attack or dissolve the styrene polymer from which the column is made, hence the actual dielectric constants of appropriate coatings should be used in detailed numerical predictions. For the purpose of this study a dielectric constant of 2.55 ·as chosen to represent

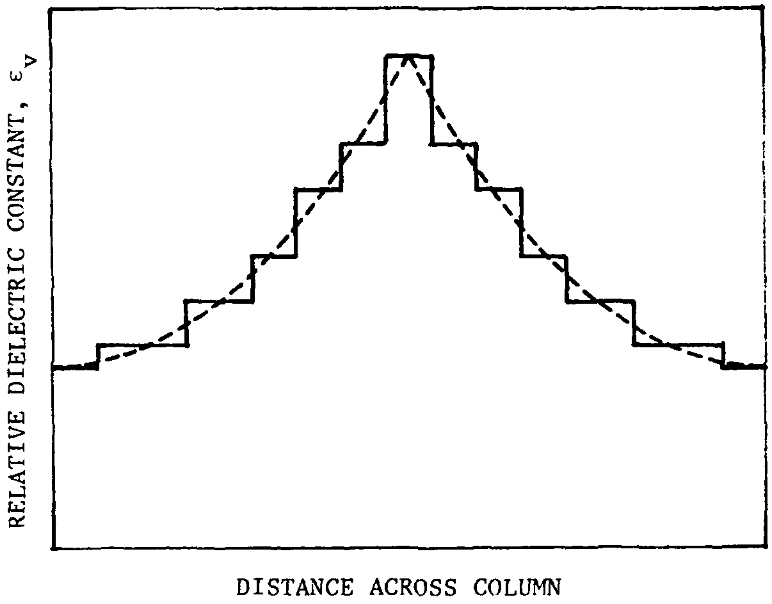

Figure 10. Stepped approximation of a smoothly varying index of refraction across the column diameter.

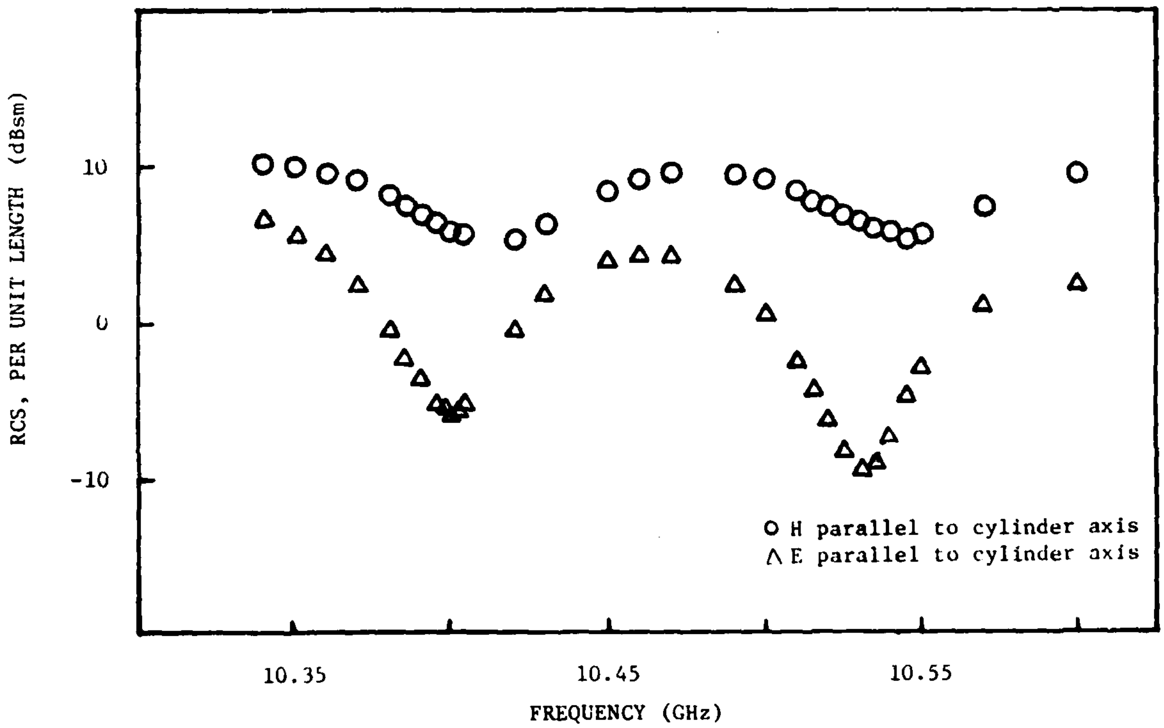

Figure 11. Data from the JMAN computer program for a 40-inch diameter cylindrical Luneburg lens.

the value of a thin surface glaze left by a hot wire.

The effect on the maximum RCS of a 40-inch diameter lossless column is shown in Figure 12. It is clear that a surface coating, no matter how thin, serves only to increase the maximum reflectivity of the column; this fact has been demonstrated at RATSCAT in assorted tests when the surface glaze left by a hot wire cutting operation was allowed to remain on the column. A standard finishing operation in the fabrication of columns at RATSCAT is to manually sand off the glaze, and Figure 12 verifies the usefulness of this finishing treatment. Thus, painting or glazing the column surface offers n RCS reduction in itself, even though it may make it easier to keep the co clean. On the other hand, the porous surface of a sanded column eventually traps gypsum and moisture, whose effects are likely to be similar to that of a surface glaze or coating. Hence, the advantage of lossless coatings is hard to assess.

Combinations of Internal Bulk Loss and Lossless Skins

Even though a lossless skin increases the maximum return from a lossless column, the skin can reduce the return of lossy cylinders slightly. This is illustrated in Figure 13, for which the real part of the dielectric constant was fixed at 1.03. The frequency coverage of this diagram is significantly greater than presented thus far. The computations were not carried out for the complete range in frequency, but the frequency intervals near the center of the diagram are spaced closely enough together to indicate the oscillatory nature of the returns.

One of the three cylinders had no surface skin (the data points are represented by squares) and was chosen as a reference. The imaginary part of its dielectric constant was -0.013, the value determined previously to yield the minimum value for the maxima in the interference pattern (see Figure 7). The RCS of this lossy column has a peak-to-peak oscillation of about 0.6 dB which is easily seen because of the expanded ordinate used in Figure 13 (the 0.6 dB oscillation is barely discernible in Figure 6 because of the compressed scale used there).

If a 2-mil lossless coating is now applied, the RCS increases by about 1 dB, and the peak-to-peak oscillation increases to about 1.2 dB. If the imagi-

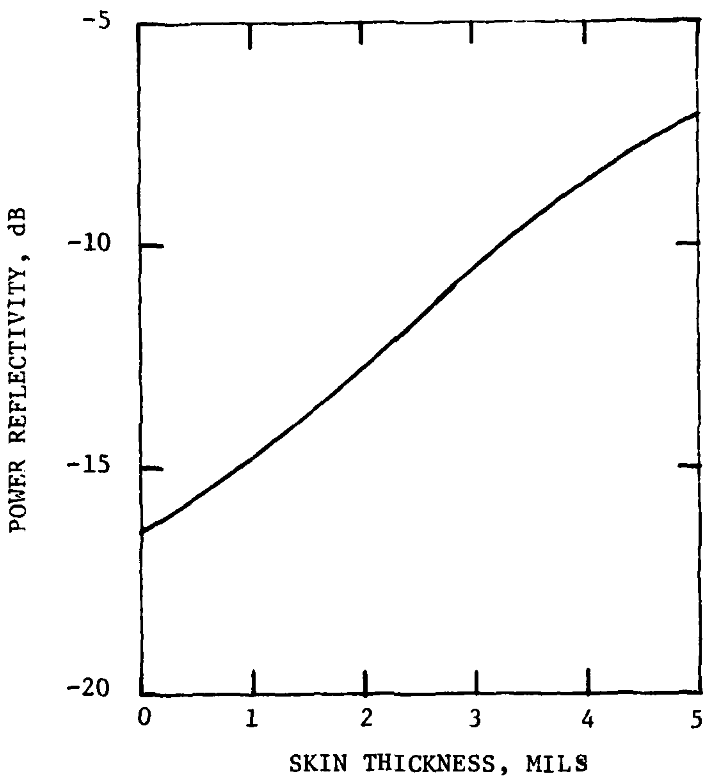

Figure 12. Maximum return of a painted lossless column 40 inches in diameter with a dielectric constant of 1.03 Frequency is near 10.4 GHz and the dielectric constant of the skin is 2.55

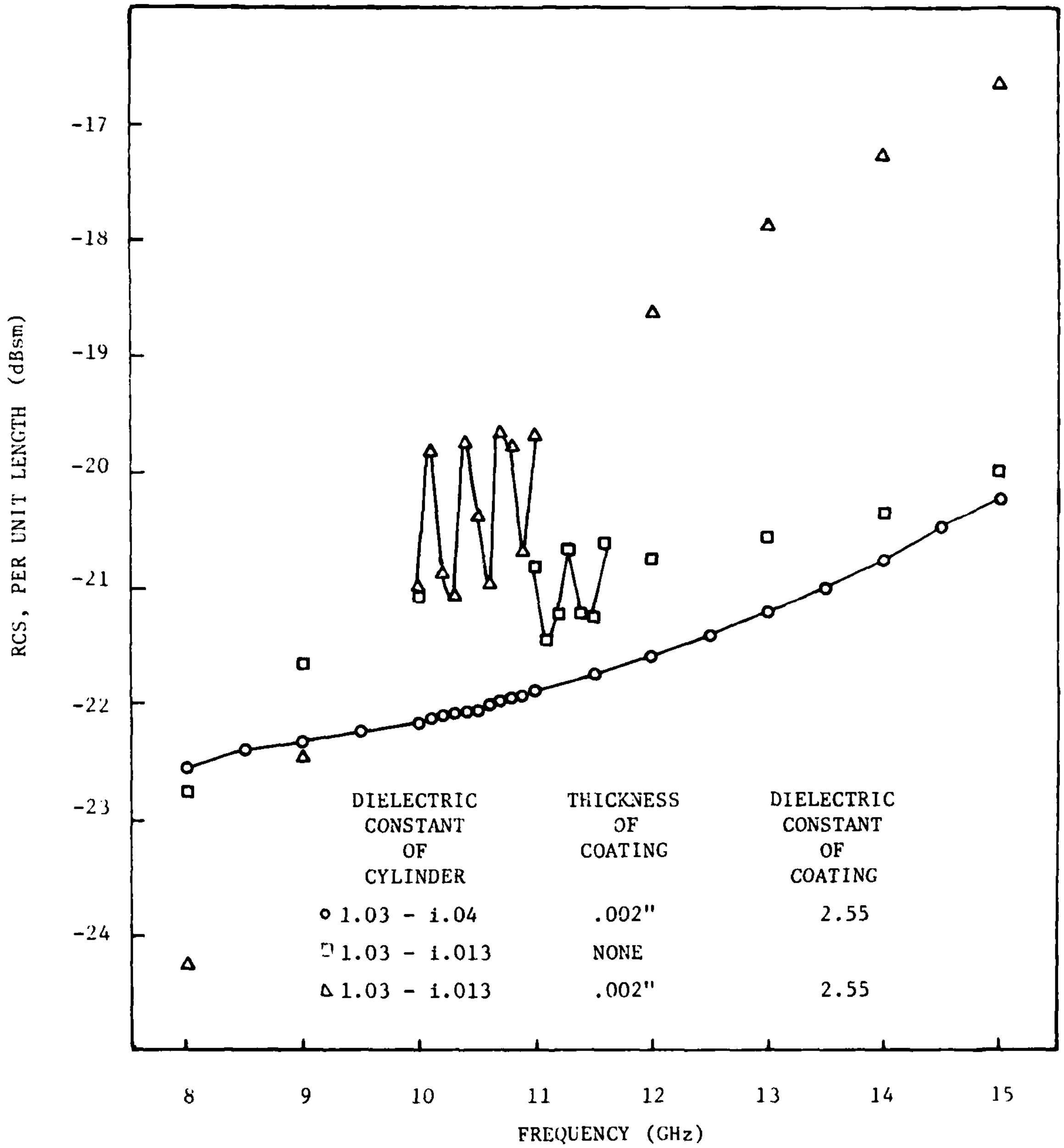

Figure 13. Data from the JMAN computer program for 40-inch diameter cylinders.

nary part of the dielectric constant is increased to -0.04, the maximum return drops about 2 dB. This was unexpected, although the likely cause immediately becomes apparent: the increased loss completely shields the rear surface, hence one of the two contributors to the RCS is removed due to the attenuation of the bulk of the column. Even so, the introduction of loss and the coating of the cylinder with a 2-mil lossless skin reduces the return by only 6 dB at X-band frequencies.

On the other hand, it is possible to achieve somewhat better than a 6 dB reduction by employing multilayer combinations of lossy and lossless skins. The computer program CONTRAST was used to investigate several combinations*, and the performance predictions in Figures 14 and 15 illustrate one particular combination. These data were predicted for frequencies from zero to 25 GHz, although it must be appreciated that the results for frequencies below about 1 GHz will be in error because the circular nature of the support column is not accommodated by CONTRAST.

Figure 14 shows a "baseline" prediction of a column similar to the best one (i.e., the lower most curve) used in Figure 13. For Figure 14, the imaginary part of the dielectric constant is -0.035, but for Figure 13 it was -0.040. Both columns had a 2-mil skin. If the column had not had a skin and if it had been lossless, its maximum reflectivity would have been about -36.6 dB. At 10 GHz, the column of Figure 14 has a reflectivity of about -42.5 dB, hence a modest reduction of 6 dB has been achieved, as noted above.

However, if we reduce the column diameter to 30 inches, reduce the skin thickness to 1.5 mils, increase the dielectric constant and introduce an outer "matching" layer just beneath the skin, the performance can be improved further, as shown in Figure 15. The reflectivity is now about -58 dB at 10 GHz, achieved primarily by the creation of a rather broad null at that frequency. At the -50 dB reflectivity level, this null has a width of about 1.5 GHz,

---

*Indeed, CONTRAST was developed as a design tool for evaluating multilayer radar absorbent materials. It is a user-interactive program that displays predicted performance graphically on one of Georgia Tech's plasma screens in real time.

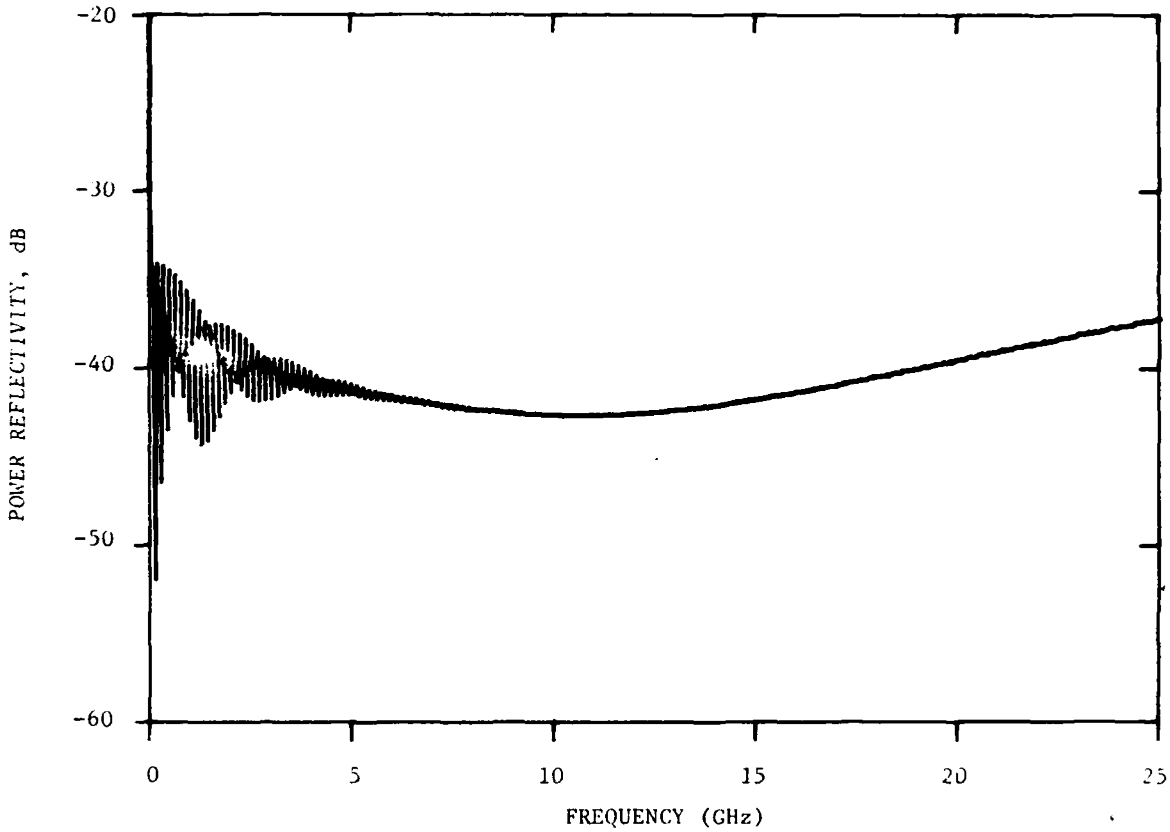

LAYER	THICKNESS	DIELECTRIC CONSTANT
1	.002"	2.550
2	40.000"	1.030 - i 0.035
3	.002"	2.550

Figure 14. Data from the CONTRAST computer program for a 40-inch thick, lossy, treated slab.

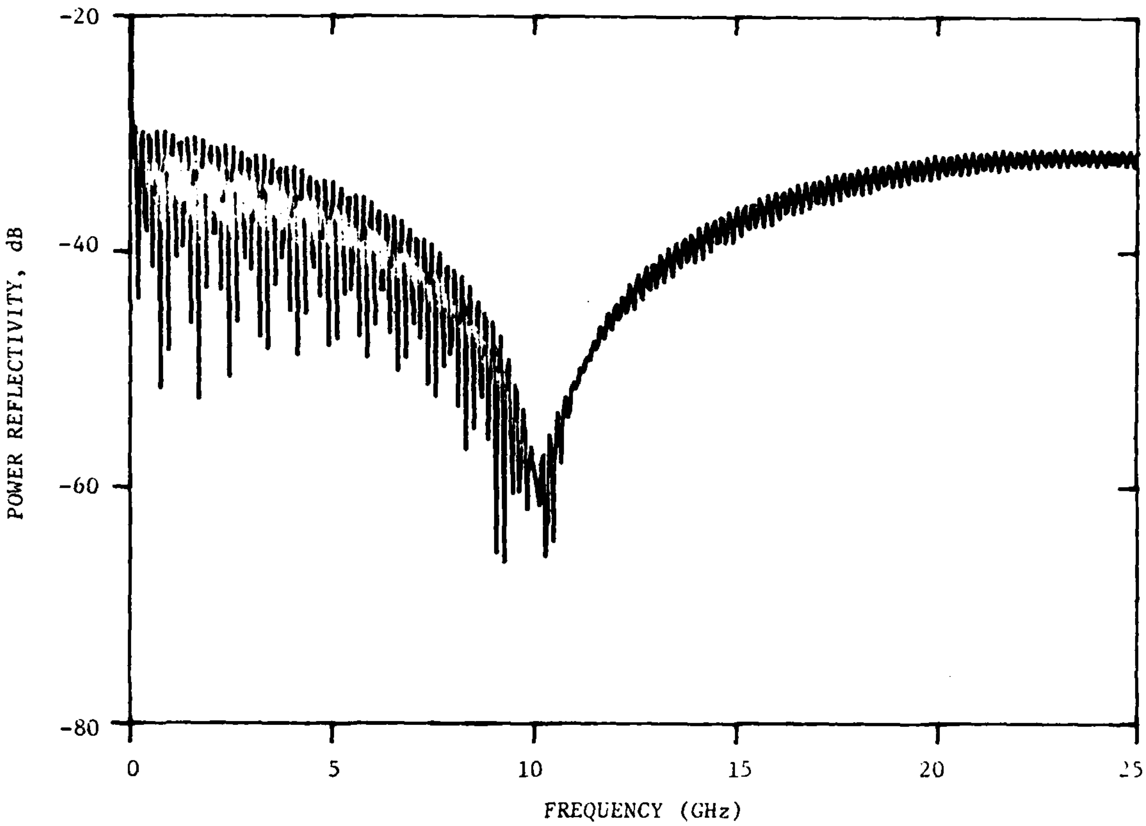

LAYER	THICKNESS	DIELECTRIC CONSTANT
1	0.0015"	2.550
2	0.210"	1.030
3	30.000"	1.070 - i 0.007
4	0.210"	1.030
5	0.0015"	2.550

Figure 15. Data from the CONTRAST computer program for a 30-inch thick, lossy, treated slab.

which is quite respectable in comparison to the width of the null (a few MHz) that would be achieved in tuning a lossless column. And the design of Figure 15 is an improvement of nearly 15 dB over an ordinary lossless column.

The design of Figure 15, however, includes several features that may not be within the capability of the state-of-the-art. It requires, for example, the following developments:

1. The ability to introduce and control a uniform loss within the bulk of a plastic foam,
2. The ability to construct a thin foam layer (0.210 inch in the example cited) surrounding the lossy foam column, and
3. The identification of a suitable coating that can be applied to the surface of the finished column.

These are not trivial, yet the improvement over a conventional column (reduction of scattered power by 15 dB over a 1.5 GHz bandwidth) is not trivial either.

Summary

The major conclusions derived from the study of column loading are summarized below:

1. The provision of a bulk loss mechanism can reduce the maximum column echo by as much as 6 dB, provided the real part of the dielectric constant remains unchanged.
2. Varying the index of refraction across the diameter of a lossless column does not reduce the column echo.
3. Painting a lossless column or otherwise providing an outer protective skin increases the column echo.
4. The combination of internal bulk loss, a concentric, lossless outer shell, and a thin outer skin can reduce the column echo as much as 15 dB over a 1.5 GHz band.

Whether the last technique can be implemented in a practical target support system at reasonable cost has not been determined. We note some very recent work at the Convair Division of General Dynamics (GD) in San Diego, California involves the fabrication of what GD engineers call "syntactic foams" [23].

---

23. Larry Carter, Convair Division, General Dynamics, San Diego, 16 June 1980 (personal communication).

Although these "foams" are vastly denser than the conventional foams used in target support columns, the method of controlling the loss may be applicable to this exotic design. The information was acquired too late to be evaluated in the signal background reduction study.

5. COLUMN SHAPING

Shaping and the application of absorbing materials are the two most useful techniques for reducing RCS. Ordinarily, the application of absorbers is effective if the added weight penalty can be tolerated, but the reduction of the RCS of foamed plastic support columns can hardly be considered ordinary. The surface reflectivity is already at a low level and, as shown in Chapter 4, the application of exterior coatings, whether they be lossy or lossless, degrades the column performance instead of improving it. Aside from the rather complex and esoteric design of Figure 15, there is no way to reduce the return from a column by adding or replacing materials.

The other alternative is to exploit column shaping, although it must be realized at the outset that shaping serves only to reduce the scattering attributable to the surface profile: the volume return analyzed by Plonus [2] will be present regardless of the surface profile and represents a floor to the attainable RCS. As pointed out in the RATSCAT capabilities brochure [1], RATSCAT already exploits the low RCS characteristics of fluted columns*. Two shapes reportedly studied at RATSCAT are the teardrop and the diamond, of which the diamond has the better performance. Another good shape is the ogival column which probably cannot be surpassed in its performance.

As is often the case in the use of shaping for RCS reduction, fluting a column improves its performance over certain aspect angle sectors at the expense of degrading it over other aspect angles. The degradation in performance must be accepted, although there are ways to overcome the degradation. One way is to take several patterns, each with the target repositioned on the fluted column to take advantage of the favorable column performance even if this covers a small range of aspect angles. A complete 360-degree pattern of the target may then be spliced together from the low background portions of the pattern set. Obviously, this is an expensive way to achieve low background patterns, but it <u>is</u> a solution.

Another form of column shaping is the use of circumferential grooves.

---

*A fluted column is one whose profile in a plane transverse to the column axis is not a circle.

The advantage of circumferential grooving is that the RCS of the column is nearly independent of the aspect angle and pattern splicing would not be necessary. The most obvious form of circumferential grooving is the vee groove design shown in Figure 16, and this design was in fact tested at Georgia Tech.

It was hoped that an analytic evaluation could be made of the vee groove design, in which the depth and taper of the grooves could be optimized. However, there are no convenient analytical tools available and, rather than develop one, Georgia Tech opted for an experimental evaluation of a single design.

Two columns were fabricated; one had the shape shown in Figure 16, and the other had a smooth shape of the same inner dimensions but lacking the grooves. Thus, the total volume of the grooved column was greater than that of the smooth one. Both had a taper of 8 degrees, a base diameter of 26 inches, and a height of 56 inches. Each was made of a collection of four 14-inch thick sections; the grooves were about 3.5 inches deep and spaced 3.5 inches apart, which is nearly 3 wavelengths at the frequency at which the measurements were made (9.65 GHz).

The columns were made from expandable bead foam obtained from a local vendor. The original billet was a block sized 17 x 48 x 192 inches and its density was very nearly 1 pound per cubic foot. According to Knott and Senior [3], its dielectric constant should have been about 1.0217, but this was not verified by measurement. As a matter of interest, the foam block was purchased at a price of $108.80. A photograph of the finished column is shown in Figure 17.

A special, electrically heated tool (shown in Figure 18) was made for cutting the grooves. This tool was made of hardened steel band bent in the shape of a vee. The ends of the band were clamped to a pair of aluminum brackets which were fastened to a bakelite board. Because of the low resistance of the tool, it required in excess of 100 amperes to get it sufficiently hot to melt the beaded foam. This heavy current was obtained by means of a step-down transformer connected to a 110 VAC bus. The entire fixture was mounted on a screw-driven carriage so that the tool could be forced to bite

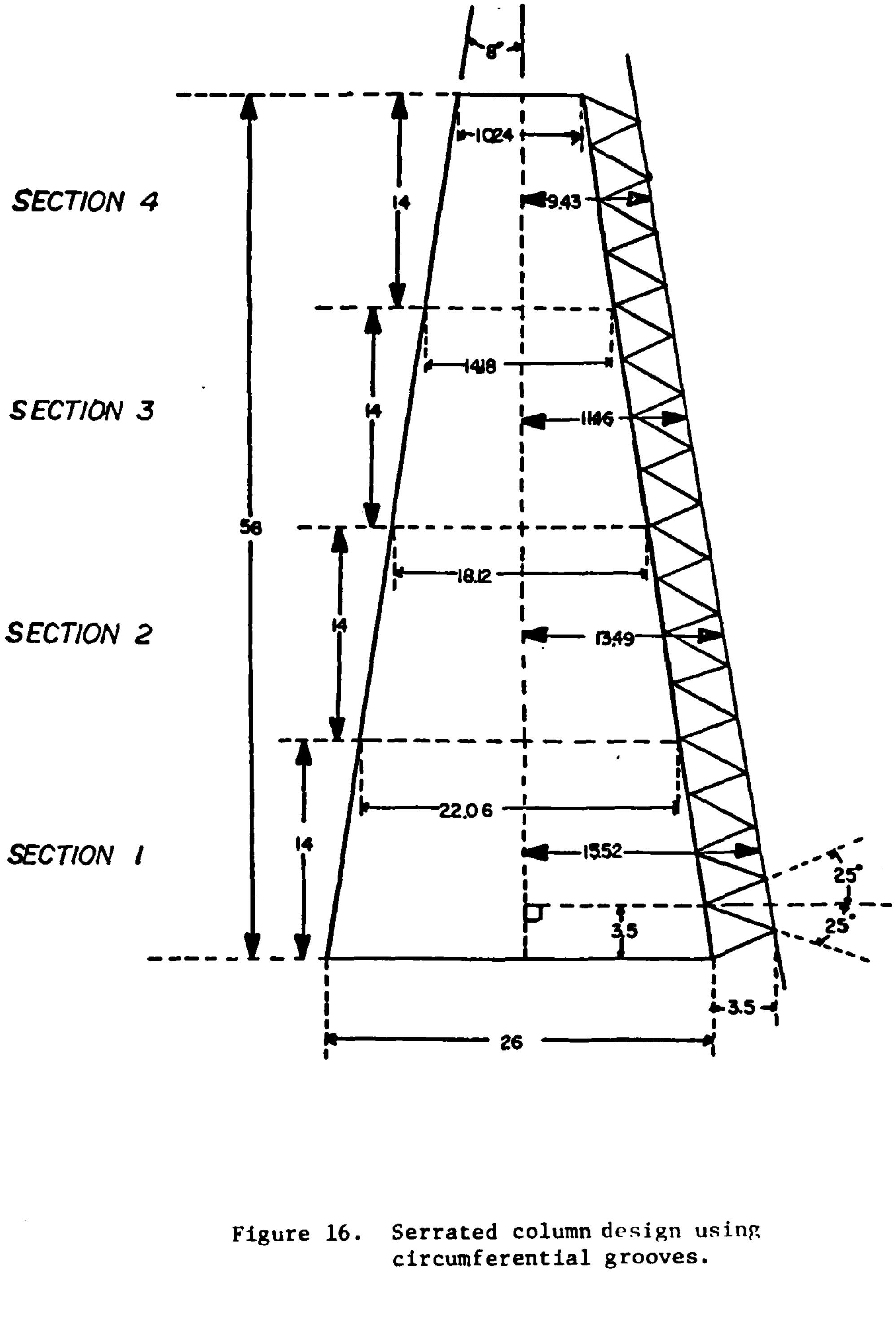

Figure 16. Serrated column design using circumferential grooves.

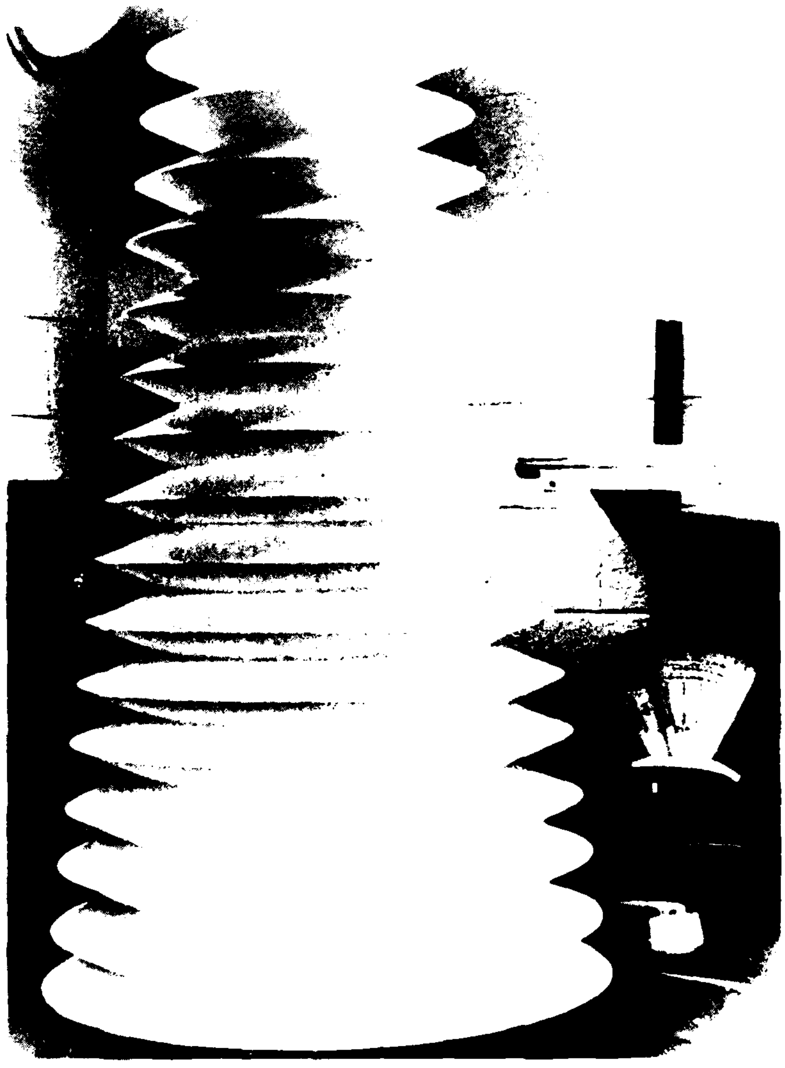

Figure 17. Serrated test column.

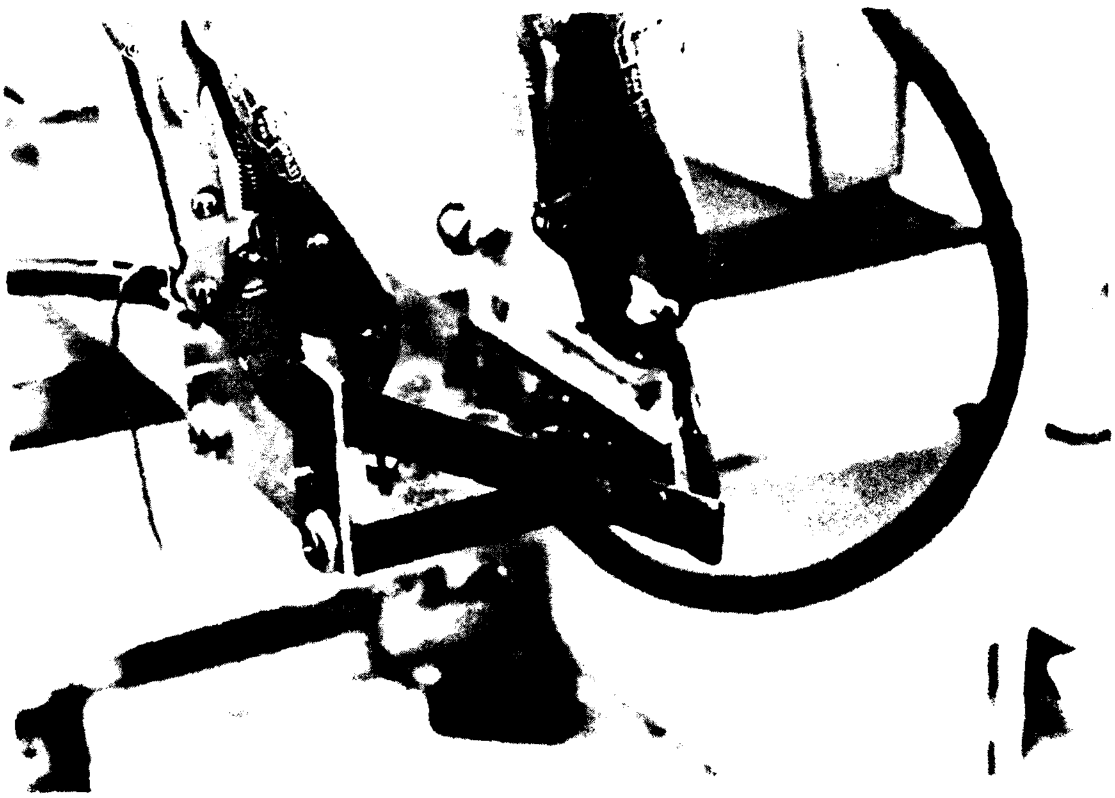

Figure 18. Vee-shaped cutting tool.

deeper into the foam work block as the block was manually rotated past the tool.

Figure 19 shows an overall view of the set-up, which was quite simple. The working block of foam was held between the two square face plates in the right center of the photo. The face plates were each fitted with five steel pegs. The shafts holding the face plates could be slipped back and forth between self-aligning bearings mounted on either side of a pair of aluminum box channels; the end of one of these channels is visible at the extreme left center of the photo.

The outboard end of the shaft on the left was fitted with a crank that was turned manually by one person while another performed the cutting operation. Fabrication of a column segment commenced with the cutting of a rectangular block of foam to the appropriate size with a conventional hot wire. Care was taken to insure that the top and bottom faces of the block were parallel. The parallel faces were then installed and locked up between the face plates of the lathe fixture, and the block was turned down to a truncated cone, again with a hot wire.

The tool of Figure 18 was then carefully positioned for cutting the first groove. One operator gently forced the tool into the side of the cone while a second operator slowly turned the cone. This was continued until the groove was carved out to the specified depth. The process was repeated until all the grooves had been carved out. The final operation was to sand off the surfaces, as shown in Figure 20.

The machining process produced four sections which were each trimmed to a thickness of 14 inches. A narrow hole was pierced through the center of each section with a heated length of 1/8-inch diameter rod, and the four sections were strung together like beads on a necklace with a piece of braided dacron line 1/16 inch in diameter. Thin plastic cards were threaded onto the line at the top and bottom of the column and the line was then knotted to keep the segments together. This was done for both columns (smooth and serrated), and the plastic cards prevented the knotted string from being pulled back through the finished column. This method of assembly was chosen as a way to hold the sections together without any bond mechanism between the faces of adjoining

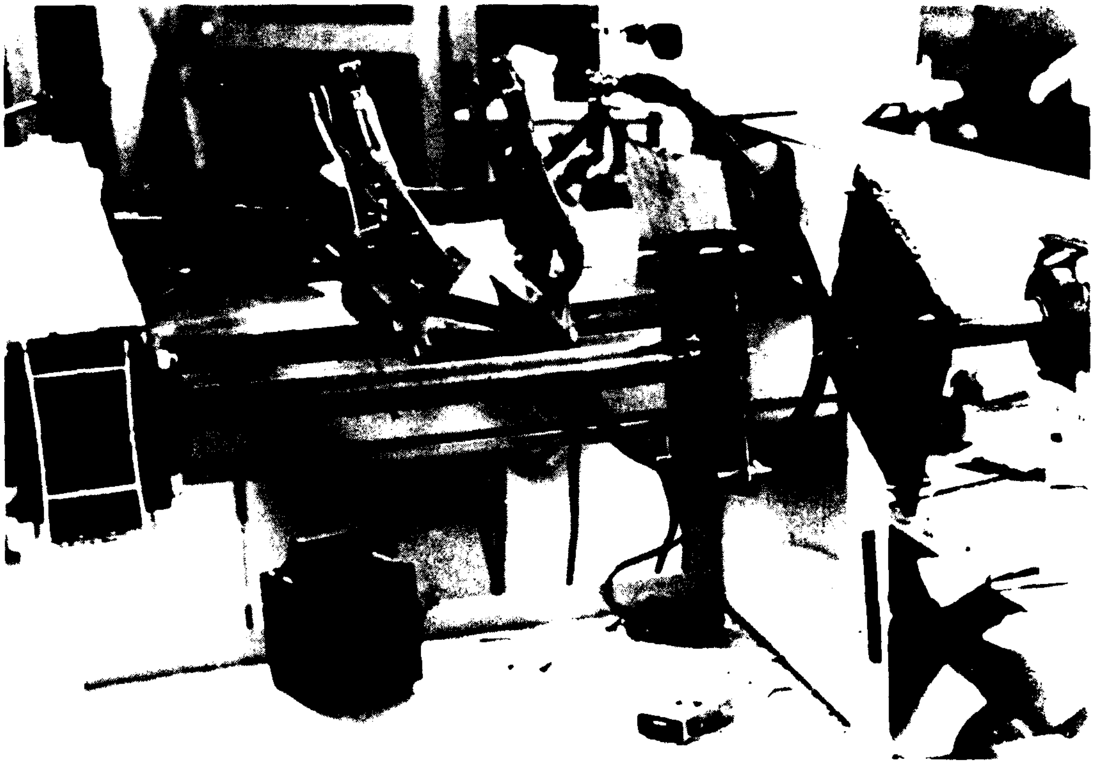

Figure 19. Lathe set-up for turning the foam blocks.

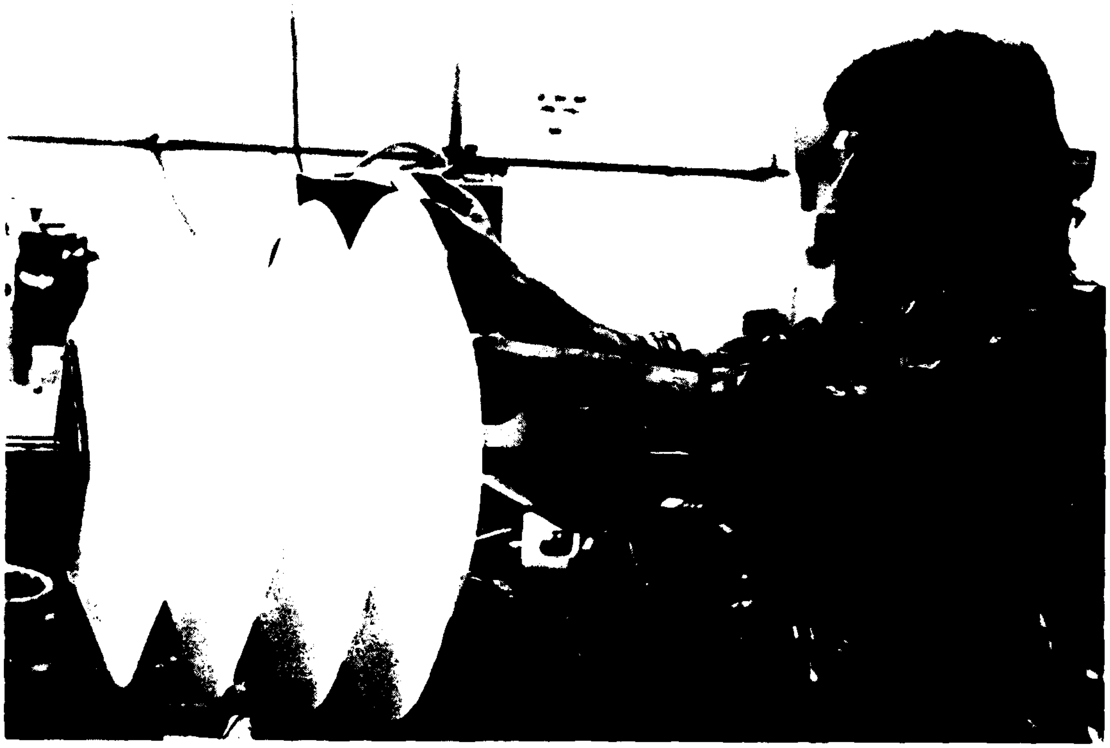

Figure 20. Final sanding operation.

sections, since tests were desired with and without glue joints. We had planned to later glue the sections together and to repeat the measurements after the columns had been measured in the unbonded condition, but this was never done.

The radar used to measure the test columns was a Georgia Tech radar designated HSS-1. The radar, whose parameters are listed in Table 3, has a selectable pulse width and PRF, and the shortest available pulse (30 ns) was used. This was necessary because the test columns were supported from a line run between a pair of 30-foot poles, and the returns from the poles could not be gated out with the longer pulse widths.

TABLE 3. HSS-1 X-BAND RADAR PARAMETERS

Power Output	15 kW
Pulse Width	30 ns
Radio Frequency	9.65 GHz
Antenna Gain	40 dB
Minimum Recovery Distance	<300 feet
Dynamic Range	70 dB
Noise Floor	-87 dBm
Noise Figure at Receiver Input	<11 dB
IF Bandwidth	35 MHz

The support poles were made from 10-foot lengths of 4-inch plastic pipe marketed commercially as drain lines. Each pole was mounted on a wooden pad staked to the ground and was guyed by lines fastened at the top and midpoint of each pole. Each pole was made of three lengths of pipe, hence they were 30 feet tall. They were far from rigid and often took on a curved shape due to non-uniform guyline tension, but they easily supported the light test columns.

The poles were erected approximately 330 feet from the radar on a grassy field at the Georgia Tech Cobb County research complex. A plan view of the site is shown in Figure 21. The poles were about 50 feet apart, and the support line between them was angled approximately 45 degrees to the radar

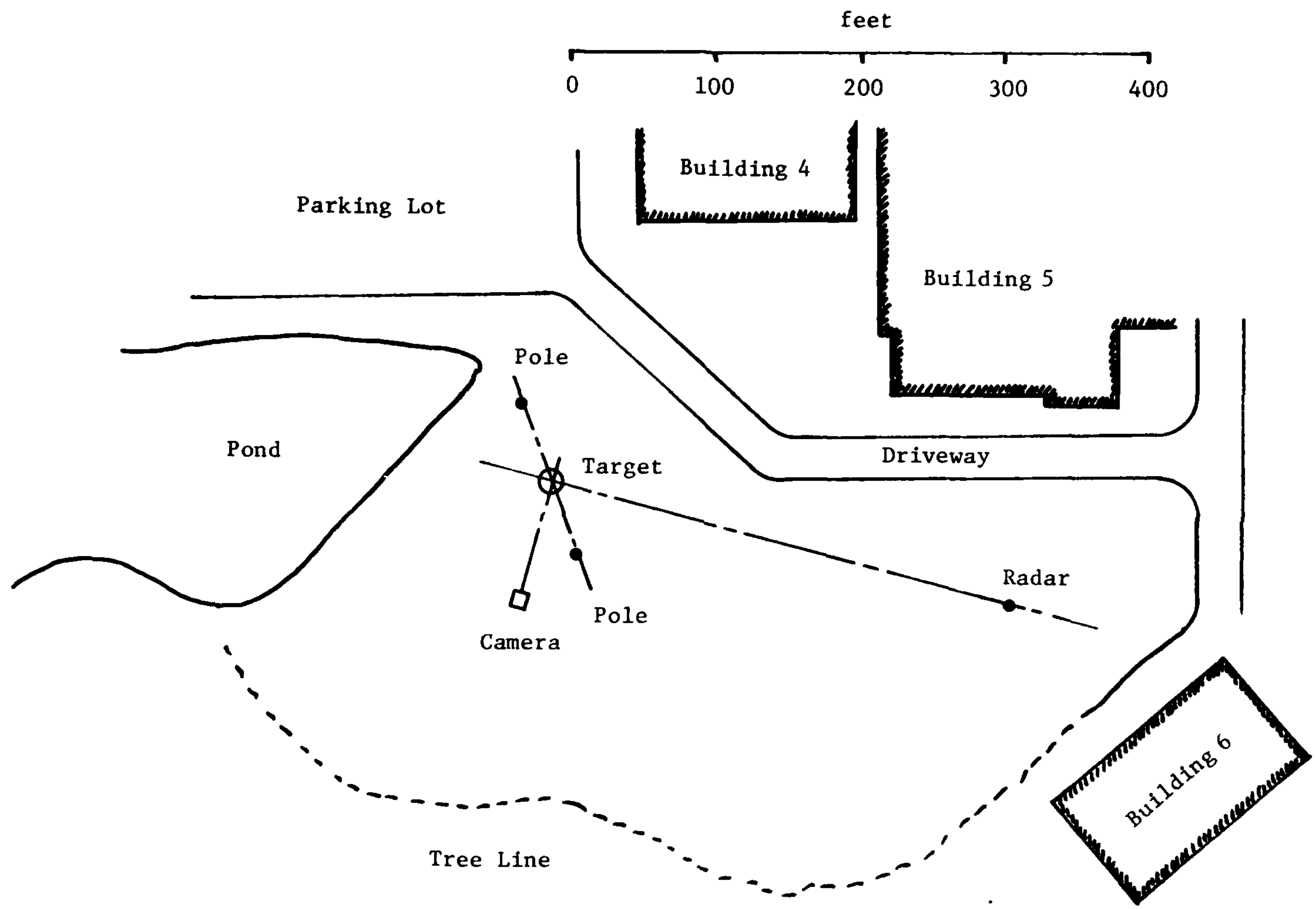

Figure 21. Measurement site.

line of sight. The purpose of this geometry was to place one pole inside the range gate and the other one outside the range gate to minimize their influence on the measured returns. As shown in Table 4, the 56-inch columns were not quite in the far field, but the range was thought to be adequate. Table 4 also shows that the poles were well outside the main lobe of the transmitting antenn~ Figure 22 is a photograph of the target scene as viewed from near the radar.

TABLE 4. MEASUREMENT PARAMETERS

Parameter	Value
Range	330 feet
$2D^2/\lambda$	430 feet
Width of mainbeam at 330 feet	9 feet
Distance between first nulls at 300 feet	19 feet

The test columns were suspended by a single line dropped from the support line running between the poles, as shown in Figures 23 through 25. In Figure 24, the smooth test column is suspended and the serrated column is on the ground in the right foreground. The columns were suspended with their axes in a vertical plane, and the aspect angle variation was obtained by pulling the bottom of the column toward or away from the radar by an attached string. The amplitude of the return signal was recorded on magnetic tape and on a strip chart, and the column was then set at a different angle by staking the bottom string at a new distance.

Continuous variations in aspect angle were not obtained, and conventional RCS patterns of the test columns were not made for several reasons. The multiplicity of strings and lines required for a harness and support sling would have contributed more signal than the test column itself. Wind buffeting the light test objects would perturb the true aspect angle so that a continuous pattern would have the appearance of noise. Consequently, the measured data are collections of discrete points versus aspect angle instead

Figure 22. Photo of target scene as viewed from near the radar.

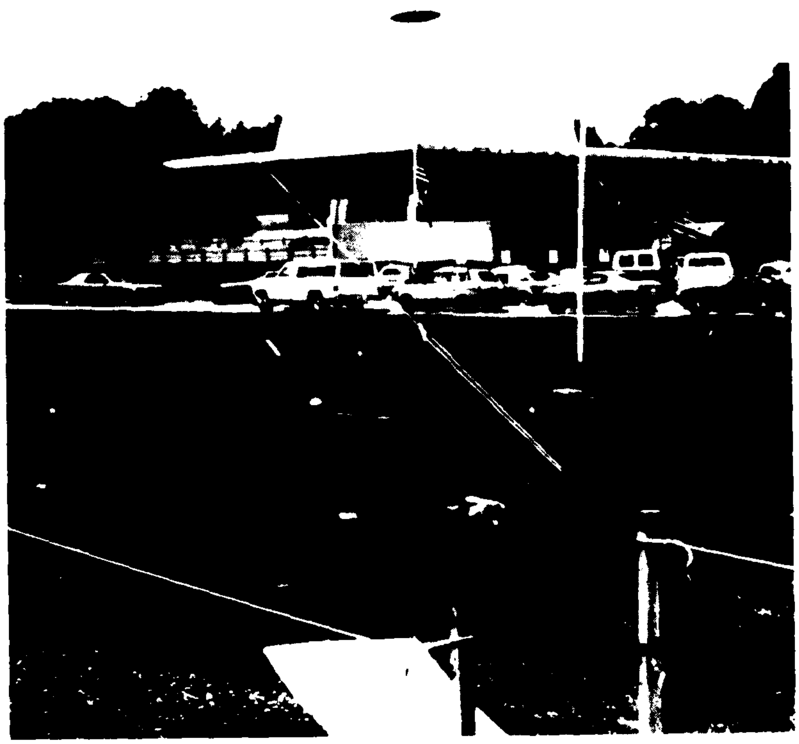

Figure 23. Closer view of target suspension.

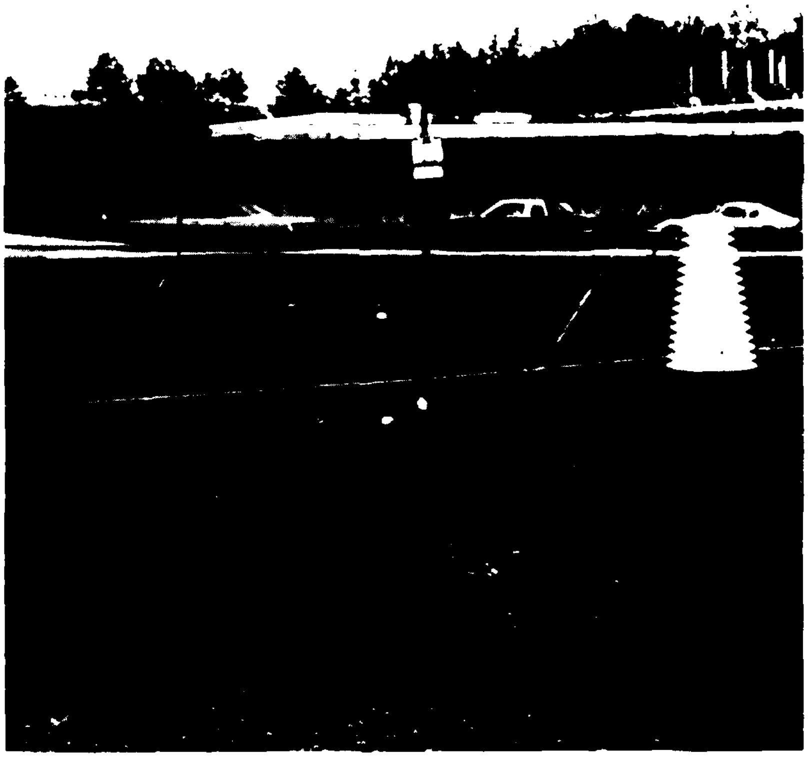

Figure 24. Smooth test column in place and serrated column on the ground.

Figure 25. Closer view of serrated column in the air.

of continuous patterns. Because of the suspension technique and the way the column was positioned, aspect angle variations were obtained in the vertical plane as opposed to the horizontal plane in conventional measurements.

The test column aspect angle was measured photographically. A 35 mm camera was stationed 60 feet off the radar line of sight, as shown in Figure 21, and trained on the target at an elevation angle of about 12.2 degrees, as shown in Figure 26a. A vertical reference pole was erected between the camera and the target. A photograph was snapped for each position of the test column. One such photograph is shown in Figure 27. Each negative was numbered and keyed to the measured video output of the radar receiver.

The developed negatives were mounted in slide frames and loaded in a projector aimed at a wall in a darkened office. A piece of paper was taped to the wall and a pair of straight lines were drawn on the paper along the image of the pole and along the rear side of the test column image. The lines were later extended until they intersected, or lines parallel to them were drawn so that the angle of intersection could be determined. This was the apparent aspect angle as seen by the camera.

The apparent aspect angle was not, however, the aspect angle presented to the radar, and the apparent angle must be corrected. Three corrections are necessary:

1. Correction for the look-up angle of the camera;
2. Correction for the column taper (a constant 8 degrees to be subtracted, since the line was drawn along the rear side of the column):
3. Correction for the radar look-up angle (a constant 2.36 degrees to be subtracted).

The camera angle correction is computed as follows: the actual angle τ subtended by the rear side of the column and the vertical is related to the apparent angle τ' as seen by the camera by the relationship

$$\tau = \arctan(\cos\beta \tan\tau')$$

where β is the camera look-up angle (i.e., 12.2 degrees).

Figure 28 is a simplified diagram of the instrumentation used in the

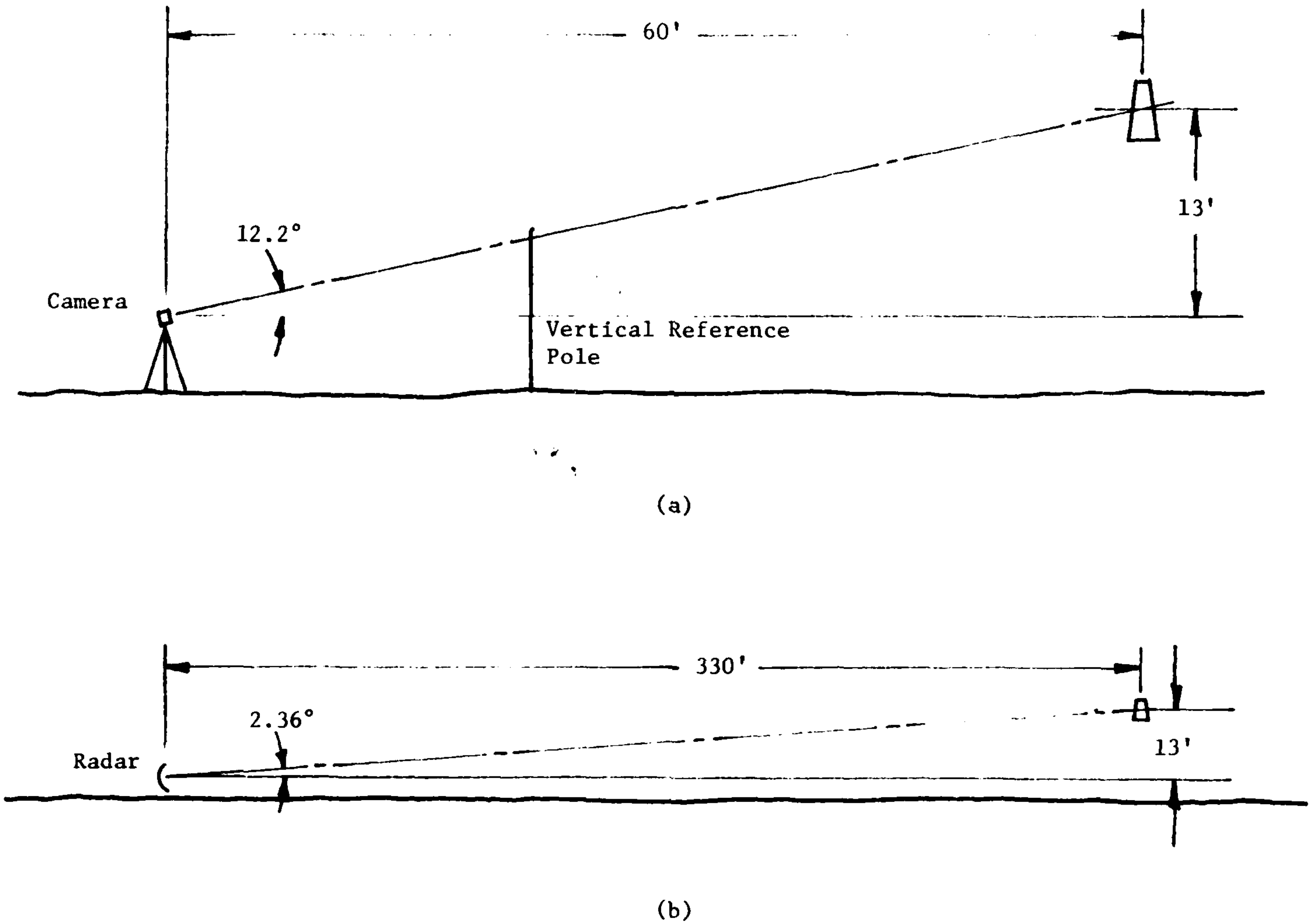

Figure 26. (a) Camera-target geometry; (b) radar-target geometry. (Not to scale.)

Figure 27. Angle measurement photo. Aspect angle was determined by comparison of target attitude with vertical reference pole in foreground.

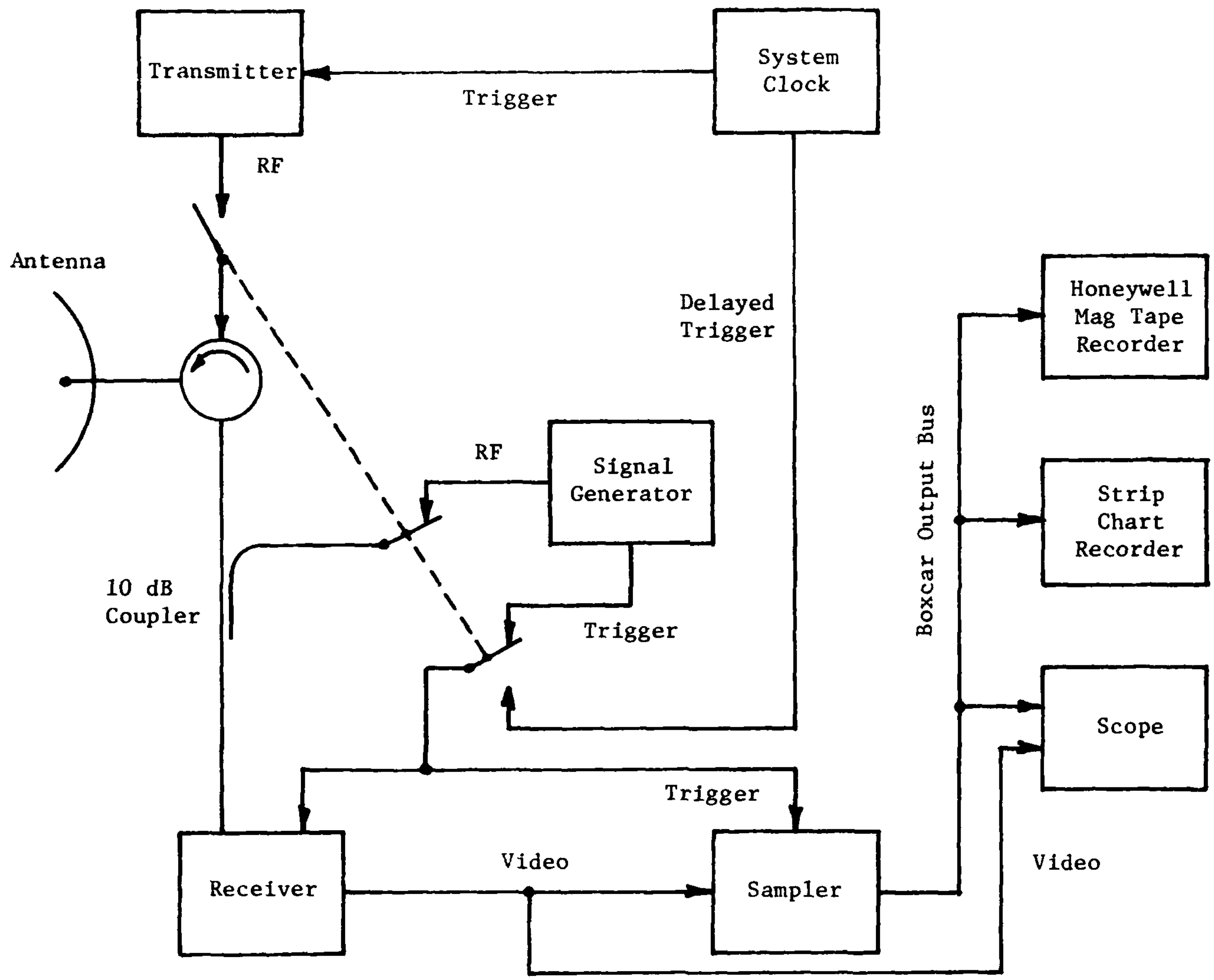

Figure 28. System instrumentation shown here in the calibration mode.

measurements. A calibrated signal generator was used to calibrate receiver linearity before a measurement run, and a sphere was used as an absolute calibration of the received signals. The measurement procedure was as follows.

1. The equipment was turned on and allowed to warm up for at least 5 minutes.

2. With the transmitter shut down, the signal generator was zeroed and calibrated with its internal standard according to the manufacturer's procedure in the CW mode. It was then switched to the internal pulse modulation mode and the trigger output was connected to the radar receiver and the sampler.

3. The signal generator output attenuator was decremented in 5 -dB steps while the chart recorder ran and was held at each step for 3 or 4 seconds, producing a stair-step trace on the strip chart. The signal output was typically varied from -10 dBm to -60 dBm. The signal generator output trigger timing was adjusted for maximum video output for this calibration.

4. While the radar receiver was being calibrated, range crews hoisted the test column onto the support line between the 30-foot poles. Three stakes, previously driven into the ground under the target and 25 feet in front and behind, provided the anchors for the string running out of the bottom of the test columns. The string had four loops in it and the combination allowed the column to be staked at 9 different positions. (Not all combinations of string loops and stake positions were used.)

5. The test column was fixed at its maximum tilt either toward or away from the radar for the first measurement of a 9-measurement sequence. In the meantime, receiver linearity calibration had been completed and the system was cabled up in its measurement configuration. The transmitter was turned on.

6. The range gate delay was adjusted for maximum video output, the video was recorded for approximately 30 seconds, and a picture was taken of the test column attitude.

7. The column was moved to the next position, another recording was made, and a picture taken of the column. This was repeated until the column had been moved through all 9 positions.

8. After two or three sequences of 9-position runs, the column was lowered and a 6-inch diameter sphere was hoisted into position. The video level was recorded, but no pictures

were taken.

9. The measurements were repeated using a different polarization, and measurements were repeated from one day to the next, as well as one week to the next, in the hope of operating under calmer conditions.

Unfortunately, extremely calm conditions were required to obtain a steadv signal from the test columns, but occasionally a peak-to-peak signal variation as low as 3 dB was observed. Most of the time, the signals varied by 10 to 15 dB because of the wind-blown target motion. Examples of the signal variation are shown in Figure 29. The target swayed slowly even under very calm conditions (upper trace), and the aspect angle varied from the peak of a sidelobe, through an adjacent null and part of the way up the next sidelobe. Under slightly more turbulent conditions, which were far more common, the variations were much more rapid (lower trace) and more erratic. Numerical values were extracted from such data by using a straightedge to draw a visual mean through the pattern. Depending on the individual trace, this mean was from 3 to 5 dB below the peak values, although the mean for some very quiet traces was nearly at the level of the peaks. Thus, the data presented in Figures 30 through 33 are averaged data, but it is difficult to establish the aspect angle window over which the data were averaged.

Figures 30 and 31 are summaries of the measurements of the serrated column taken for vertical polarization. A total of four test runs are included in each figure. There does not seem to be any distinct pattern, and the lack of any regularity in the data is probably due to random target motion. Figure 32 contains three data runs for horizontal polarization; fewer data were measured for horizontal than for vertical polarization because of the interfering effect of the long horizontal support line running between the tops of the 30-foot poles. This may be the reason for the high cross sections on the right side of the figure.

Figure 33 contains two measurement runs (one for each polarization) of the smooth test column. Only two runs are available for this target, and although the RCS values seem a little higher than those for the serrated column, no definite conclusions can be drawn.

The lack of data in the center of the diagrams in Figures 31 through 33

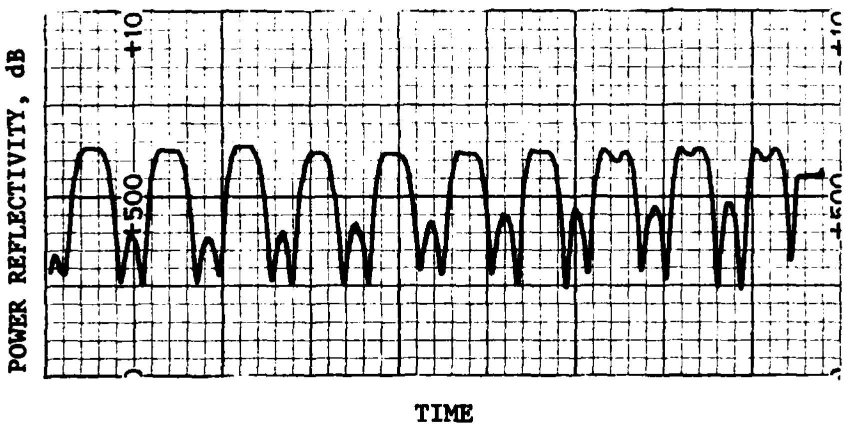

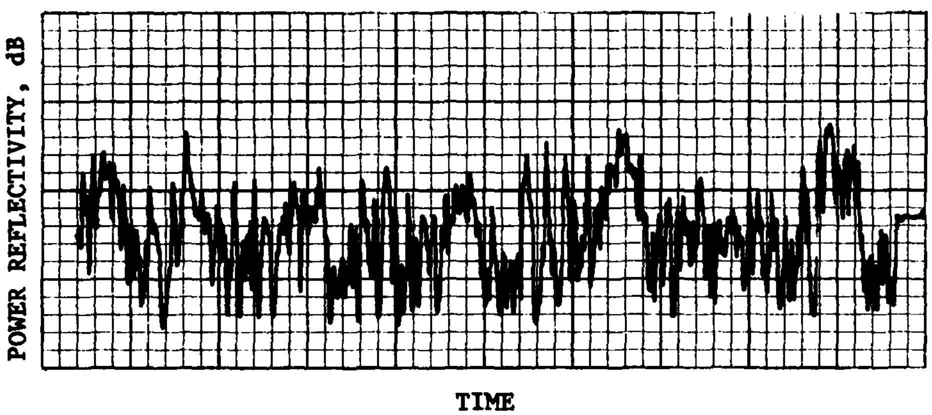

Figure 29. Examples of data recorded on a very calm day (top) and a moderately calm day (bottom). Vertical scale: approximately 1.5 dB per division.

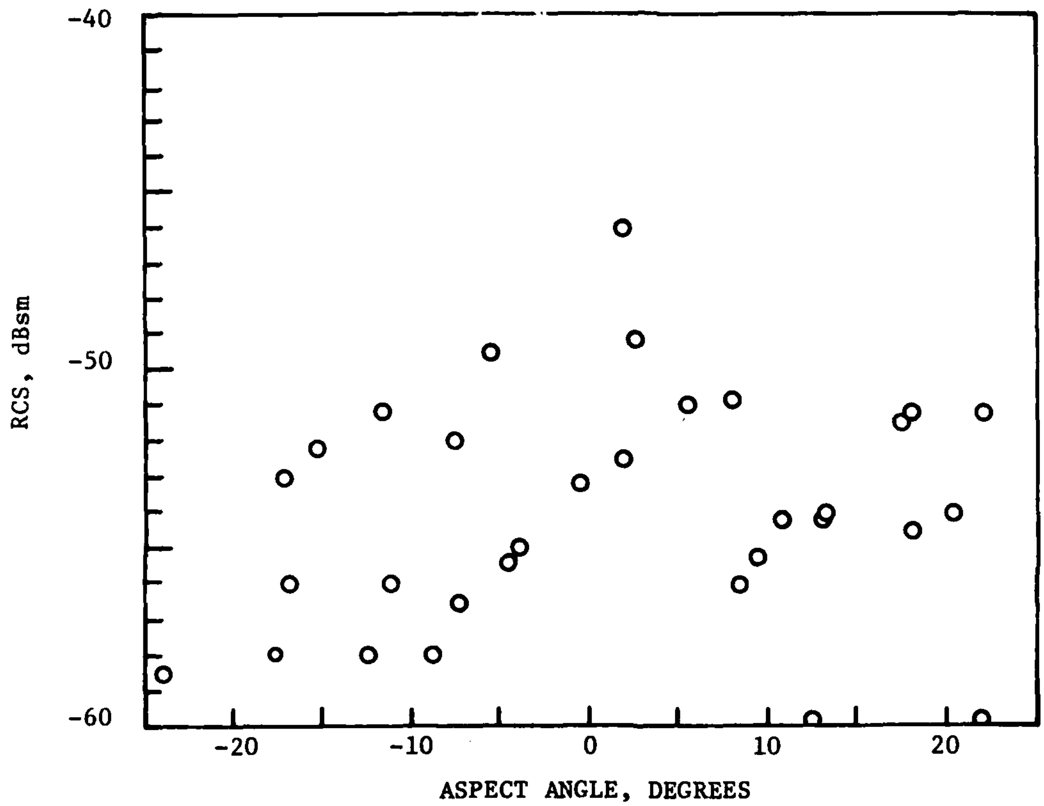

Figure 30. Serrated column RCS; first four runs for vertical polarization.

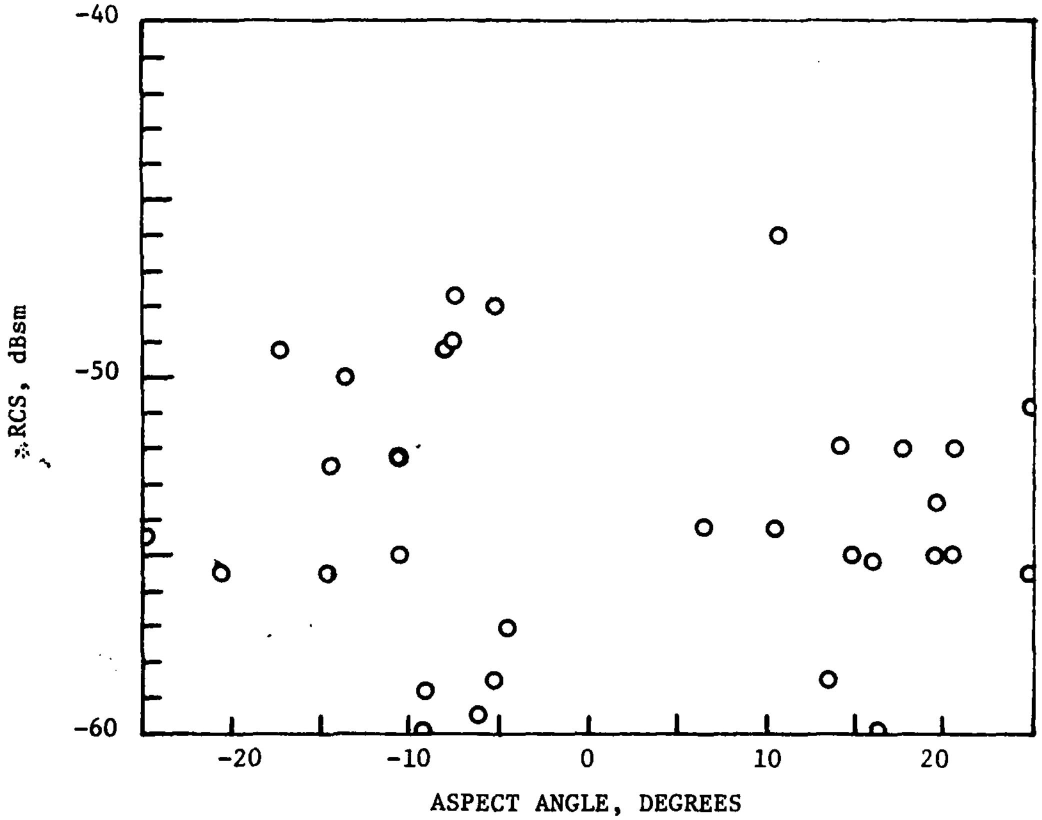

Figure 31. Serrated column RCS; second four runs for vertical polarization.

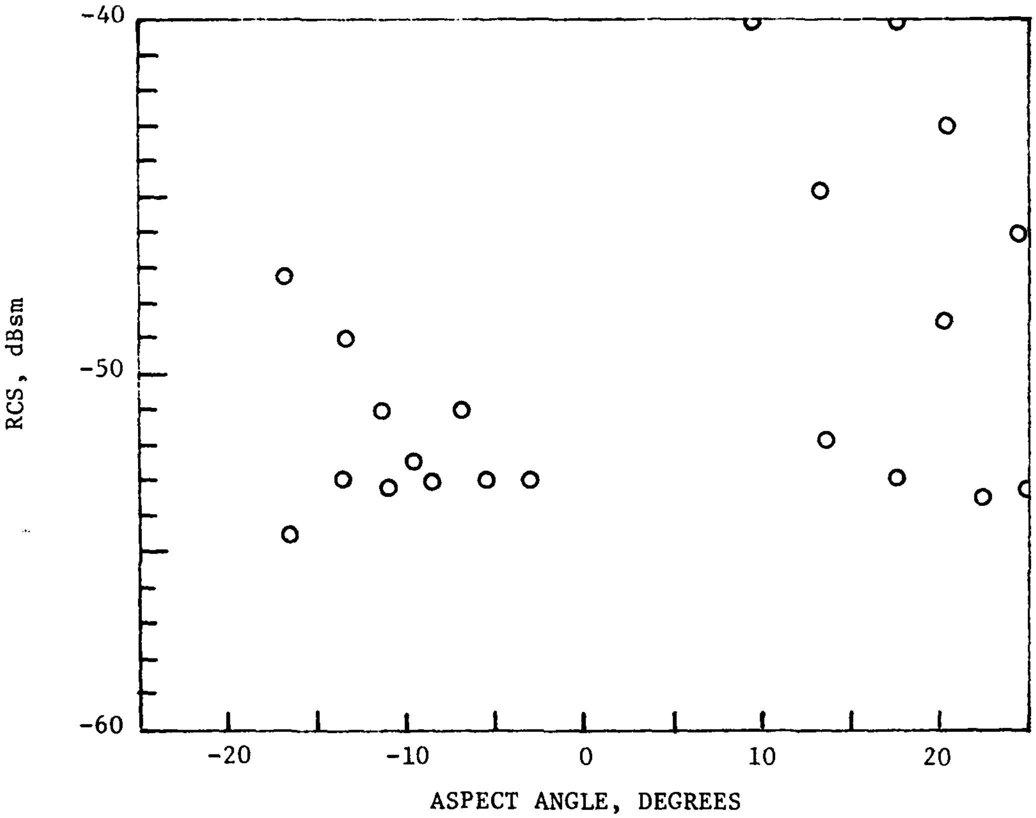

Figure 32. Serrated column RCS; three runs for horizontal polarization.

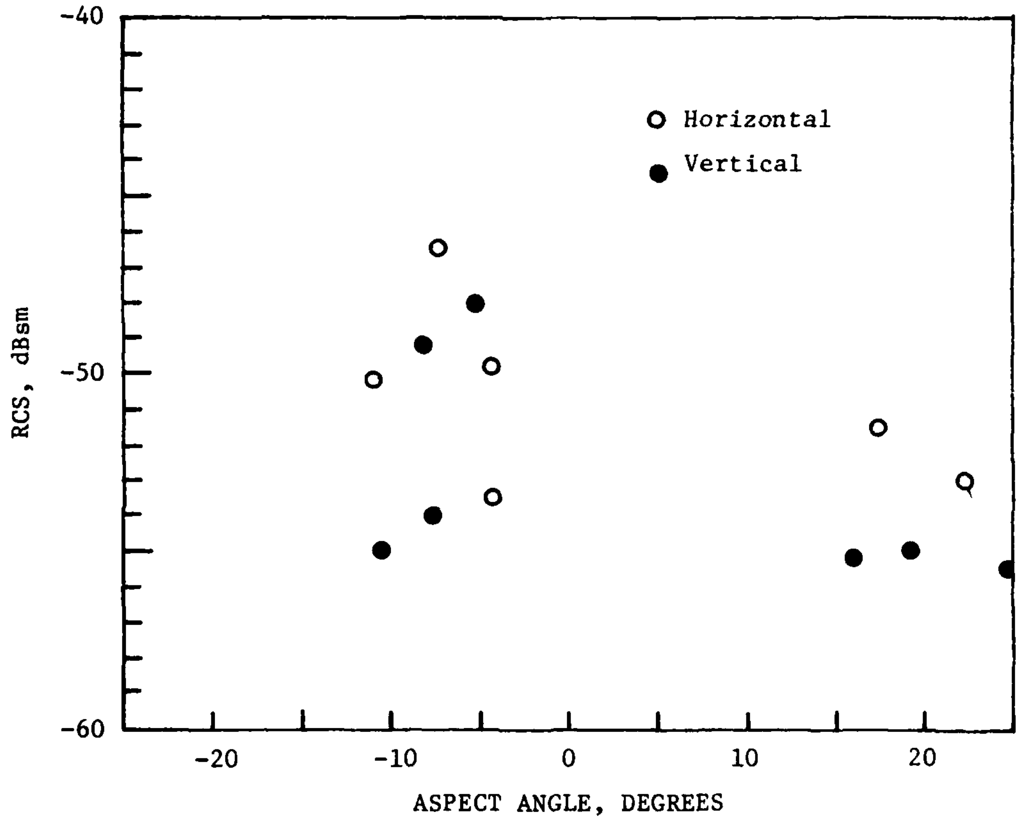

Figure 33. Smooth column RCS (both polarizations).

is due to the loss of a stake when the grass under the target was cut. The other two stakes were inadvertently moved after the grass was mowed, shifting the target aspect angles to the right.

We had planned to bond the segments of both columns together after these initial tests and repeat the tests so that the effects of bonding could be assessed. However, calm weather continued to elude the experimenters and in time the contract ran out. Therefore, no assessment was made of bond lines between column segments.

The volume of the smooth column is 8.9 cubic feet and that of the serrated column about 11 cubic feet. Using the value of -58 dBsm per cubic foot from the Michigan studies [3], the incoherent return from the test columns would be of the order of -48 dBsm. Most of the data in Figures 30 through 33 lie somewhat below this level and at least in a gross sense, the numerical values seem reasonable. The tests were inconclusive as regards the goal of assessing the effectiveness of circumferential grooves; the experiment was too coarse to establish that effectiveness.

6. LOW FREQUENCY BACKGROUND SIGNALS

A. THE SYMPTOMS

RATSCAT is faced from time to time with the requirement to measure RCS at frequencies below 500 MHz, and range personnel have experienced difficulty in conducting the measurements. The problems apparently stem from two distinct sources: deficiencies in instrumentation and vagaries in the ground plane performance. The precise identification of measurement problems is elusive, however, and one gets different viewpoints depending on who one talks to at the site. As far as can be determined, there is no documentation describing the symptoms of the measurement problems. Moreover, there seems to have been no systematic approach to isolating and correcting the problems. When faced with a measurement requirement below 500 MHz, range personnel attempt to optimize instrumentation performance as best they can within the time allotted, but eventually the data must be collected. They do not always have the luxury of more time to devise a satisfactory improvement in instrumentation performance.

One of the symptoms, as described by range personnel, is a peculiar "ringing" of the system. No oscilloscope photographs are available to document the effect, but Figure 34 is a replica of a sketch of the receiver video made by one of the RATSCAT range operators in 1979. Instead of dropping back to zero shortly after main bang, the received signal decays slowly enough that there is still some residual return in the vicinity of the target, shown in Figure 34 to be about 750 feet away in range. The residual signal has a small effect if the target return is large enough, but quite often the target return is not much above the background signal and at times may even be less.

Another symptom of low frequency operation is an apparent reflection from the pit, even in the absence of a support column or test target. For frequencies less than 500 MHz, the RATSCAT 60-foot dish is used as the transmitting and receiving antenna, although there are some exceptions. Pit 5b, 780 feet to the south, and Pit 6, 830 feet to the west, are the available target locations, but Pit 5b seems to be used more than Pit 6.

Range operators have reported that a small rotator placed on the ground at a similar range well away from the pit gives a much smaller residual return than one of the pits. This fact leads one to consider the possibility of a propagating ground wave being reflected by the discontinuity in the ground due to the pits. This will be discussed in a moment.

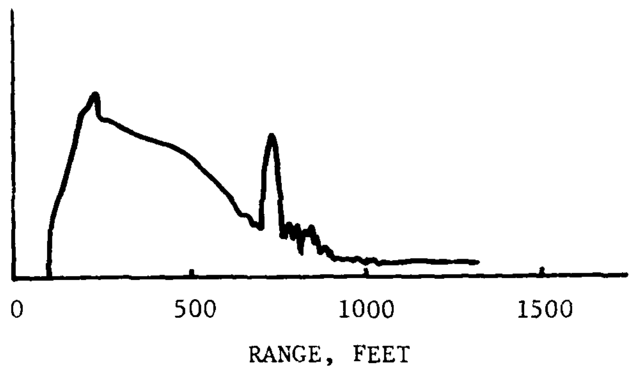

Figure 34. Sketch of video pulse.

B. POSSIBLE IMPROVEMENTS IN INSTRUMENTATION

Range personnel have ascribed the ringing phenomenon of Figure 34 to a combination of factors, but no systematic tests seem to have been performed to isolate them. The RATSCAT mode of operation discourages time-consuming diagnostic work because of tight schedules, and this is one of the causes of persistent problems at the site, at high frequencies as well as low.

The use of a single antenna to transmit and receive requires a duplexer to isolate the transmitter from the receiver. This mode of operation is different from all other frequency bands, for which separate transmitting and receiving dishes are used. The directivity of these higher frequency antennas is high enough that adequate isolation can be achieved without the need for duplexers, hence, range operators are less familiar with low frequency instrumentation and techniques than they are with higher frequency equipment. Indeed, most RATSCAT personnel cite one or two people as being ... "low frequency experts," and these experts are automatically expected to ...ate in all low frequency test programs.

A suspected reason for the ringing is the long cable runs between the instrumentation and the antenna feed of the 60-foot dish. Range operators say that the line length can be as much as 100 feet, and they suspect that a poor VSWR at one or more of the duplexer ports can reflect energy back and forth along the line, thereby leaking signals into the receiver line even after the duplexer has isolated the receiver. However, no one seems to have ever tested this conjecture; a simple test is to replace the antenna feed with a well-matched load. Such a test would help isolate another possible reason.

It has been reported that a circulator has improved the transmitter/receiver isolation, but it is not known if this improvement has been achieved uniformly across the VHF/UHF bands. Other techniques to eliminate background signals include a cancellation scheme, in which a sample of the transmitted signal is attenuated and delayed in time and then combined with the received signal (in the absence of a target) in a "bucking" mode. Range personnel report that this procedure has been only partly successful.

The background problem has been alleged to be worse for circular polarization than for linear, suggesting interactions between the feed dipoles. In addition, no systematic checks have been made of the input impedance of the feed as a function of frequency. Such checks need to be made to secure the best possible operating conditions.

Range operators have suggested that the long cable runs be eliminated by placing the transmitter and receiver closer to the antenna feed. The 60-foot dish is certainly big enough and strong enough to physically accommodate an instrumentation cluster, and solid state technology would allow a compact package to be designed, built, and installed. Before such a change is made, however, it would be prudent to make a simple test of the idea to demonstrate the validity of eliminating the long cable runs. Unfortunately, again because of the RATSCAT mode of operation, time for such testing has never been set aside.

Perhaps understandably. The feed is 50 feet above the ground and not easily accessed, either temporarily or in a permanent installation. Set-up and adjustment of the equipment for a test would require a few days, and time is at a premium. Nevertheless, it is only through often painful test procedures that problem areas can be isolated and corrective steps taken.

Less fully appreciated are the facts that the 60-foot antenna is not especially large in terms of wavelengths for frequencies below 150 MHz, and that the far sidelobes and spillover can be appreciable. Consequently, some of the ringing may be due to ground scattering in the vicinity of the antenna itself or from terrain located behind the antenna. A simple, although possibly inconclusive test, would be to aim the antenna at the zenith (its stowed position) to see how this influences the background signals. If there is a marked change, the ground reflections (clutter) are worse than was thought. If the change is small, ground clutter cannot be ruled out because the spillover still illuminates the terrain near the antenna and, possibly, the duplexer/circulator operation is still not optimum. Tests made with the antenna feed replaced by a well-matched load with the antenna pointing upward could yield more diagnostic clues. The load should be placed at the far end of the cable runs, and also at the near end, for such tests.

As in any sequence of diagnostic testing, the purposes of the test and the interpretation of the outcome of the tests should be carefully thought out. This requires a thorough understanding of the system and the physical and electrical processes involved. Haphazard testing may eventually uncover the reasons for abnormal low frequency background signals, but at no less expense than a carefully conceived plan.

C. POSSIBLE GROUND PLANE EFFECTS

At frequencies of 500 MHz and less, the RATSCAT ground plane does not reflect energy like it does at the higher frequencies. Penetration of waves into the ground can be significant, and the ground reflection can be considerably different for one polarization than it is for the other. Thus, achieving circular incident polarization at the target may be difficult. Even if it can be achieved through careful orientation of the antenna feed and adjustment of the two linear polarizations used to obtain circular polarization, the received signal will not be circularly polarized due to polarization selectivity of the ground plane.

There is no easy way to correct for the depolarizing effect of the ground. One way, which requires data manipulation and processing after the data are recorded, is to measure the target twice, once with one linear polarization and once with the other (say, horizontal and vertical). If the data are collected with a coherent system, so that phase and amplitude are available from both measurement runs, the circularly polarized pattern of the target can be synthesized by adding together the two linear data sets, with one shifted in phase by 90 degrees, as appropriate. This doubles the measurement time, but is a possible way to correct for the depolarizing effect of the ground at these low frequencies.

Because of the electrical characteristics of the soil at these frequencies, it is possible to launch a "trapped wave" which gets stuck to the ground. In actual fact, the energy can be concentrated in the layer of relatively dry gypsum between the water table and the surface of the ground, although the energy content of the wave above the ground is substantial. For the purposes of analysis, we assumed that the water table is flat, smooth, and perfectly conducting so that it can be treated as a ground plane. The gypsum layer above it constitutes a dielectric medium of (assumed) constant thickness which can support the trapped wave mode of propagation.

Analytical Development

The coordinate system shown in Figure 35 is chosen as the geometric framework for an analytical description of the trapped wave phenomenon. The ground surface and the water table are assumed flat, smooth, and parallel, and these two planes are assumed to be separated by t, the thickness of dielectric layer. In terms of a representation in k-space (wavenumber space), an exact solution of Maxwell's equations for a single field component is

$$Hy\ (x,y,z) = \int_{-\infty}^{\infty}\int_{-\infty}^{\infty}\int_{-\infty}^{\infty} \frac{\beta_x}{\gamma^2}\Psi(k_y,k_z)\ e^{-i(k_x x + k_y y + k_z z)}\ dk_x\ dk_y\ dk_z \qquad (11)$$

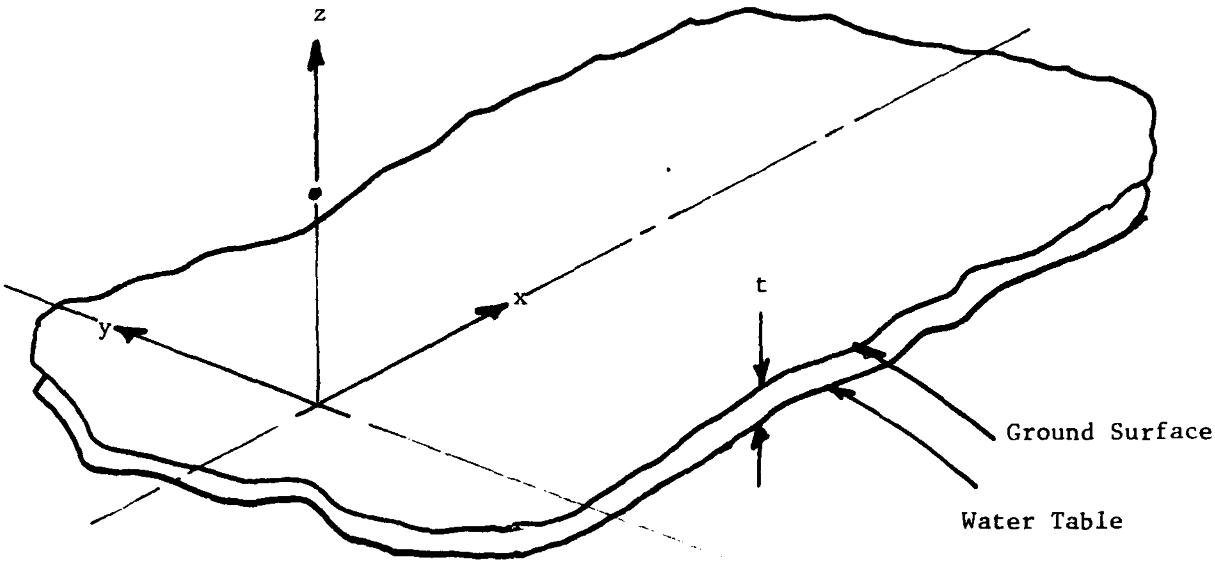

Figure 35. Geometry for trapped wave analysis. Dielectric layer between the ground surface and the water table has thickness t. Propagation is in the x direction.

where:

β_x $= (k^2 - k_y{}^2 - k_z{}^2)^{1/2}$

γ $= (k^2 - k_x{}^2 - k_y{}^2 - k_z{}^2)^{1/2}$

k = propagation constant in the medium of interest

Ψ = a potential function to be determined

k_x, k_y, k_z = wavenumbers along the three coordinate directions

At $x=0^+$, the singularity in the integrand at $k_x = \beta_x$ allows the evaluation

$$H_y(0,y,z) = i2\pi \int_{-\infty}^{\infty}\int_{-\infty}^{\infty} H_y(0,y,z)\, e^{i(k_y y + k_z z)}\, dy\, dz \ . \qquad (12)$$

But if H_y $(0,y,z)$ is the magnetic field distribution over the source plane $x=0$, $\Psi(k_y,k_z)$ can be determined from the transform of H_y $(0,y,z)$. Therefore,

$$\Psi(k_y,k_z) = \frac{1}{i2\pi} \int_{-\infty}^{\infty}\int_{-\infty}^{\infty} H_y(0,y,z)\, e^{i(k_y y + k_z z)}\, dy\, dz \ . \qquad (13)$$

Thus, the field distribution H_y $(0,y,z)$ over the plane $x=0^+$ allows a description of the field in the half-space $x > 0$ (for all y and z).

In general, at least two magnetic field components are required to satisfy the Maxwellian divergence relationship. For the specific case of vertical polarization, H_x and H_y are required, and the three components of electric field, (E_x, E_y, E_z), must be allowed. It can be shown that the components have the following form:

$$H_x(x,y,z) = -\int_{-\infty}^{\infty}\int_{-\infty}^{\infty}\int_{-\infty}^{\infty} \frac{k_y\ \beta_x}{k_x\ \gamma^2}\ \Psi(k_y,k_z)\ e^{-i(k_x x + k_y y + k_z z)} dk_x dk_y dk_z \qquad (14)$$

$$H_y(x,y,z) = \int_{-\infty}^{\infty}\int_{-\infty}^{\infty}\int_{-\infty}^{\infty} \frac{\beta_x}{\gamma^2}\ \Psi(k_y,k_z)\ e^{-i(k_x x + k_y y + k_z z)} dk_x dk_y dk_z \qquad (15)$$

$$E_x(x,y,z) = -\int_{-\infty}^{\infty}\int_{-\infty}^{\infty}\int_{-\infty}^{\infty} \frac{k_x\ \beta_x}{\omega\varepsilon\ \gamma^2}\ \Psi(k_y,k_z)\ e^{-i(k_x x + k_y y + k_z z)} dk_x dk_y dk_z \qquad (16)$$

$$E_y(x,y,z) = -\int_{-\infty}^{\infty}\int_{-\infty}^{\infty}\int_{-\infty}^{\infty} \frac{k_y k_z \beta_x}{\omega\varepsilon k_x \gamma^2}\ \Psi(k_y,k_z)\ e^{-i(k_x x + k_y y + k_z z)} dk_x dk_y dk_z \qquad (17)$$

$$E_z(x,y,z) = \int_{-\infty}^{\infty}\int_{-\infty}^{\infty}\int_{-\infty}^{\infty} \frac{(k_x^2 + k_y^2)\beta_x}{\omega\varepsilon\ k_x\ \gamma^2}\ \Psi(k_y,k_z) e^{-i(k_x x + k_y y + k_z z)} dk_x dk_y dk_z \qquad (18)$$

where ω = radian frequency of the wave

ε = permittivity of the medium

Two important observations may be noted from these expressions: (1) the values of a single field component over an infinite plane completely determines the total field structure for $x > 0$, (2) the field structure for $x > 0$ is unique only for a given distribution over the plane $x = 0$. Other, and different, distributions for $x \neq 0$ can yield the same far field distribution. (The plane $x = 0$ contains the transmitting antenna.)

The principal fields radiated by the radar system for vertical polarization are E_z and H_y, yet the boundary conditions at the ground plane (the water table) involve E_x and H_y, and E_y and H_x. Since propagation above the ground plane is in the x-direction, however, attention will be confined to H_y and E_x.

Two sets of fields exist within the dielectric layer, one set having a component of propagation downward and the other set having a component of propagation upward. Both sets have forward components of propagation, of course. The boundary conditions need to be invoked over horizontal planes (z = constant). For waves having downward components of propagation, the fields can be represented as

$$H_{yD1} = \int_{-\infty}^{\infty}\int_{-\infty}^{\infty}\int_{-\infty}^{\infty} \frac{\beta_z}{\gamma^2} \Psi_{D1}(k_x,k_y)\ e^{-i(k_x x + k_y y + k_z z)}\ dk_x dk_y dk_z \qquad (19)$$

$$E_{xD1} = \int_{-\infty}^{\infty}\int_{-\infty}^{\infty}\int_{-\infty}^{\infty} \frac{k_z\ \beta_z}{\omega\varepsilon\ \gamma^2} \Psi_{D1}(k_x,k_y)\ e^{-i(k_x x + k_y y + k_z z)}\ dk_x dk_y dk_z \qquad (20)$$

where $\beta_z = (k^2 - k_x^2 - k_y^2)^{1/2}$ and Ψ_{D1} and Ψ_{D2} are the potential functions associated with the waves. For waves having upward components of properties (being reflected from the water table) the fields can be represented as

$$H_{yD2} = \int_{-\infty}^{\infty}\int_{-\infty}^{\infty}\int_{-\infty}^{\infty} \frac{\beta_z}{\gamma^2} \Psi_{D1}(k_x,k_y) e^{-i(k_x x + k_y y + k_z z)}\ e^{-ik_z t}\ dk_x dk_y dk_z \qquad (21)$$

$$E_{xD2} = \int_{-\infty}^{\infty}\int_{-\infty}^{\infty}\int_{-\infty}^{\infty} \frac{k_z\ \beta_z}{\omega\varepsilon\ \gamma^2} \Psi_{D2}(k_x,k_y) e^{-i(k_x x + k_y y + k_z z)}\ e^{-ik_z t}\ dk_x dk_y dk_z \qquad (22)$$

Integrating over all k_z,

$$E_{xD1}(x,y,z) = \int_{-\infty}^{\infty}\int_{-\infty}^{\infty} \frac{\beta_z}{\omega\varepsilon} \Psi_{D1}(k_x,k_y)\, e^{-i(k_x x + k_y y - \beta_z z)}\, dk_x dk_y \tag{23}$$

$$E_{xD2}(x,y,z) = -\int_{-\infty}^{\infty}\int_{-\infty}^{\infty} \frac{\beta_z}{\omega\varepsilon} \Psi_{d2}(k_x,k_y)\, e^{-i(k_x x + k_y y + b_z z)}\, e^{-i\beta_z t}\, dk_x dk_y \tag{24}$$

At $z = -t$, the total tangential electric field must vanish, since the water table has been assumed to be perfectly conducting. Therefore,

$$E_{xD1}\ (x,y,-t) + E_{xD2}\ (x,y,-t) = 0$$

which in turn requires that

$$\Psi_{D1}\ (k_x,k_y)\ e^{-i\beta_z t} = \Psi_{D2}\ (k_x,k_y)$$

Consequently, the transforms of the total fields H_y and E_x within the dielectric layer are

$$H_{yDT}(k_x,k_y) = \left(e^{i\beta_z z} + e^{-i\beta_z (z + 2t)}\right) \Psi_{D1}(k_x,k_y) \tag{25}$$

$$E_{xDT}(k_x,k_y) = \frac{\beta_z}{\omega\varepsilon} \left(e^{i\beta_z z} + e^{-i\beta_z (z + 2t)}\right) \Psi_{D1}(k_x,k_y) \tag{26}$$

where H_{yDT} and E_{xDT} are the total fields.

Similarly, the reflected fields above the ground have the form

$$H_{yR}(k_x,k_y) = \Psi_R\ (k_x,k_y)\ e^{-i\beta_{oz}z} \tag{27}$$

$$E_{xR}(k_x,k_y) = -\frac{\beta_{oz}}{\omega\varepsilon_o}\ \Psi_R\ (k_x,k_y)\ e^{-i\beta_{oz}z} \tag{28}$$

where: $\beta_{oz} = (k_o^2 - k_x^2 - k_z^2)^{1/2}$

$k_o = \sqrt{\omega\ \mu_o\varepsilon_o}$ = freespace wavenumber

ε_o = permittivity of free space

μ_o = permeability of free space.

At the interface between the ground (dielectric layer) and the air above, z=0, and (25) through (28) become

$$H_{yDT}(k_x,k_y) = (1 + e^{-i2\beta_z t})\ \Psi_{D1}\ (k_x,k_y) \tag{29}$$

$$E_{xDT}(k_x,k_y) = \frac{\beta_z}{\omega\varepsilon}\ (1 - e^{-i2\beta_z t})\ \Psi_{D1}\ (k_x,k_y) \tag{30}$$

$$H_{yR}(k_x,k_y) = \Psi_R\ (k_x k_y) \tag{31}$$

$$E_{xR}(k_x,k_y) = -\frac{\beta_{oz}}{\omega\varepsilon_o}\ \Psi_R\ (k_x,k_y) \tag{32}$$

Equations (29) through (32) allow the total magnetic field within the dielectric layer to be expressed as

$$H_{yT}(k,y,z) = \int_{-\infty}^{\infty}\int_{-\infty}^{\infty}\int_{-\infty}^{\infty} \frac{\beta_z}{\gamma^2}\left(1 + e^{-i(k_z + \beta_z)t}\right)\Psi_{D1}(k_x,k_y)\ \cdot\ e^{-i(k_x x + k_y y + k_z z)}\ dk_x dk_y dk_z \tag{33}$$

where:

$$\Psi_{D1}(k_x,k_y) = \int_{-\infty}^{\infty} \frac{\varepsilon(k_o^2 - k_y^2 - u^2)^{1/2}(u + \beta_{oz})\Psi(k_y,-u)\, e^{i(\beta_z t - uz_a)}}{2(k_o^2 - k_x^2 - k_y^2 - u^2)(i\varepsilon_o\beta_z \sin\beta_{oz}t + \varepsilon\beta_{oz}\cos\beta_z t)}\, du \quad (34)$$

The integral (33) can be evaluated, providing certain simplifying assumptions can be satisfied. Specifically, the function $\Psi(k_y,-u)$ is assumed to be separable so that it can be expressed as the product of a pair of functions,

$$\Psi\,(k_y,-u) \longrightarrow \Psi_y(k_y)\ \Psi_u(-u)$$

Moreover, $\Psi_u(-u)$ should correspond to a uniform illumination of the antenna aperture and the electrical thickness $\beta_z t$ (of the dielectric layer) should be small. Under these assumptions, the approximate evaluation of (33) is

$$H_{yT}(x,y,z) = H_a\, e^{-\Gamma k_o z_a}\, e^{-\Gamma k_o t}\, \sinh[\tfrac{1}{2}\,(\Gamma k_o w)(\Gamma k_o t)]\, \cdot$$

$$\frac{\cos\{\Gamma(kz + kt)[1 - \frac{\varepsilon_o}{\varepsilon_D}\,(\Gamma kt)^2]^{1/2}\}}{\cos\{\Gamma kt[1 - \frac{\varepsilon_o}{\varepsilon_D}\,(\Gamma kt)^2]^{1/2}} \cdot$$

$$\int_{-\infty}^{\infty} \Psi(k_y)\, e^{-ik_y y}\, e^{-ix[(k_o\Omega)^2 - k_y^2]^{1/2}}\, dk_y \quad (35)$$

where H_a = magnetic field intensity in the aperture,

z_a = height of the aperture,

w = aperture width along the z-direction

$\Gamma = (1 - \frac{\varepsilon_o}{\varepsilon_p})^{1/2}$

$\Omega = [1 + \Gamma^2(\Gamma k_o t)^2]^{1/2}$

The integral in (35) can be evaluated by means of the convolution theorem, resulting in

$$\int_{-\infty}^{\infty} \frac{x\ f(s)\ H_1^{(2)}\ \left(k_o\Omega[x^2 + (y - s)^2]^{1/2}\right)\ ds}{[x^2 + (y - s)^2]^{1/2}} \tag{36}$$

where $H_1^{(2)}(p)$ is the outward Hankel function of order 1 and argument p and f(s) is the transform of $\Psi(k_y)$.

For large arguments, the Hankel function can be approximated by

$$H_1^{(2)}\ (p) \approx (\frac{2}{\pi p})^{1/2}\ e^{-i(p - \frac{3\pi}{4})}$$

whence the integral in (35) becomes

$$(\frac{2}{\pi})^{1/2}\ e^{i\ \frac{3\pi}{4}} \int_{-\infty}^{\infty} \frac{xf(s)}{[x^2 + (y - s)^2]^{1/2}} \cdot \frac{e^{-ik_o\Omega[x^2 + (y - s)^2]^{1/2}}}{k_o\Omega[x^2 + (y - s)^2]^{1/2}} ds \tag{37}$$

Invoking a far field condition that the only significant contributions occur for $s << (x^2 + y^2)^{1/2}$, the integral in (37) can be approximated by

$$\frac{x}{\rho}\left(\frac{2}{\pi k_o \Omega\rho}\right)^{1/2} e^{i\frac{3\pi}{4}} e^{-ik_o\Omega\rho} \int_{-\infty}^{\infty} f(s)\, e^{ik_o\Omega\, y\, s/\rho}\, ds \tag{38}$$

where $\rho = (x^2 + y^2)^{1/2}$ is the radial distance from the aperture to a point in the dielectric layer.

Thus, in substituting (38) into (35), the total magnetic field intensity at a point in the dielectric is

$$H_{yT}(x,y,z) \approx \frac{x}{\rho}\left(\frac{2}{\pi k_o \Omega\rho}\right)^{1/2} H_a e^{i\frac{3\pi}{4}} e^{-\Gamma(k_o z_a + k_o t)} e^{-ik_o\Omega\rho} \cdot$$

$$\frac{\cos\left\{\Gamma(kz + kt)\left[1 - \frac{\varepsilon_o}{\varepsilon_D}(\Gamma kt)^2\right]^{1/2}\right\}}{\cos\left\{\Gamma kt\left[1 - \frac{\varepsilon_o}{\varepsilon_D}(\Gamma kt)^2\right]^{1/2}\right\}} \sinh\left\{\frac{1}{2}(\Gamma k_o w)(\Gamma k_o t)\right\} \cdot$$

$$\int_{-\infty}^{\infty} f(s)\, e^{ik_o\Omega\, y\, s/\rho}\, ds \tag{39}$$

Interpretation

Equation (39) is complicated despite the approximations and assumptions made to obtain it. Nevertheless, several significant conclusions may be reached. First, the field intensity falls off exponentially with the aperture height, as is evidence from the term $e^{-\Gamma k_o z_a}$. Thus, the coupling of energy to the trapped wave mode decreases exponentially with antenna height. Second, the product $e^{-\Gamma k_o t} \sinh\{\frac{1}{2}(\Gamma k_o w)(\Gamma k_o t)\}$ is essentially a linear function of the layer thickness t, provided $\Gamma k_o t$ is not large. This, and the ratio of the two cosine functions, shows that the coupling to the trapped wave can vary considerably with the layer thickness, suggesting that large variations of measurement conditions may take place from day to day as the water table moves up and down.

For $y \ll x$, the term $\frac{x}{\rho}$ is essentially unity, hence the decay in field strength with radial distance is given by the next term, $(\pi k_o \Omega \rho)^{1/2}$. Consequently, the power attenuation varies as ρ^{-1}, as opposed to ρ^{-2} with normal free space propagation modes, and the trapped wave does not decay as rapidly as a free space wave. This is due to the radial transmission mode and the discontinuity presented by the pit in the dielectric layer can be a significant source of reflection. Unlike the vertical field profile for normal ground plane operation in which the field intensity becomes small at the ground surface, the field intensity at the ground can be significant in the presence of a trapped wave. Finally, because the velocity of propagation above and below the ground surface differs, the incident wave fronts are tilted, and energy tends to be transferred from the wave propagating above the ground to the trapped wave propagating in the dielectric layer.

As shown in Figure 36a, the trapped wave will be reflected by the discontinuity in the ground surface introduced by the pit itself. The trapped wave return is likely to lag the free space return, as shown in Figure 36b, but not by enough to allow their separation by gating. One way to prevent the trapped wave from impinging on the pit discontinuity is to provide a buried, metallic ogival shield, as shown in Figure 36c. The shape of this shield is chosen to deflect the trapped wave in directions other than back to the radar, although the precise shape may not be critical. The shield should be placed in range such that the residual return may be separated in time by gating techniques.

Another method would be to bury a specially designed absorber termination in front of the pit. Since this absorber has to match the impedance of the soil to that of a short circuit, it would not be a commercially available item. The absorber would likely have to be several wavelengths long and several wavelengths wide.

Neither of these methods is attractive because of the cost and because of the uncertainty of their effectiveness. A cheaper alternative might be to lay down a metallic mat on the ground surface in an attempt to create a better ground plane. Even this is not without its limitations because of the way the

AD-A099 560 GEORGIA INST OF TECH ATLANTA ENGINEERING EXPERIMENT --ETC F/G 17/9
RADAR BACKGROUND SIGNAL REDUCTION STUDY.(U)
JUL 80 E F KNOTT, C J RAY, M S WEST F29601-79-C-0050
UNCLASSIFIED GIT/EES-A-2403-F NL

2 of 2
AD
A099560

END
DATE
FILMED
7-81
DTIC

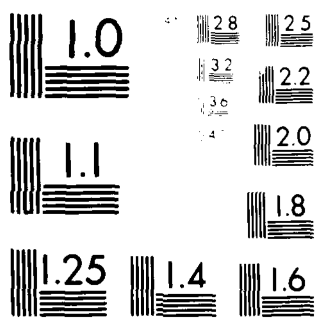

MICROCOPY RESOLUTION TEST CHART
NATIONAL BUREAU OF STANDARDS-1963-A

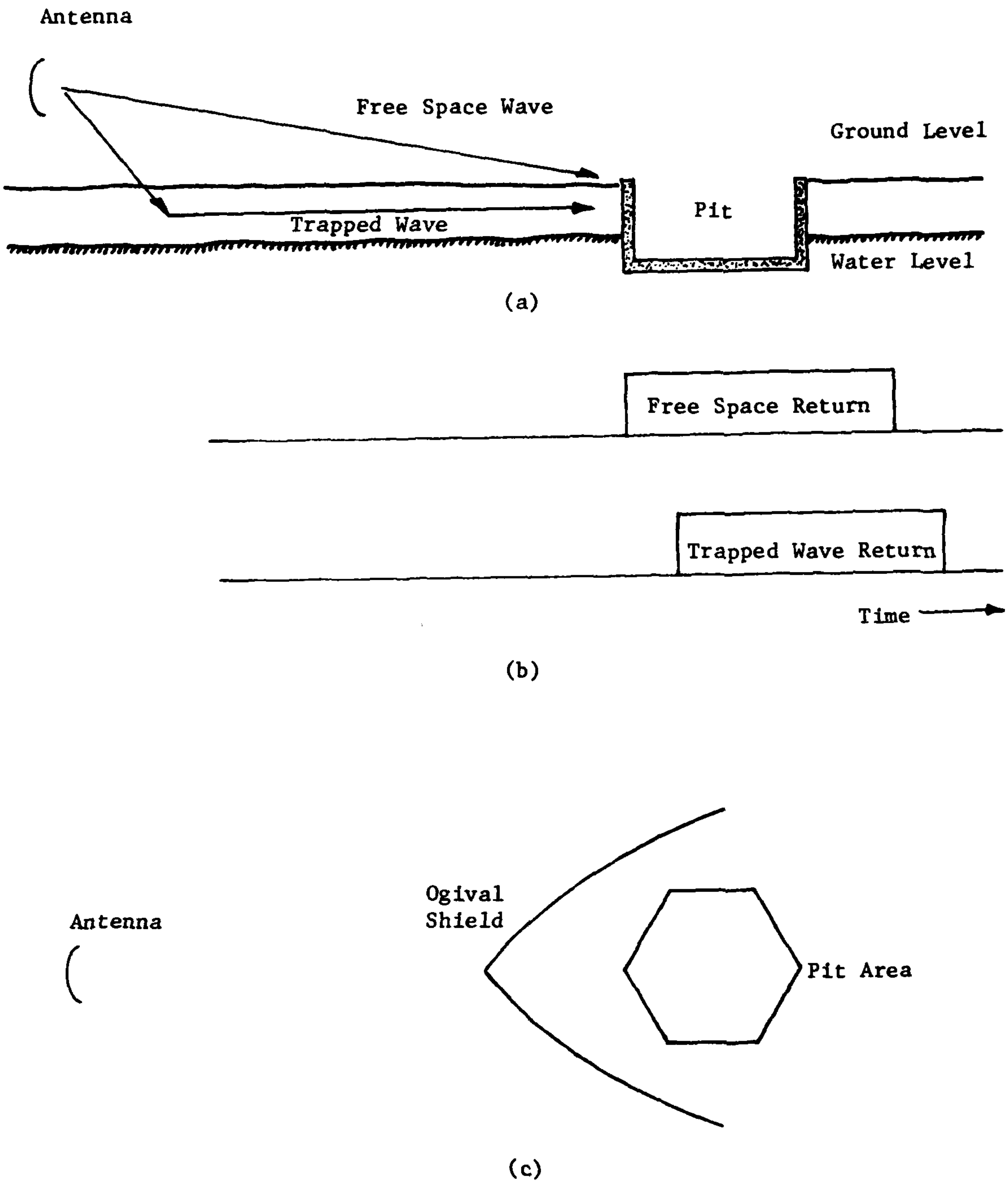

Figure 36. (a) Trapped wave propagation; (b) trapped wave return from pit lags the free space return; (c) buried ogival shield may deflect trapped wave reflection away from the radar.

RATSCAT gypsum attacks metals and accumulation of windblown sand on the ground plane.

In short, there seem to be no easy ways to suppress interference effects due to a trapped wave. Before any countermeasure is seriously considered, a sequence of tests should be devised to verify that the phenomenon actually exists. This could be done by means of probing the incident field structure along a vertical path below the ground as well as above it, both near the pit, as well as at some other location where there is no apparent discontinuity. The tests should be performed when the water table is high as well as when it is low to assess the variability. A soil moisture profile should be taken simultaneously so as to aid in the interpretation of test results. And further tests should be devised if these tests prove to be inconclusive.

7. VECTOR FIELD SUBTRACTION

The concept of vector field subtraction (VFS) is quite simple and is based on the assumption that the net signal in the receiving system arises from the target and unwanted background signals. Thus, vector field subtraction can be implemented as follows:

1. Measure the target plus background,
2. Measure the background alone, and
3. Subtract the background from target plus background.

The procedure implicitly assumes that the target and background signals are completely decoupled, so that the presence or absence of one does not affect the signal return of the other. How closely this assumption is satisfied for typical targets has never been established, but it seems eminently reasonable.

The implementation of the concept obviously requires the measurement of the phase and amplitude of the target plus background as a function of aspect angle and the measurement of the background alone as a function of aspect angle. Since the subtraction must be performed with all due regard to the phasor characteristics of the data, phase must be measured as well as amplitude. Nevertheless, the subtraction process may be corrupted by the presence of noise in the receiving system as well as time varying clutter signals that are independent of the rotator position.

The aspect angles must be as closely duplicated as possible from one run to the next so that the proper quadruplet of numbers are manipulated (phase and amplitude from two measurement sets). The quality of the corrected data depends on how well the alignment in aspect angle is preserved for the two data sets and this was demonstrated in a sequence of mathematically generated data. Other conditions implicit in the VFS concept include the assumption that the column return is not significantly affected by the physical loads imposed by the target and the propagation, due, for example, to soil moisture content and atmospheric refractive index, remain unchanged between the measurements of the two primary data sets (target plus column, column alone). The mathematically generated data are primarily for the assessment of the aspect angle alignment between the data sets, and all other factors are assumed to remain unchanged.

The only documented test of vector field subtraction that could be found is a short description in reference 4. The test was apparently performed at a frequency in L-band and, as judged from the broadness of the pattern, the test object (a metallic cone sphere) was less than 3 wavelengths long. Other tests were reported to have been conducted at RATSCAT, and RATSCAT's brochure [1] states that three VFS systems are in use at the site.

For the purposes of assessing the effectiveness of these systems in suppressing background signals, Georgia Tech suggested that these data be retrieved from RATSCAT data banks and forwarded for analysis, but this appeared to be unfeasible. An alternative was for phase and amplitude data to be collected on a simple vehicle and forwarded to Georgia Tech for analysis, and this in fact was suggested to a representative of the 6586th Test Group.

The cost of mounting a measurement program on-site for the sole purpose of collecting phase and amplitude data for a VFS assessment would have been prohibitively costly, even if the range time were available. Moreover, there were no test programs in progress or on the schedule which would have allowed a "piggy back" set of measurements to be made at minimal additional cost. Therefore, in the absence of actual test data, Georgia Tech undertook to assess the usefulness of the VFS technique using mathematically generated data. These data are presented in Figures 37 through 48 below.

The data presented in these figures all follow the same format. The upper left diagram (labeled "a" in each figure) is the uncorrupted pattern of a right circular cylinder generated mathematically. Consequently the pattern that consists of the broadside lobe plus six sidelobes on either side is very regular. The dynamic range exceeds 50 dB, and although the aspect angle variation presented is only ±10 degrees from broadside, the actual aspect angle variation is not important for the purpose of the study. The relative slip between two sets of measurements determines the efficacy of the VFS procedure.

The upper right diagram in each figure (labeled "b") is an assumed (synthesized) contribution from the support column over the same aspect angle range as covered by the pure cylinder return. The support column return was deliberately constructed from a regular, but slowly varying, component and a component that resembles noise. Both components were adjusted to different levels in the mathematical exercise so that the effect of the column contribution could be assessed.

The lower left diagram of each figure (labeled "c") shows the vector sum of the column return and the target return and corresponds to the target return as it might be measured in the presence of the background return shown in diagram b of each figure. If the background could be perfectly subtracted, the original target pattern in diagram a would be recovered. However, a small misalignment has been assumed between diagrams a and c, and the pattern actually recovered is shown in the lower right hand corner of each figure. Thus, a comparison of the upper left and lower right patterns gives a measure of the effect of aspect angle misalignments.

Figure 37 shows the effect of a relatively slowly varying support column return that is of the order of 20 dB below the main lobe. The recovered target return for the broadside lobe is very close to that of the actual target return for these aspects. Note that the pattern misalignment was 1 degree, which is approximately 0.7 the width of a sidelobe. A 1-degree misalignment would probably never occur in a practical application of the VFS technique, but a 70% sidelobe misalignment could very easily occur for electrically large targets. This is why the relative angles in terms of pattern detail, rather than the actual aspect angles, are important in this study. The sidelobes of Figure 37d are a good deal noisier than the main lobe, but the mean sidelobe levels are closer to the true value than those of the corrupted pattern in Figure 37c. Thus, slowly varying background signals allow a reasonably accurate measurement of the true target pattern, even for large aspect angle misalignments.

When the background is very noisy and has appreciable dynamic range, as in Figure 38b, a 70% sidelobe misalignment has the effect of making the recovered pattern even worse than the perturbed pattern. Figure 39 shows the effect of a small offset (0.05 degree, or only 3.5% of the width of a sidelobe) with the same column perturbation of Figure 38. The effect shown in Figure 39 suggests that reducing the alignment error does not significantly improve the efficacy of the background signal subtraction. This is because of the large dynamic range of the background return and the rapidity of the variation. If the mean level of the background is lowered as suggested in Figure 40b, however, the subtraction produces better results, even if the dynamic range of the background is unchanged. Note that the sidelobes of the recovered pattern are significantly perturbed by the background, but that the pattern of Figure 40d shows deeper nulls than the uncorrected pattern of Figure 40c.

For small misalignments, a slowly varying background has less effect as shown in Figure 41, but larger misalignments degrade the recovered pattern as shown in Figures 42 and 43. If the misalignment is large enough and the periodicity of the background signal close enough to that of the target, the lobe structure of the recovered pattern becomes severely distorted. Note that even the main lobe is influenced, and the distortion becomes even worse if the background signal is increased to within a few dB of the peak of the main lobe, as in Figure 44. Reducing the misalignment to 0.05 degree, as in Figure 45, in the presence of large background signals improves the situation somewhat, but the recovered pattern is not nearly as good as one would like. Reducing the mean level of the background some 20 dB has the expected effect of markedly improving the accuracy of the recovered pattern as suggested by Figure 46, even though the misalignment may be large. A smaller offset error would improve the accuracy, of course. Finally, Figures 47 and 48 reinforce what Figures 38 and 39 have shown -- that background signals with large dynamic range and significant levels seriously degrade the recovered pattern, whether the offset is large or small.

These comparisons illustrate an important point: a centralized support structure having a fairly constant return with aspect angle is extremely desirable for vector field subtraction.

In addition to controlling the effects of the various parameters involved in vector field subtraction, compensating approaches can be used to minimize errors. None of these techniques were actually employed in the current analysis because, although they are theoretically defensible, the proof of their applicability requires real data. Perhaps the most useful technique concerns

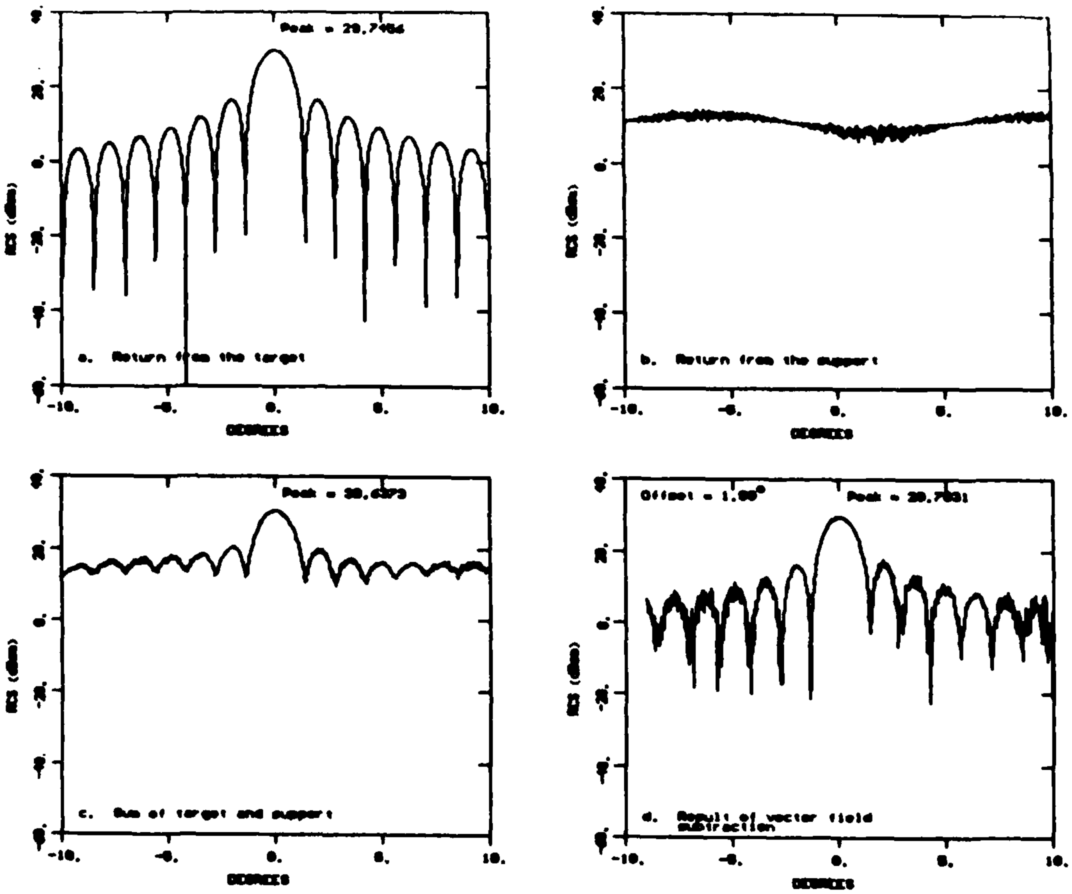

Figure 37. Vector field subtraction for slowly varying background and a 1-degree angle misalignment.

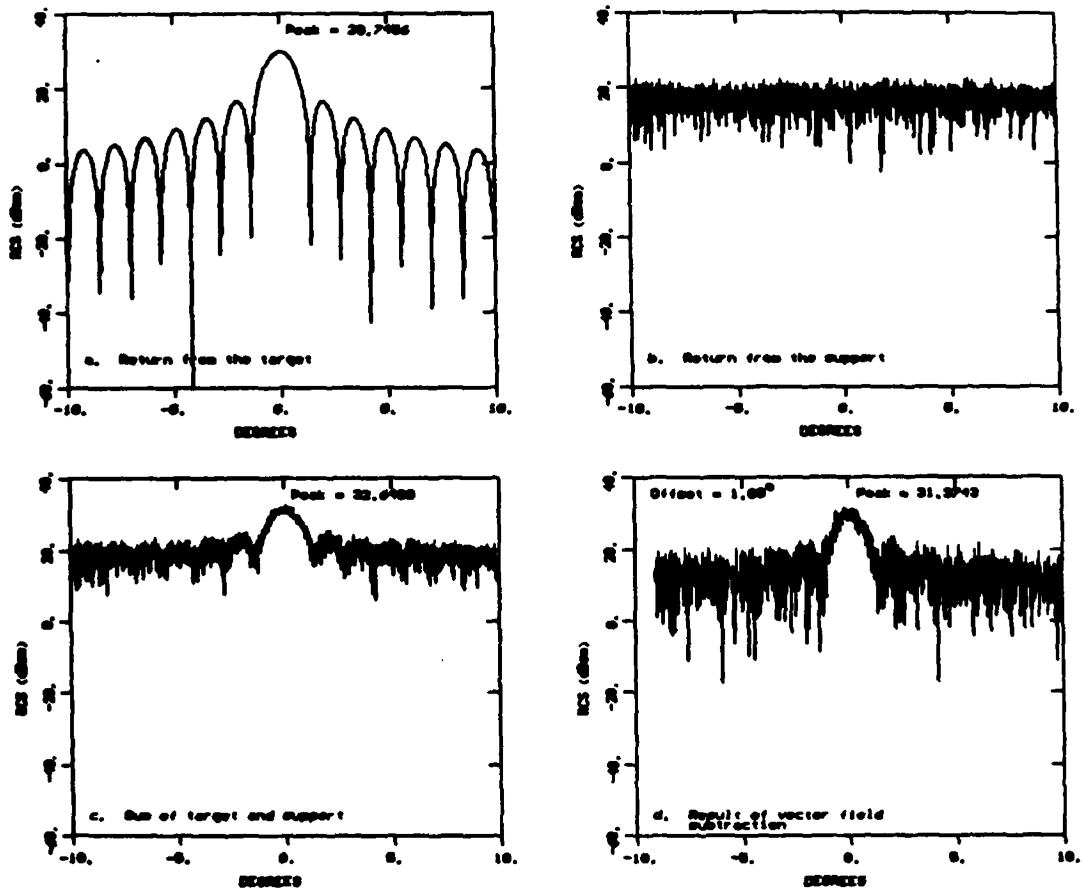

Figure 38. Vector field subtraction for very noisy background and a 1-degree angle misalignment.

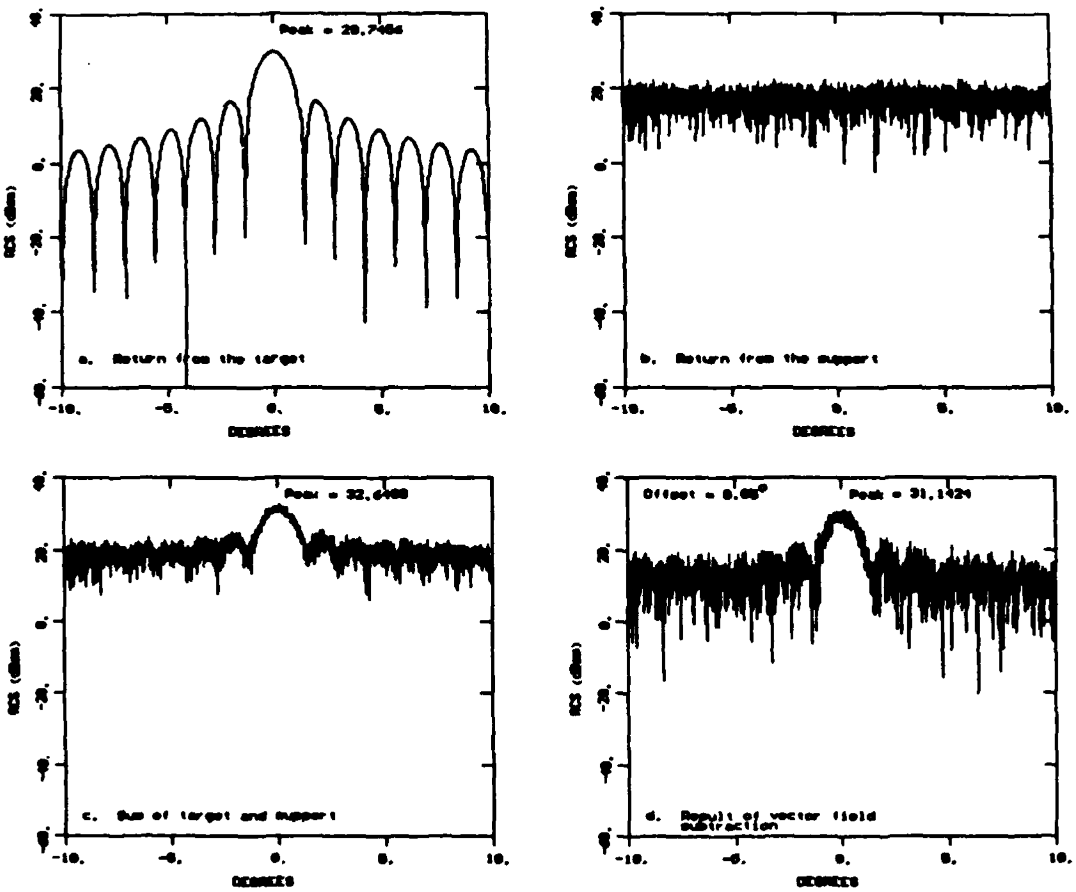

Figure 39. Vector field subtraction for a very noisy background and a 0.05-degree angle misalignment.

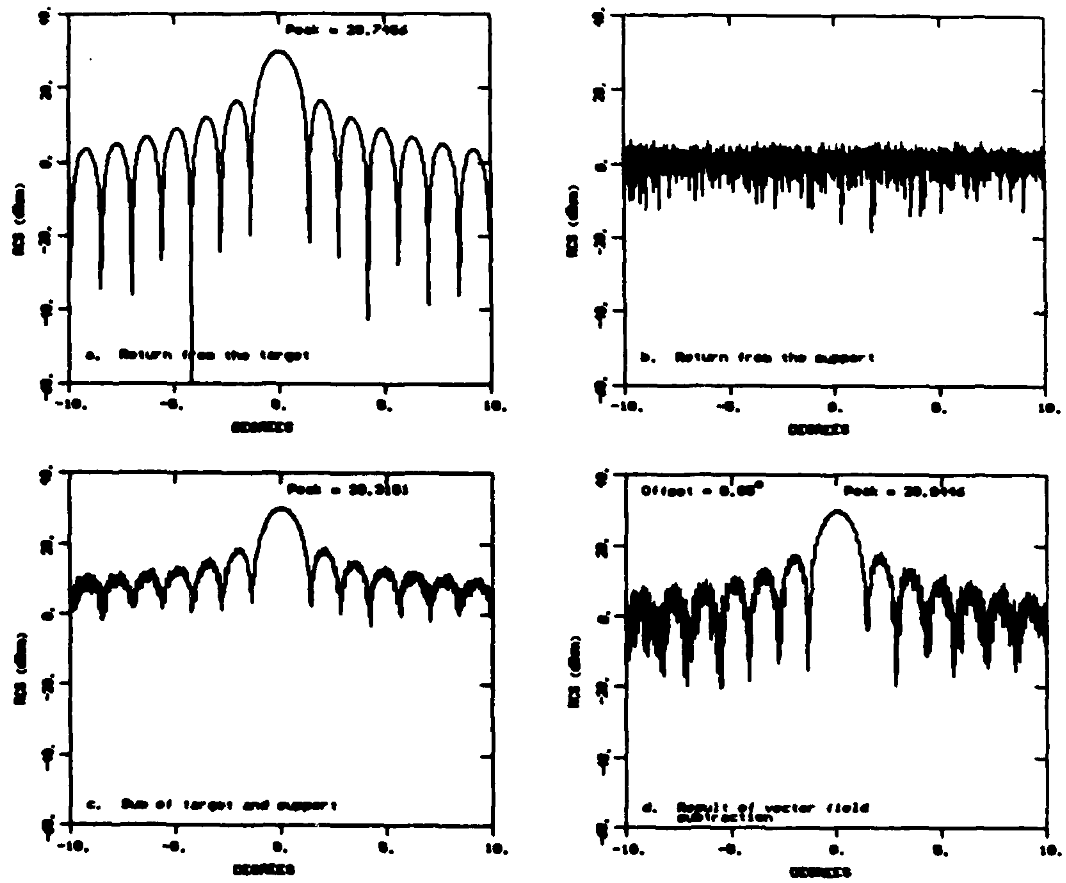

Figure 40. Reducing the mean level of the background improves the result, even if the background dynamic range remains unchanged for a 0.05-degree misalignment.

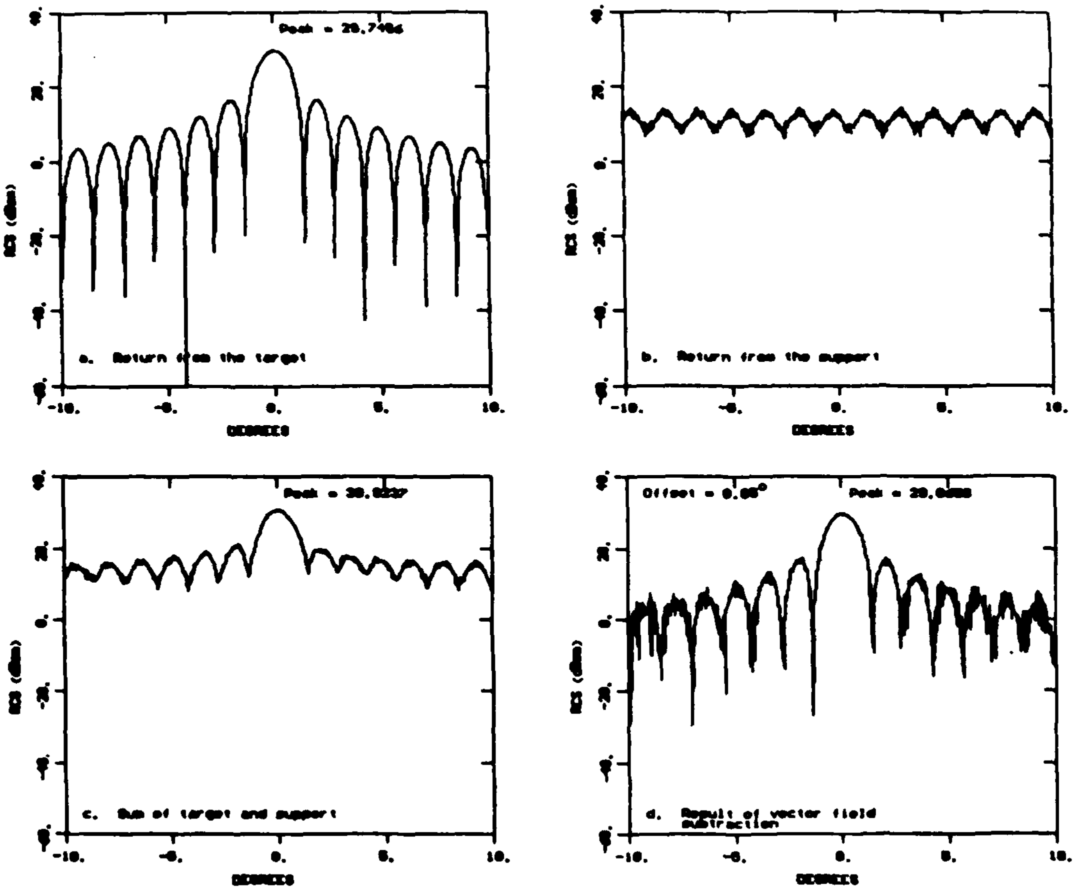

Figure 41. Slowly varying background seems less degrading for a small misalignment of 0.05 degree.

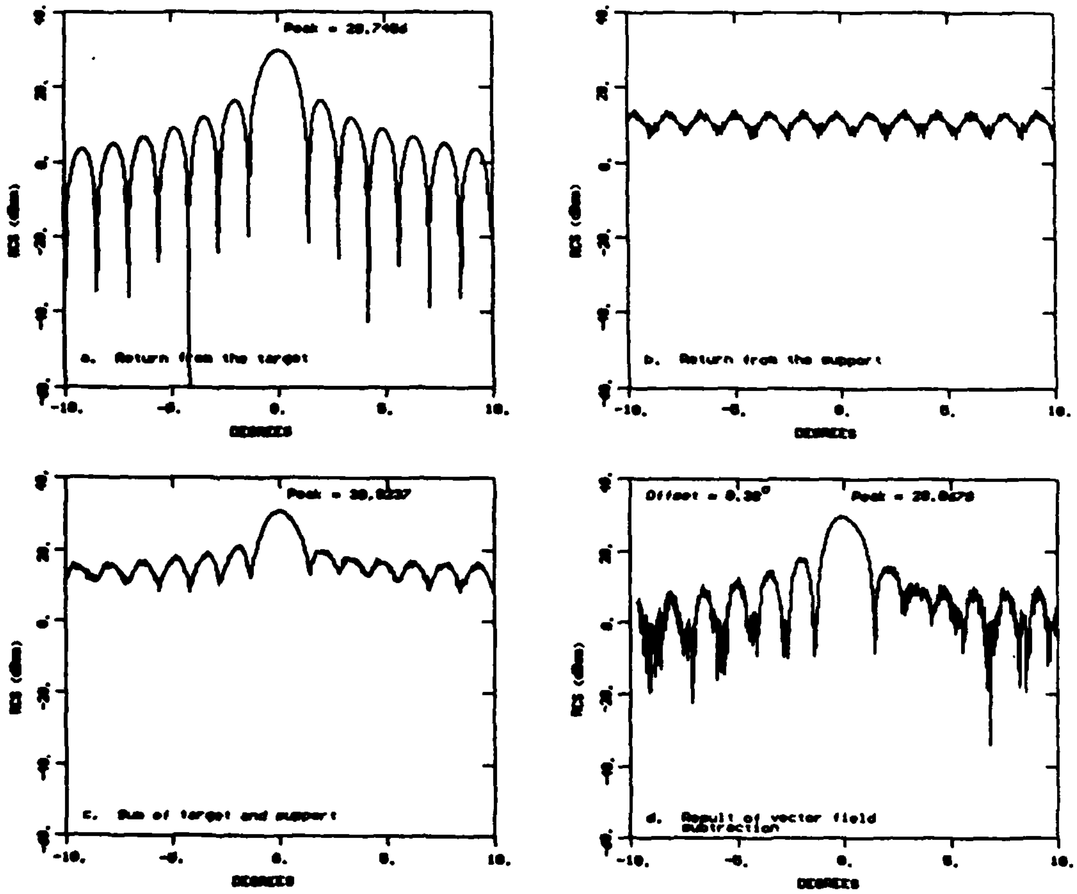

Figure 42. Effect of slowly varying background with 0.3-degree misalignment.

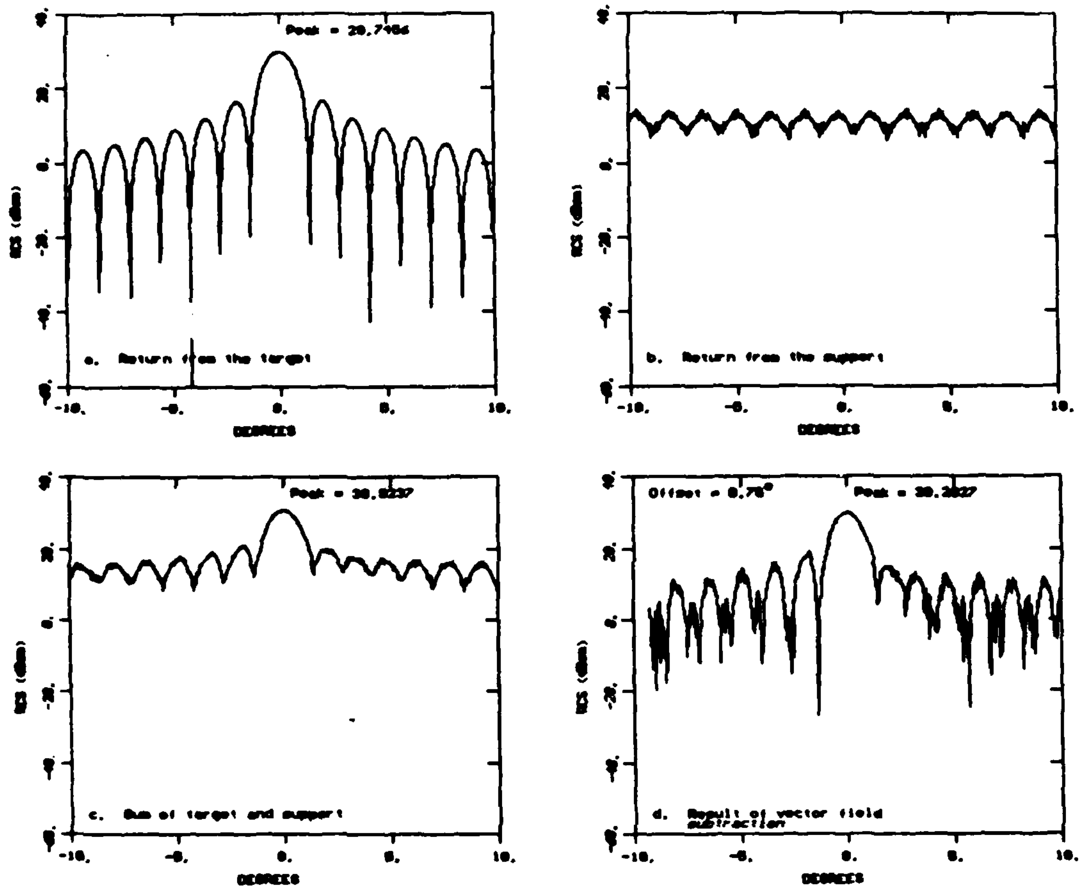

Figure 43. Effect of slowly varying background can introduce false lobes for large misalignments, 0.75 degree in this case.

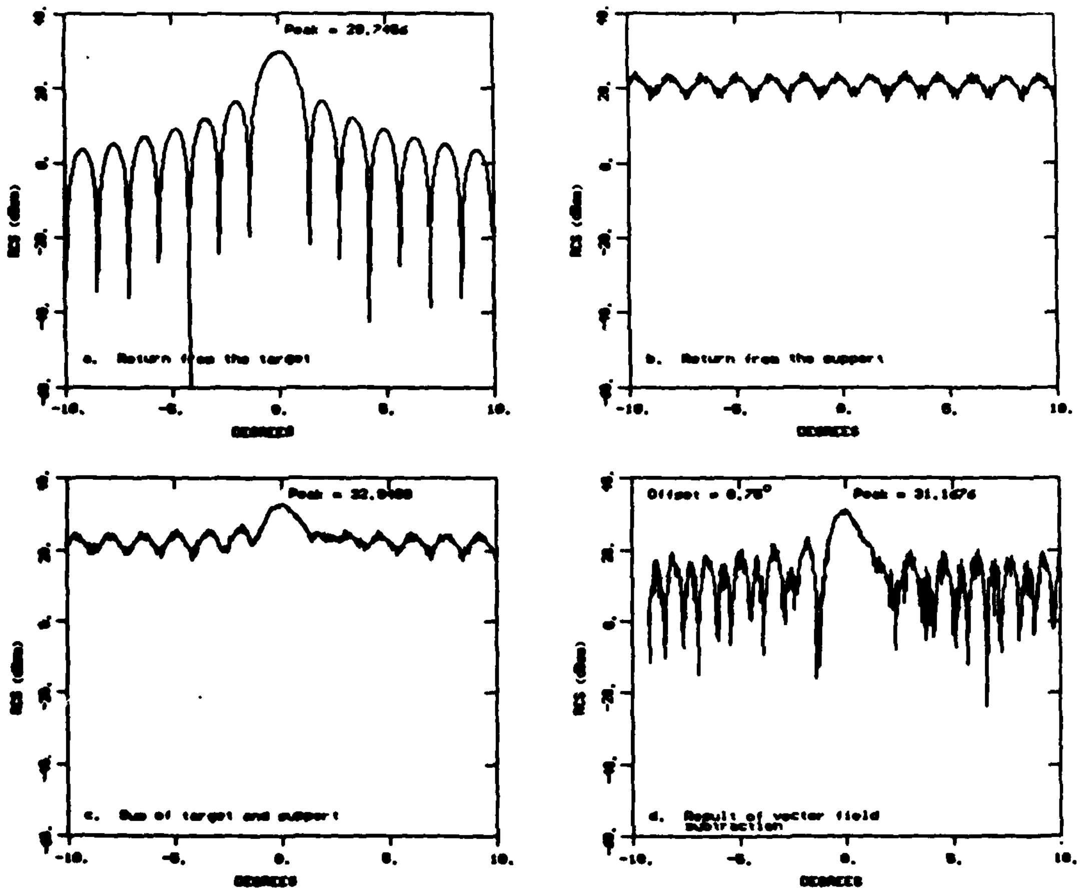

Figure 44. Severe pattern distortion occurs for large misalignments and strong background signals. (Misalignment here is 0.75 degree.)

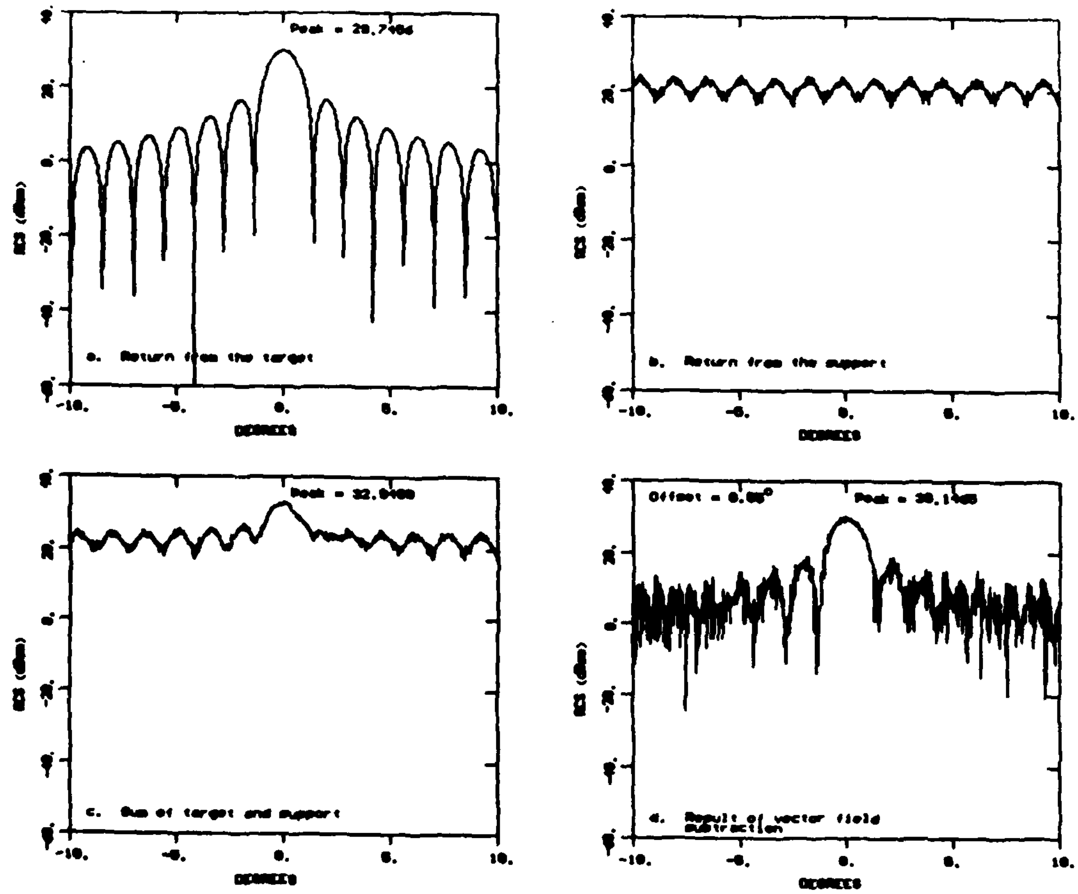

Figure 45. Reducing the misalignment to 0.05 degree makes some improvement.

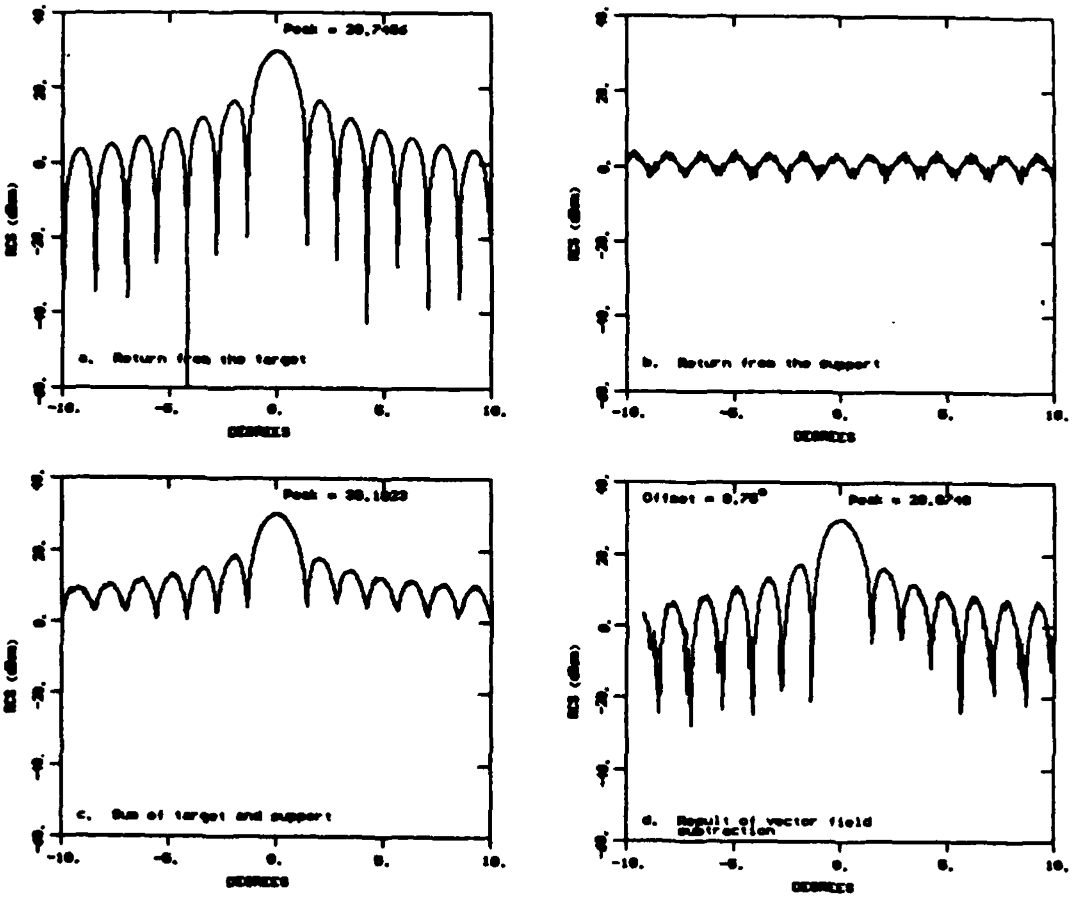

Figure 46. Reducing the background level improves the VFS accuracy, even for large effects (0.75 degree here).

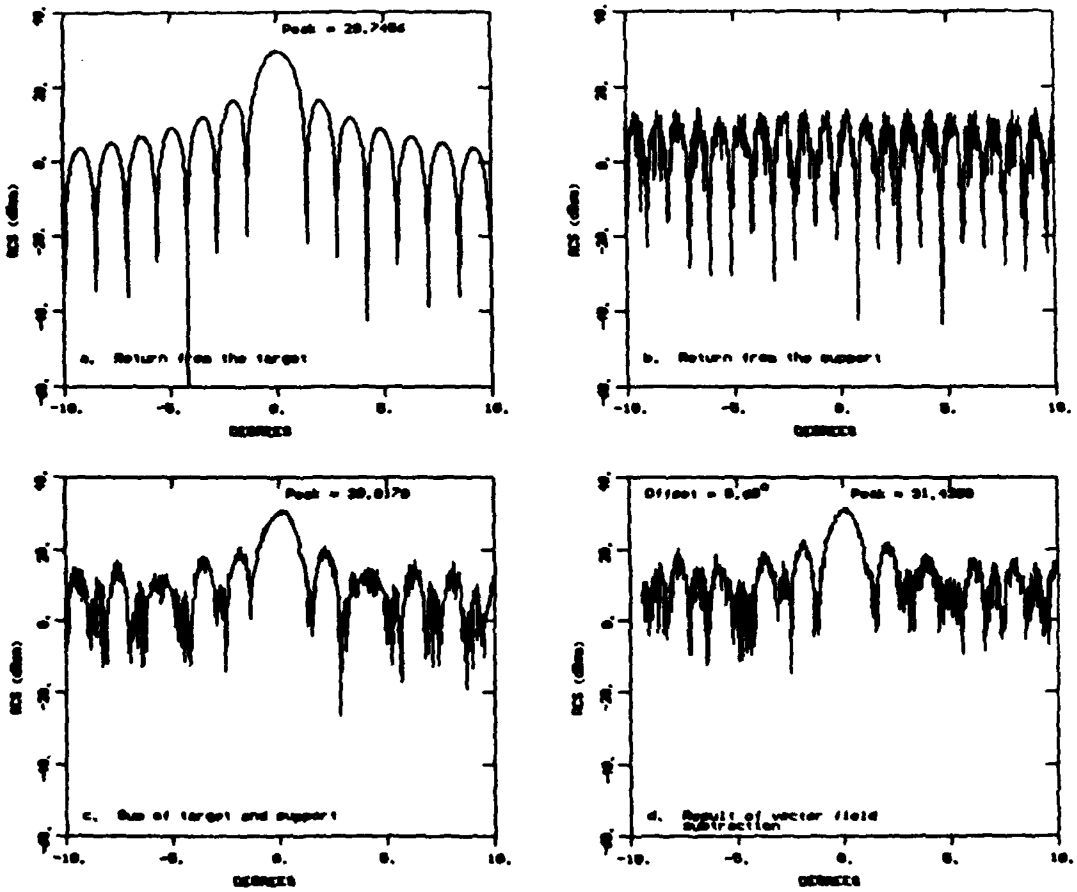

Figure 47. Effect of wide dynamic background signal
is large for a 0.75-degree misalignment.

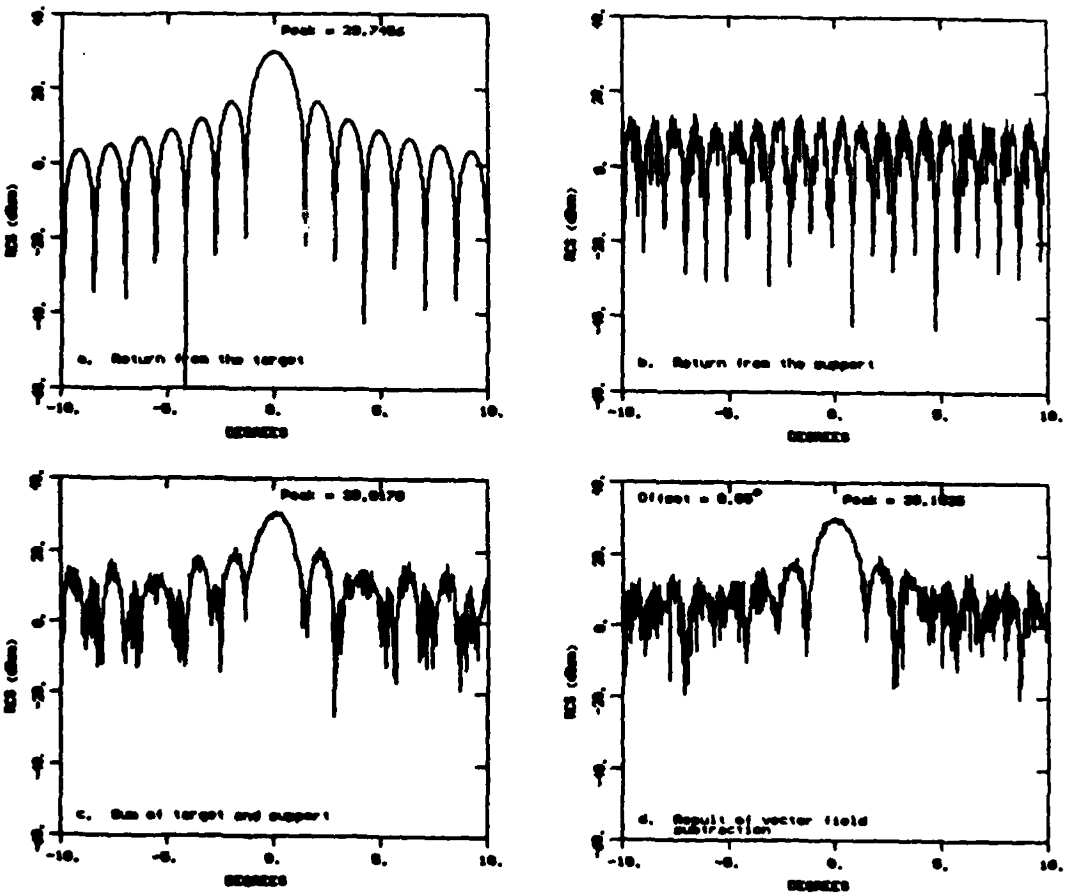

Figure 48. Wide dynamic background has large effects even for small misalignments (0.05 degree here).

the application of the cross-correlation function to correct possible misalignment problems in the data. In particular, the following technique is suggested.

1. Perform the usual measurements of amplitude and phase for the support, and then the target plus support.
2. Choose a nominal alignment for the two measurements and perform vector field subtraction for each.
3. Vary alignment over a range of samples in both directions about the nominal alignment and again perform vector field subtraction for each.
4. Calculate the cross-correlation between the support and each vector field subtraction result.

Presumably, the best alignment in aspect angle generates the smallest cross-correlation. Alternatively, the alignment that generates the highest cross-correlation between the column return and the column-plus-target return is the best alignment for performing vector field subtraction.

Note that this in no way exhausts the possibilities in digital signal processing for improving vector field subtraction, but further suggestions would depend heavily on the nature of the support being used or the target being measured. In particular, as a final example, suppose that the power returns from both the support and the support plus target are essentially the same in a certain frequency band. Then it could be conjectured that this power is due almost entirely to the presence of the support. Hence, by bandpass filtering both sets of data in this region, a noticeable improvement in vector field subtraction could be obtained.

Vector field subtraction is a useful technique, but it is not without its limitations. The numerical study illustrated the effects of aspect angle misalignment between the two data sets (column-plus-target and column alone) for a variety of cases. The study was based on mathematically generated data, however, and experimental tests are highly desirable. A systematic test program takes time, but there is a need for it. Under carefully controlled conditions, the resulting data will show the limits of the technique and the situations in which it is best applied. The scope of the present contract was too limited for this to be done, yet a study needs to be performed using actual test data.

Very late in the contract we discovered that a VFS system had been instrumented at Teledyne Micronetics in San Diego, California [23]. According to reports a test object up to 70 wavelengths long had been measured, and the support column return can indeed be suppressed. The test conditions and the degree of success are unknown, and the system limitations were not explained. However, the very fact that a system has been built and measurements conducted for an object several dozens of wavelengths long suggests that VFS should be explored futher.

8. SOLID SUPPORT STRUCTURES

Solid support structures were not studied per se because they are, in general, large scatterers. An exception is the absorber-coated pylon which, as was mentioned earlier, has a remarkably low RCS for such a large structure. Its shape is not unlike that of an airfoil, except that it has a sharp leading edge in addition to a sharp trailing edge and the profile is ogival. That is, the profile of a transverse section is formed by a pair of circular arcs which meet at the leading and trailing edges.

The leading edge of this huge vane faces the radar, and the entire structure is tilted toward the radar. This effectively removes the specular return due to the leading edge. A thin coating of absorber on the exterior surface effectively suppresses traveling waves launched toward the trailing edge where they would otherwise be reflected.

The chord at the base of the pylon is large and tapers to a much smaller value at the top of the pylon. The rotator head at the top of the pylon mates with the target by means of a mounting fixture installed on the target itself. Thus, the target must be disfigured in order to be attached to the pylon, a distinct disadvantage.

Other disadvantages are its high cost and the several days that it takes to erect it or remove it from its mounting piers. The high cost discourages the acquisition of more pylons and the time-consuming installation prolongs range schedules. Despite these shortcomings, the absorber-covered pylon is a step forward in target support technology.

The target support need not be metallic. One can conceive of using solid plastic tubes to support test objects, although it should be emphasized that the load bearing capacity of such a support system would be less than that of a metal column. Plastic support structures would have to be restricted to relatively small targets, say less than 15 or 20 feet long, weighing perhaps no more than a few hundred pounds.

Surprisingly enough, the return from a plastic column is only a few dB less than that from a metal one. In general, one can expect the return to be proportional to the voltage reflection coefficient, R,

$$R = \frac{1 - \sqrt{\varepsilon}}{1 + \sqrt{\varepsilon}}$$

where ε is the dielectric constant of the plastic material. By way of example, a fiberglass column having a dielectric constant of 4 (which is not unreasonable), has a power reflectivity of -4.77 dB. Hence, the column return is barely 5 dB below that of a metal cylinder of the same size.

By making the plastic column circular and carefully centering it on the rotator, it may be possible to perform a vector field subtraction to remove the column contribution. As was shown in the previous chapter, a centralized background contribution is more easily removed from the measured data than one which varies rapidly, hence a single central support is desired. What is to be avoided is a multiplicity of solid supports placed well away from the center of the rotator.

9. CONCLUSIONS AND RECOMMENDATIONS

The background signals contributing to the RCS measurement errors arise from different mechanisms for frequencies above and below 500 MHz. Below 500 MHz, background signals are due to ground plane anomalies and equipment deficiencies; above 500 MHz, they are due to the target support column. The technical effort expended during this contract was directed mostly toward the high frequency sources of background signal, but some effort was devoted to the low frequency problem as well.

A. CONCLUSIONS

Major conclusions drawn from this radar background signal reduction study are as follows:

New materials, new techniques

A search of the literature revealed no evidence that new materials or techniques have been developed since RATSCAT began using expandable bead foam 16 years ago. In actual fact, the absorber-coated metal pylon (see below) is an example of new technology, but the concept has not appeared in the open literature. Since no new materials were identified, the materials reflectivity characterizations specified in Task 4.4 were not performed.

Special column treatments

Most forms of column treatment, such as wrapping or control of dielectric properties, do not improve column performance. Some of these ideas have been generated at RATSCAT, and one or two isolated (and inconclusive) experiments have been conducted on-site. But one study showed that any kind of exterior sheath, whether it be lossy or lossless, serves only to increase the column RCS. In general, this is also true of internal bulk loading.

However, a combination of distributed internal losses and a pair of thin outer concentric shells reduced the return of a 30-inch diameter column by 15 dB over a 1.5 GHz bandwidth (see Figure 15). This is a significant reduction. The results were obtained by the exercising of Georgia Tech computer programs and must be considered "theoretical" results that remain to be tested experimentally. The specification of the desirable electrical parameters ignores how these parameters might be achieved in reality. The necessary loss could be achieved by the inclusion of carbon particles in the material before it is foamed, but it is not known how the strength of the foam would be affected. Moreover, one risks increasing the real part of the dielectric constant of the material along with the necessary increase in the imaginary part, and this would negate the performance obtained by the introduction of loss.

Shaping

The use of column shaping to reduce the return was tested experimentally, but shaping could not be evaluated due to experiment difficulties. The objective of the experiments performed during the contract was to compare the returns from smooth and circumferentially grooved test columns, and thereby assess the performance. Unfortunately, it was not possible to obtain RCS patterns of the columns and, instead, the data were averaged (by nature) over aspect angle windows. The data do not show that one column performs better than the other, but without RCS patterns to compare, no firm conclusion can be drawn.

Low frequency background

Not enough diagnostic work has been performed by range personnel to separate instrumentation deficiencies from ground plane anomalies. The contract scope was too limited to allow Georgia Tech to perform diagnostic work and our conclusions are based on interviews with range engineers and upon a theoretical study of the trapped surface wave phenomenon. The equipment limitations can be overcome by improved design and installation of hardware, but the ground plane anomalies are not as easily treated.

Vector field subtraction

VFS remains a good candidate for background signal reduction, provided the target and background signals are restricted to certain characteristics. In theory, accurate measurements of the phase and amplitude of two RCS patterns (with and without the target) at known aspect angles allow the perfect subtraction of background signals. In practice, random noise and aspect angle misalignments will degrade the recovered pattern. Some limitations of VFS were identified using mathematically generated data sets and, had actual measured data been available, other limitations might have been found. Our study shows that VFS has good potential for reducing background signal effects, but the study did not establish accuracy levels as functions of typically operating parameters, such as target size, column size, and radar frequency.

Solid supports

RATSCAT's absorber-covered metal pylons represent improvements in state-of-the-art target support technology. Despite their low RCS, however, the pylons have their disadvantages. The target must be modified to mate with the rotator head atop the pylon, it takes a considerable time to install or remove the pylon, and there is a distinct hazard of target/pylon coupling. The pylon cannot (and should not) be used for targets such as small missiles and projectiles.

Solid plastic supports were not studied. Mutual coupling between the target and the support is as likely with plastic columns as it is with metal columns, and there is no easy way to remove such effects. The return from a solid plastic support can be nearly as large as that from a base metal column. However, if a single central column could support a target, VFS might be a useful technique for removing the unwanted column return. Whether this is in fact the case was not established.

B. RECOMMENDATIONS

Specific recommendations based on these conclusions are listed below in the order of their importance.

Vector field subtraction

VFS should be evaluated in an experimental program. The performance capabilities of the technique should be determined as a function of the relative levels of the target and background signals and the rate with which the signals change with changing aspect angle. The latter is related to the target size in wavelengths and the inhomogeneities in the support column. The evaluation should be performed with simple targets, such as right circular cylinders, and with columns whose returns can be artificially enhanced. Accurate RCS patterns of the test objects must be available as standards of comparison for the reconstructed patterns. VFS should also be evaluated for a practical target such as a missile.

Low frequency background signals

Diagnostic testing should be performed to separate ground plane anomalies from equipment deficiencies. In Section 6 several tests were suggested as ways to help identify the signal sources and aids to further troubleshooting. These involve replacing the antenna input terminals with a good matched load, both at the end of the cable run as well as at the receiver. Other tests are to point the antenna at the zenith and in a direction away from the pit area and note the change, if any, in the signal. Some of these tests may be inconclusive and other tests may suggest themselves in the process of experimentation.

If the tests show that trapped waves are the cause for background signals, a decision must be made how to suppress the signals. The cost of designing, fabricating, testing, and installing a background signal suppression shield may be high, hence scale model tests might be useful before the decision is made to implement any reduction scheme by shielding. An alternative is to improve the ground plane by laying a few acres of runway matting on the desert floor. If the tests show that the instrumentation is inadequate, a design study should be undertaken to correct the problem. This might be in the form of an instrumentation package, for example, mounted near the antenna feed terminals instead of in the pedestal of the 60-foot dish.

Column treatments

The feasibility of the design summarized in Figure 15 should be established. Specifically, the mechanism of introducing loss (the inclusion of carbon black, for example) should be investigated and it should be determined if this also increases the real part of the effective dielectric constant. If it does not, then the fabrication techniques of adding a concentric outer shell and a skin should be established. Finally, a trial column should be fabricated and its RCS methodically measured and compared with those of conventional columns.

The usefulness of the serrated (circumferentially grooved) support column should be established experimentally. Measurement objectives are to obtain RCS patterns of smooth and serrated columns in both the elevation plane and the azimuth plane for assessing performance. If the shaped column performs better than a smooth one, a further sequence of measurements should be performed on a series of groove designs to determine if there is an optimum groove angle and/or depth for a given frequency.

10. EPILOG

There is no painless panacea for reducing background signals or reducing their effects on RCS measurements. Nevertheless, in almost every case, the quality of RCS data can be improved. Multiple patterns can be taken using fluted columns, and the patterns can be spliced together. Vector field subtraction is a promising technique, even if it imposes careful sampling techniques and requires the collection of four times as much data as usually required in routine RCS measurements. Low frequency ground plane anomalies can be removed by covering the ground with conducting mesh. These do not exhaust the possibilities and they are technically achievable. What may not be so acceptable is their cost; accurate data are seldom acquired cheaply.

The importance of the RATSCAT mission and the nature of current and future test requirements demands more attention at the basic research and development level than has been given. To more adequately define deficiencies in instrumentation and procedures, and to devise adequate corrective measures, it is often necessary to perform tests and experiments not strictly related to sponsored test programs at the site. It seems only logical that a scientific "troubleshooting" team be assembled to address these basic problems, and perhaps such a team already exists. The team should not be constrained to support a given test program, but should be assigned the general task of improving RATSCAT's performance and capabilities. As part of that task, the team should be capable of conceiving and designing definitive experiments, conducting or directing the measurements, interpreting the results, and making recommendations. The mode of operation must be logical, methodical, and thorough.

11. REFERENCES

1. "RATSCAT Facilities and Capabilities," 6585th Test Group, Holloman Air Force Base, New Mexico, 1978.

2. M. A. Plonus, "Theoretical Investigations of Scattering from Plastic Foams," IEEE Transactions on Antennas and Propagation, Vol. AP-13, January 1965, pp. 88-93.

3. E. F. Knott and T. B. A. Senior, "Studies of Scattering by Cellular Plastic Materials," University of Michigan Radiation Laboratory Report 5849-1-F, April 1964.

4. H. C. Marlow, D. C. Watson, C. H. Van Hoozer and C. C. Freeny, "The RATSCAT Cross-Section Facility," Proceedings of the IEEE, Vol. 53, August 1965, pp. 946-954.

5. "Radar Cross Section Target Supports - Plastic Materials," Technical Report RADC-TDR-64-381, Rome Air Development Center, June 1964.

6. T. B. A. Senior, M. A. Plonus, and E. F. Knott, "Designing Foamed-Plastic Target Supports," Microwaves, December 1964, pp. 38-43.

7. T. B. A. Senior and E. F. Knott, "Estimates of the 'Volume' Return from Styrofoam," Proceedings of the Radar Reflectivity Measurements Symposium held at MIT Lincoln Laboratories, Report RADC-TDR-64-25, Vol. I, April 1964, pp. 521-526.

8. "Radar Cross Section Target Supports - Metal Columns and Suspension Devices," Technical Report RADC-TDR-64-382, Rome Air Development Center, June 1964.

9. C. C. Freeny, "Radar Target Scatter Site (RATSCAT) Background Subtraction Investigation," Technical Report RADC-TDR-67-436, Rome Air Development Center, June 1964.

10. "The Engineering Data Bank - Foams," Modern Plastics Encyclopedia, Vol. 54, No. 10A, 1977, pp. 485-487.

11. R. W. Barito and W. O. Eastman, "Plastic and Elastomeric Foams," Chapter 7, Handbook of Plastics and Elastomers, 1975

12. Plastic Foams, Part II, eds. K. C. Frisch and J. H. Saunders (Marcel Dekker, Inc., New York 1973), Chapter 9, "Rigid Urethane Foams," Chapter 10, "Polystyrene and Related Thermoplastic Foams;" Chapter 11, "Phenolic Foams," Chapter 12, "Urea-Formaldehyde Foams," Chapter 13, "Epoxy-Resin Foams," Chapter 15, "Miscellaneous Foams;" Chapter 17, "Effects of Cell Geometry on Foam Performance," and Chapter 21, "Military and Space Applications of Cellular Materials."

13. T. H. Ferrigno, Rigid Plastic Foams, 2nd Edition, Reinhold Publishing Corp., New York, 1967.

14. Calvin J. Benning, Plastic Foams: The Physics and Chemistry of Product Performance and Process Technology, Vol. II: Structure, Properties, and Applications, Wiley-Interscience, New York, 1969.

15. Yale L. Meltzer, Foamed Plastics - Recent Developments, Noyes Data Corporation, Park Ridge, New Jersey, 1976.

16. E. A. Meinecke and R. C. Clark, Mechanical Properties of Polymeric Foams, Technomic Publishing Co., Inc., Westport, CT, 1973.

17. A. R. Ingram, "Novel Foams From Styrene-Acrylonitrile Copolymers," Journal of Cellular Plastics, 1, 1965, pp. 69-75.

18. R. E. Skochdopole and L. C. Rubens, "Physical Property Modifications of Low-Density Polyethylene Foams," Journal of Cellular Plastics, 1, 1965, pp. 91-96.

19. "Ethafoam Brand Polyethylene Foam," Dow Chemical Company Form No. 172-125-78.

20. J. K. Bachus and P. G. Gemeinhardt, "Rigid Urethane Foams," in Plastic Foams, Part II, ed. K. C. Frisch and J. H. Saunders, Marcel Dekker, Inc., New York, 1973, pp. 451-524.

21. M. M. Horst, M. T. Tuley, and K. B. Langseth, "Radar Modeling Studies," Final Report on Applied Physics Laboratory Subcontract 600403, Georgia Institute of Technology, Engineering Experiment Station, July 1978.

22. J. A. Stratton, Electromagnetic Theory, McGraw-Hill, New York and London, 1941, pp. 493-494.

23. Larry Carter, Convair Division, General Dynamics, San Diego, 16 June 1980 (personal communication).

24. Warrey Fey, Teledyne Micronetics, San Diego, 13 June 1980 (personal communication).

DATE
ILMED
-8